TO: ARPA
ATTN: Debra Amick

FINAL TECHNICAL REPORT

September 1994

INNOVATIVE PROCESSING OF COMPOSITES FOR ULTRA-HIGH TEMPERATURE APPLICATIONS

by

Reza Abbaschian
Department of Materials Science and Engineering
University of Florida
Gainesville, Florida

Sponsored by: The Advanced Research Projects Agency
Monitored by: The Office of Naval Research

ARPA Grant No. N00014-91-J-4075

BOOK I of IV

Executive Summary

The overall objective of this program was to provide a fundamental understanding of the processing science and technology necessary to fabricate ceramic-matrix, intermetallic-matrix, and metal-matrix composites with superior mechanical properties in high temperature and oxidizing environments. The composites are intended for use as structural materials for advanced aerospace applications at temperatures exceeding 1200°C (2200°F).

In order to accomplish the program objective, interactive research groups were established in three key areas of (a) Fiber Fabrication, (b) Coatings and Infiltration, and (c) Composite Fabrication. The objective of the fiber fabrication group was to develop new fibers which have superior strength and toughness at high temperatures and in oxidizing environments. The research effort focused on the development of two types of fibers: (1) glass-free mullite-based fibers, and (2) oxygen-free silicon carbide fibers. The coatings program had two primary objectives: (1) to control the characteristics of matrix/reinforcing phase interfaces (e.g., to control chemical reactions and bonding at a matrix/fiber interface) and (2) to develop coatings that will improve the oxidation resistance of metal-matrix and intermetallic-matrix composites. Coatings methods utilized included chemical vapor deposition, sol-gel processing, and solution coating with polymeric precursors to ceramics.

The composite fabrication group investigated various methods to incorporate reinforcing phases (i.e., fibers, whiskers, and particulates) into ceramic-, metal-, and intermetallic-matrices. Processing methods investigated included colloidal processing, chemical vapor infiltration, reactive hot-compaction and *in situ* coating, and microwave sintering. The objectives were not only to utilize innovative processing techniques, but also to develop and improved scientific understanding of processing-microstructure relationships in composites fabrication.

This annual report consists of seven sections compiled in four books as described below:

BOOK I

Section 1 Processing and Properties of Silicon Carbide Fibers
Principal Investigators: C.D. Batich
M.D. Sacks

Section 2 Processing of Mullite Composite Fibers
Principal Investigators: J.H. Simmons
M.D. Sacks
A.B. Brennan

Section 3 Chemical Vapor Deposition (CVD) and Chemical Vapor Infiltration (CVI)
Principal Investigator: T.J. Anderson

BOOK II

Section 1 **Processing and Properties of Intermetallic Matrix Composites**
Principal Investigator: **R. Abbaschian**

Section 2 **Mechanical Alloying of $MoSi_2$**
Principal Investigator: **M.J. Kaufman**

BOOK III

Section 1 **Processing of Ceramic Matrix Composites**
Principal Investigator: **M.D. Sacks**

Section 2 **Processing of $BaO\text{-}Al_2O_3\text{-}2SiO_2$ Fibers**
Principal Investigator: **D.E. Clark**

BOOK IV

Section 1 **Processing and Mechanical Property Characterization of Tape Cast, Multilayer, Alumina/Nickel Laminated Composites**
Principal Investigator: **J.J. Mecholsky**

BOOK I

Section 1

Processing and Properties

of

Silicon Carbide Fibers

Principal Investigators: C.D. Batich
M.D. Sacks

Polymer-Derived Silicon Carbide Fibers with Low Oxygen Content and Improved Thermomechanical Stability

PI's: C.D. Batich and M.D. Sacks

Objectives

The two overall objectives of this program are as stated in the past two years:

(1) To develop and characterize high performance, SiC fibers (designated "UF fibers") which have improved thermomechanical properties compared to commercially available SiC fibers and which are suitable for use in ceramic-matrix composites for high temperature (>1300°C) structural applications.

(2) To establish related R&D programs with industrial partners which will result in (i) process scale-up to provide sufficient quantities of high performance, multifilament fiber tows and weaves to fully evaluate fiber properties and (ii) to allow the fabrication of composite test panels and (iii) commercialization of UF SiC fibers in ≤5 years.

Summary of Research and Development Activities

University of Florida researchers developed novel pre-ceramic polymers which were used to prepare continuous, fine-diameter, low-oxygen-content SiC fibers with improved thermomechanical properties compared to commercially available fine-diameter fibers (e.g, Nicalon®).

A patented process was developed to produce "UF Fibers" by dry spinning of polycarbosilane polymers. A basic patent and two divisionals have now been issued to the UF (Toreki and Batich). The key variables in this process were polymer molecular weight, polymer/solvent ratio, and type and concentration of organosilicon spinning aids. Under appropriate conditions, the process resulted in (i) fiberizing solutions with excellent spinnability, (ii) green and partially-pyrolyzed fibers with good handleability, (iii) green fibers which could be directly pyrolyzed to a ceramic without melting (i.e., the process was carried out without an oxidative or irradiative cross-linking step), (iv) high ceramic yield after pyrolysis, and (v) fibers with fine-diameter, smooth surfaces, and round cross-sections.

The average tensile strengths for batches of UF Fibers with ~10-15 μm diameter were as high as ~3.3 GPa (~480 ksi) at room temperature. Due to the fine diameters and high tensile strengths, UF Fibers would be well-suited for textile weaving operations.

The microstructure of as-fabricated UF Fibers showed a carbon-rich, weakly-crystalline structure with very fine (~3-5 nm) β-SiC crystallites. Thus, fibers had relatively low elastic modulus (~200 GPa) compared to stoichiometric SiC, even after heat treatment at temperatures up to 1700°C.

UF Fibers had low oxygen content (~1-2 wt%), e.g., compared to Nicalon® fibers (8-15 wt% oxygen). This resulted in improved thermomechanical stability compared to commercially-available fibers, as indicated by lower weight losses, lower specific surface areas, and improved strength retention after heat treatment at elevated temperatures. Scanning Auger microprobe (SAM) analysis showed that the residual oxygen in UF fibers was concentrated near the fiber surfaces, apparently due to contamination from atmospheric oxygen and water vapor during the spinning and pyrolysis operations. In samples with high levels of surface oxygen contamination, reaction between siliceous (Si-O containing) and carbon-rich materials resulted in some surface degradation of the fibers after high temperature (≥1500°C) heat treatment. Fibers with improved thermomechanical stability were produced by reducing the partial pressure of oxygen during pyrolysis. Scanning electron microscopy (SEM) observations and specific surface area measurements showed that surface degradation reactions were greatly inhibited in fibers with lower oxygen contamination.

Investigations were also directed toward development of fully-crystalline, stoichiometric silicon carbide fibers with higher elastic modulus, while still retaining high tensile strength and excellent thermomechanical stability. By varying polymer chemistry and heat treatment conditions, the capability to vary the fiber Si:C ratio from highly carbon-rich (as in UF Fibers) to the 1:1 ratio in stoichiometric SiC was achieved in this program.

A method was developed to incorporate boron into the fibers so that a more simplified process resulted. This resulted in a Ph.D. dissertation and an invention disclosure has been submitted to the university (6). An additional invention disclosure on improved polymer synthesis has just been submitted to UF by W. Toreki.

Further development of near-stoichiometric, high-strength, high-modulus SiC fibers (designated "UF-HM Fibers") was carried out under a spin-off program sponsored by the Integrated High Performance Turbine Engine Technology (IHPTET) Fiber Development Consortium. Some of the accomplishments of the latter program were: (1) Polymer synthesis and spin dope preparation were scaled up by more than one order to magnitude. (2) Conditions for spinning and winding continuously for extended periods of time with a 30-hole spinneret were determined at the semi-works facility at DuPont's Experimental Station in Wilmington, DE. (3) Typical average tensile strengths in the range of 300-500 ksi (2.1-3.45 GPa) for UF-HM Fibers were achieved. The maximum average tensile strength for a set of fibers was ~550 ksi (~3.8 GPa). (4) Compositional and microstructural characterization of UF-HM fibers was carried out. X-ray diffraction (XRD) and transmission electron microscopy (TEM) showed that fibers consisted primarily of β-SiC with small amounts of α-SiC. TEM showed that grains were mostly in the range of ~0.05-0.2 μm, but larger grains (up to ~0.5-0.6 μm) were also present. Electron microprobe analysis (EMA) indicated showed that fibers had stoichiometric or near-stoichiometric SiC composition. The near-stoichiometric composition was also confirmed by apparent density measurements using the sink-float method. Fiber densities were

usually in the range of 3.1-3.2 g/cm^3 with an average value of ~3.15 g/cm^3. The latter density is ~98% of the value for fully dense (pore-free), stoichiometric SiC.

Continued scale-up and development of UF-HM Fibers is anticipated under the sponsorship of the IHPTET Fiber Development Consortium.

Publications

1. Wm. Toreki, C.D. Batich, M.D. Sacks, M. Saleem, and G.J. Choi, "Polymer-Derived Silicon Carbide Fibers with Improved Thermomechanical Stability," pp. 761-769 in Better Ceramics Through Chemistry V, edited by M.J. Hampden-Smith, W.G. Klemperer, and C.J. Brinker, Mat. Res. Soc. Symp. Proc. Vol. 271, Materials Research Society, Pittsburgh, PA, 1992.

2. Wm. Toreki, G.J. Choi, C.D. Batich, M.D. Sacks, and M. Saleem, "Polymer-Derived Silicon Carbide Fibers with Low Oxygen Content," Ceram. Eng. Sci. Proc., 13 (9-10) 198-208 (1992).

3. Wm. Toreki and C.D. Batich, U.S. Patent No. 5,171,722, "SiC Fibers Having Low Oxygen Content and Methods of Preparation," December 15, 1992, USP 5,242,870 (September 7, 1993), and USP 5,278,110 (January 11, 1994).

4. Wm. Toreki, C.D. Batich, M.D. Sacks, M. Saleem, G.J. Choi, and A.A. Morrone, "Polymer-Derived Silicon Carbide Fibers with Low Oxygen Content and Improved Thermomechanical Stability," J. Composites Sci. Technol., 51 145-159 (1994).

5. M.D. Sacks et al., "Properties and Microstructure of Near-Stoichiometric Silicon Carbide Fibers," in preparation.

6. Chemical Modifications of Polymer-Derived Silicon Carbide Fibers to Enhance Thermomechanical Stability. Ph.D. dissertation December 1993, Guang Jin Choi; Invention disclosure (#1261) by G. Choi, C. Batich, W. Toreki and M. Sacks.

A copy of reference 4 is attached.

POLYMER-DERIVED SILICON CARBIDE FIBERS WITH LOW OXYGEN CONTENT AND IMPROVED THERMOMECHANICAL STABILITY

William Toreki, Christopher D. Batich, Michael D. Sacks,*
Mohamed Saleem, Guang J. Choi & Augusto A. Morrone

Department of Materials Science and Engineering, University of Florida, Gainesville, Florida 32611, USA

Abstract

Continuous silicon carbide fibers (UF fibers) with low oxygen content (~1–2 wt%) were prepared in a range of diameters (~8–50 μm) by the dry spinning of organosilicon polymer solutions and subsequent pyrolysis of the polymer fibers. Room-temperature mechanical properties were similar to commercially-available Nicalon™ fibers, as average tensile strengths ~3 GPa were obtained for some batches with fiber diameters in the range of ~10 μm. Furthermore, UF fibers showed significantly better thermomechanical stability compared to Nicalon, as indicated by lower weight losses, lower specific surface areas, and improved strength retention after heat treatment at temperatures up to 1700°C. The structure and composition of UF fibers were also characterized using scanning electron microscopy, transmission electron microscopy, X-ray diffraction, Auger depth profiling analysis, neutron activation analysis, and atomic absorption.

Keywords: fibers, silicon carbide, polymer, polycarbosilane, thermomechanical properties

INTRODUCTION

There has been considerable interest in fiber-reinforced ceramic-matrix composites (CMCs) for high temperature structural applications since Yajima *et al.*[1,2] first developed continuous silicon carbide fibers with fine diameter and high tensile strength. CMCs with high strength and high fracture toughness at elevated temperatures have been developed by combining Nicalon™ SiC fibers (Nippon Carbon Co., Tokyo, Japan) with a variety of matrix materials, including glasses, glass-ceramics, and crystalline ceramics.[3–5] Despite the impressive properties achieved, there is still a need for SiC fibers with improved thermomechanical properties. The mechanical properties of Nicalon fibers often deteriorate at (or below) the temperatures required for processing CMCs, as well as below the maximum useful temperatures for many of the ceramic matrix materials used in structural applications. Thermal degradation of Nicalon fibers is highly dependent upon atmosphere, but significant weight losses can occur at temperatures as low as 1200°C and decreases in tensile strength can occur at temperatures below 1000°C.[7–15] Studies have shown that these effects are associated with the presence of oxygen (~8–15 wt%) and excess carbon in the fibers. Carbothermal reduction reactions (i.e. between carbon and siliceous material) lead to the evolution of volatile species (primarily CO and SiO) which results in large weight losses, formation of porosity, and the growth of SiC grains and other strength-degrading flaws in the fiber microstructure.[7,15]

Nicalon fibers are prepared by melt spinning of a low-molecular-weight organosilicon polymer (i.e. polycarbosilane). As-spun fibers are then heated at low temperature (~150–200°C) in air in order to cure (cross-link) the polymer. This treatment prevents the fibers from re-melting during the subsequent pyrolysis step (in which the polymer is converted at higher temperatures to a SiC-rich ceramic). However, curing in air also leads to the high oxygen content in Nicalon fibers. To produce fibers with improved thermomechanical stability, alternative processes for fabricating SiC fibers with minimal oxygen 'contamination' have been investigated.[16–22]

Frechette *et al.*[16] produced stoichiometric polycrystalline SiC fibers with low oxygen content by using a process which is a hybrid of polymer melt spinning and ceramic powder/liquid extrusion. SiC particles and molten organic polymer were mixed, extruded through a spinneret, and wound on a rotating drum to

* To whom correspondence should be addressed.

form 'green' fibers. This was followed by 'binder burnout' (i.e. pyrolysis of the organic polymer) and subsequent sintering of the SiC 'powder compact' at high temperatures (>1900°C). The sintered fibers had high relative density (i.e. minimal residual porosity) and an ~1–2 μm average grain size. The fibers had average tensile strengths at room temperature in the range ~1.0–1.2 GPa and the strength level was maintained after heat treatment at 1550°C. A related process for producing polycrystalline SiC fibers with low oxygen content was developed by Silverman *et al.*[17] Fibers were produced using concentrated SiC particle slurries prepared with xylene as the liquid media and polycarbosilane (PC) as a binder. Mixtures were extruded through a spinneret and subsequently heat treated to pyrolyze the PC and to sinter (at 2000°C) the fibers to high relative density (>99%). The fiber tensile strength and strength retention after heat treatment were similar to that reported by Frechette *et al.*[16] The average elastic modulus was ~380 GPa, i.e. only slightly below the value for bulk polycrystalline SiC samples.

Despite the excellent thermal stability, there are several limitations associated with the powder processing routes utilized by Frechette *et al.* and Silverman *et al.* to produce SiC fibers. First, since the starting particle sizes for the SiC powders are relatively large (i.e. average sizes of the order of ~0.5 μm), the grain sizes in the sintered fibers are also relatively large (i.e. compared to those observed in polymer-derived fibers). This, in turn, limits the maximum tensile strength that can be achieved. Secondly, powder processing routes currently have a lower limit of ~25 μm for the fiber diameter,[16,17] i.e. ~10 μm larger than Nicalon. The larger fiber diameter and lower strength of the fibers (e.g. compared to Nicalon) limit the flexibility and, hence, weavability of the fibers. Consequently, there is still considerable interest in using organosilicon polymers as precursors for the development of SiC fibers with low oxygen content.[18–22]

Lipowitz *et al.*[18,19] developed stoichiometric, polycrystalline SiC fibers using polycarbosilane and methylpolydisilylazane polymers. Fibers were melt spun, cross-linked, and heat treated at temperatures above 1600°C in argon in order to react excess carbon and oxygen in the fibers. As noted earlier, PC-derived fibers normally become very weak and develop a porous, large-grained microstructure during this type of heat treatment. However, Lipowitz *et al.* incorporated 'sintering additives' (unspecified chemistry) in the polymer which allowed fibers to retain their integrity (and fine grain size) during the carbothermal reduction reactions discussed earlier. The resulting fibers had fine diameter (8–10 μm), high relative density, small average grain sizes (in the range ~0.03–0.5 μm, depending on the Si:C ratio), low oxygen content (<0.1%), high tensile strength (up to 2.6 GPa), high elastic modulus (up to 420 GPa), and good strength retention after high temperature (1800°C) heat treatment in argon. The key limitation in this process was apparently a difficulty in producing continuous fibers. Although details were not provided, the authors indicated that further developments in rapid cross-linking technology were needed, as well as improvements in the fiber spinnability and green strength.

Takeda *et al.*[20,21] have reported the development of low-oxygen-content (0.4 wt%), fine-diameter (~15 μm) SiC fibers. These fibers are prepared in a similar manner as Nicalon (i.e. by melt spinning of PC), except that cross-linking is accomplished by electron beam irradiation (i.e. instead of using oxidation). The high-temperature stability of the fibers increased dramatically as the oxygen content of the fibers decreased. Fibers with 0.4 wt% oxygen retained high strength (~2.4 GPa) and high modulus (~250 GPa) after heat treatment at 1500°C in argon. The main drawback of this method is that cross-linking of the polymer by electron beam irradiation is a slow and costly processing step.

The present authors have also fabricated PC-derived SiC fibers (designated 'UF fibers') with low oxygen content (~2 wt%) and good thermal stability.[22] In contrast to the melt spinning techniques used by Takeda *et al.* and Lipowitz *et al.*, UF fibers are prepared using a solution-based fiber spinning process. In this paper, more detailed information is provided on the processing, structure, and properties of these fibers.

EXPERIMENTAL METHODS

Synthesis and processing

Polycarbosilane (PC) was synthesized by pressure pyrolysis of polydimethylsilane (Huls, Bristol, PA) in a stainless steel autoclave (model 4651, Parr Instrument Co., Moline, IL) under a nitrogen atmosphere. PCs with controlled average molecular weight (in the range ~1,000–12,000 (see note 1)) were produced by varying the pyrolysis temperature and time. The PC was purified by dissolving the reaction product in chloroform, filtering the solutions, and subsequently precipitating the PC in an excess of acetone. The product was vacuum dried at ~60°C and stored under vacuum in a desiccator.

Control over molecular weight (MW) was a key requirement for successfully producing PC fibers by solution processing. PCs with low MW (e.g. <5,000) were highly soluble in common organic solvents (e.g. toluene, hexane, chloroform, etc.), but useful fibers could not be produced because the polymer melted during subsequent heat treatment. (Furthermore,

there is low ceramic yield after pyrolysis of low-molecular-weight PCs.) In contrast, high-molecular-weight PCs (e.g. >10 000) did not melt during heat treatment, but the polymer solubility was too low to prepare useful fiber spinning solutions. Therefore, fibers were spun using intermediate-molecular-weight PCs (~5 000–10 000) which not only enabled preparation of highly concentrated solutions (e.g. typically ~70 wt%), but also allowed fibers to be pyrolyzed without melting. The latter consideration is particularly important because it allows the formation of fibers without introducing an oxidative curing step. Thus, any oxygen present in the pyrolyzed fibers results from impurities in the starting materials and/or contamination due to exposure to oxygen or water vapor during the various processing steps.

Several additives were found to be effective in improving the spinnability of the PC solutions and the strength of as-spun fibers. These included vinylic polysilazane (MW ≈ 50 000) and polyisobutylene (MW ≈ 50 000). The former polymer was prepared according to procedures described in detail previously,[23] while the latter polymer was commercially available (Vistanex®, Exxon Chemical Co., Houston, TX). The mixed polymer solutions were passed through a 2–4 μm glass frit filter to remove insoluble material (e.g. particulate impurities, polymer 'microgel' particles, etc.) Some solutions were also passed through 0.1 or 0.2 μm PTFE filters. After filtration, solutions were concentrated on a rotary evaporator at ~60°C until ~30 wt% solvent remained. Rheological characteristics of the spinning solution were determined using a cone-plate viscometer (Model HBT, Brookfield Engineering Laboratories Inc., Stoughton, MA).

Fibers were formed at room temperature by extruding the polymer solutions through stainless steel spinnerets (~70 or ~120 μm diameter orifices) under nitrogen pressure. Three to five filaments were extruded simultaneously in most experiments. Continuous 'green' fibers were collected by winding on a rotating drum which was placed approximately 30 cm below the spinneret. A range of fiber diameters were produced by varying the spinneret orifice size, nitrogen pressure, winding speed, and solution viscosity. After fiber spinning, batches (typically a few grams) were cut from the drum (~15–20 cm lengths) and heat treated in a tube furnace to pyrolyze the polymeric fibers to a SiC-containing ceramic. Most of the samples were heated at ~0.5°C/min to 150°C, then ~3.5°C/min to 1000°C, followed by a hold of 1 h at 1000°C. It was determined later that higher heating rates could be used without any adverse effect on fiber properties, so the schedule was changed to ~1°C/min to 150°C and ~7°C/min to 1000°C. The pyrolysis atmosphere was nitrogen, argon, or argon with a small amount of hydrogen (~1–2%). Fibers with controlled diameters in the range of ~8–50 μm were produced after pyrolysis.

Fiber characterization

Weight loss behavior of green and pyrolyzed fibers was determined by thermal gravimetric analysis (TGA) (Model TGA-7, Perkin-Elmer, Norwalk, CT; Model STA-409, Netzsch Co., Exton, PA). Specific surface areas of heat-treated fibers were determined by the BET method using nitrogen or krypton gas adsorption measurements (Model ASAP 2000, Micromeritics, Atlanta, GA). Fibers were also examined by scanning electron microscopy (SEM) (Model JSM-6400, JEOL, Tokyo, Japan) and transmission electron microscopy (TEM) (Model 200 CX, JEOL).

Elemental compositions of carbosilane polymers and heat-treated fibers were determined by outside analytical laboratories (IRT Corp., San Diego, CA; Radio-Analytical Services, University of Kentucky, Lexington, KY; Galbraith Laboratories Inc., Knoxville, TN) using neutron activation analysis (for oxygen, nitrogen, and silicon), atomic absorption (for silicon), and LECO combustion analysis (for carbon, hydrogen, and nitrogen). Phase analysis of heat-treated fibers was carried out by X-ray diffraction (XRD) (Model APD 3720, Philips Electronic Instruments Co., Mt. Vernon, NY) using Ni-filtered Cu Kα radiation.

Compositional analyses of individual pyrolyzed fibers were also carried out by scanning Auger microprobe (SAM) analysis (model PHI 660, Perkin Elmer Corp., Eden Prairie, MN). Fibers were mounted horizontally and a 10 kV electron beam (30 nA) was focused on a small area (<0.01 μm^2) on the center portion of the fiber surface. A detailed survey spectrum (10 scans) was collected over the entire kinetic energy range (50–2050 eV). The analyzed surface was then etched by sputtering for 6 s with an Ar^+ ion beam; this was followed by re-analysis of the same fiber area, but only over the spectral regions for C, Si, and O. This process was repeated in rapid sequence (five scans for each analysis) for an extended period (~18 min total sputtering time) in order to obtain a depth profile for the fiber elemental composition. The results were corrected for relative atomic sensitivities and displayed as atomic percentage versus sputtering time. (The sputter rate was adjusted to correspond to approximately 100 Å per minute for a tantalum oxide standard.) After depth profiling was completed, a detailed survey spectrum (10 scans) of the fiber interior was collected.

Fiber tensile strengths were determined at room temperature according to ASTM procedure D3379.[24] Both green and pyrolyzed fibers were tested. In addition, pyrolyzed fibers were tested after additional heat treatments in the range 1200–1700°C (0.5–2.0 h) in argon or argon/1–2% hydrogen atmospheres.

Individual fibers were attached to paper tabs using an epoxy adhesive and loaded in tension (0.5 mm/min cross-head speed) until failure using a mechanical testing apparatus (Model 1122, Instron Corp., Canton, MA). The gage length was 25 mm and at least eight fibers (but usually 10–15) were tested for each batch. To calculate tensile strengths, fiber diameters were determined using an optical microscope equipped with a micrometer in the eyepiece. Rupture strains and elastic modulus values were obtained from the stress–strain data collected during the strength measurements. Modulus values were calculated without any corrections for the compliance of the mechanical testing system.

Fiber tensile strengths were also measured at elevated temperatures at the High Temperature Materials Laboratory at Oak Ridge National Laboratory. Individual fibers with a 178 mm gage length were mounted directly in pneumatic grips. Measurements were made in air at 1400°C.

RESULTS AND DISCUSSION

As noted earlier, successful formation of fibers required both control over the PC molecular weight and the use of spinning aids. In addition, it was necessary to control the polymer/solvent ratio in the spinning solution in order to prepare useful fibers. If the polymer solution had a large excess of solvent, fibers did not maintain their shape after exiting the spinneret and it was not possible to form continuous fibers. With a smaller excess of solvent, continuous fibers were formed but they would stick together on the wind-up drum (i.e. due to insufficient solvent evaporation during the time period between exiting the spinneret and winding on the drum). In contrast, if polymer solutions were too concentrated (solvent deficient), it was difficult to extrude the solutions through the spinneret (i.e. due to the high viscosity). This tended to produce discontinuous brittle fibers with rough surfaces. In the appropriate range of solvent/polymer concentrations, fibers could be spun continuously for periods up to ~20 min. (The primary cause of interruptions in spinning was gas bubbles in the polymer solutions. These bubbles developed mostly from entrainment of gas during preparation and mixing of the polymer solutions, but also possibly from nitrogen introduced during the extrusion of the solutions through the spinneret. In some cases, the continuous spinning time was only limited by the amount of polymer solution contained in the reservoir in the spinneret head.) The spinning solutions showed slightly shear thinning rheological flow behavior with a typical viscosity of the order of 25 Pa s at a shear rate of 40 s^{-1}. Figure 1 shows typical plots of shear stress versus shear rate and viscosity versus shear rate for solutions used in fiber spinning. The measurements were made by first increasing the shear rate from 1 to 40 s^{-1} and then decreasing the shear rate back to 1 s^{-1}. Solutions showed negligible thixotropy under these measuring conditions.

Stress–strain measurements were carried out on green fibers (as-spun) and fibers heated at 400°C for 0.5 h. The green fibers had an average tensile strength of ~20 MPa and average rupture strain of ~1.0% (see note 2). The fibers showed only elastic deformation before failure. In contrast, the 400°C-pyrolyzed fibers exhibited considerable plastic deformation. The average tensile strength increased to ~45 MPa and the average rupture strain increased to ~4%. Hasegawa *et al.*[26] observed similar mechanical properties for oxidatively cured PC-derived fibers (i.e. Nicalon-type) heated at 400°C for 1 h in nitrogen or in vacuum.

Figure 2 shows TGA results for unpyrolyzed fibers that were heated at a rate of 20°C/min in flowing argon to 950°C. The ceramic yield (~80 wt%) is relatively high, especially compared to yields (~60 wt%) reported for low-molecular-weight PCs (such as used in melt spinning of Nicalon-type fibers).[25,26] In fact, the ceramic yield for the UF fibers is comparable to values reported for *oxygen-cured* PC fibers.[15,26] The high yield, in combination with the observation that the polymers do not melt during heat treatment, suggest that the intermediate-molecular-weight PCs prepared in this study have significantly greater intramolecular branching and ring structure development compared to low-molecular-weight PCs.

Pyrolyzed fibers (750–1200°C) have a visual appearance similar to Nicalon (i.e. black color). SEM observations of a 1000°C-pyrolyzed sample (Fig. 3) show fibers have round cross-sections and relatively smooth surfaces. Fracture surfaces (Fig. 3) have a glassy appearance which reflects the fact that the pyrolyzed fibers consist of weakly crystalline, extremely fine-grained β-SiC and amorphous carbon. Electron diffraction on a 1200°C-pyrolyzed sample shows a ring pattern (Fig. 4(A)) which corresponds to the three strongest reflections in β-SiC (111, 220, and 311). The TEM bright field image in Fig. 4(B) shows that the crystal domains in this sample are only of the order of a few nanometers. These microstructural features are similar to those observed in Nicalon fibers heated at relatively low temperatures ($\leq$ 1200°C).[8,9,15]

Figure 5 shows a plot of average tensile strength (at room temperature) versus fiber diameter for various UF fiber batches pyrolyzed at 1000°C in nitrogen. The strength decreases with increasing fiber diameter. (This effect is usually attributed to the increased probability of encountering strength-limiting flaws as the fiber diameter increases.[27] It has also been reported that large-diameter fibers may develop large processing flaws,[27] but this possibility was not investigated for UF fibers.) Figure 5 shows that some UF batches with fiber diameters in the range of ~10

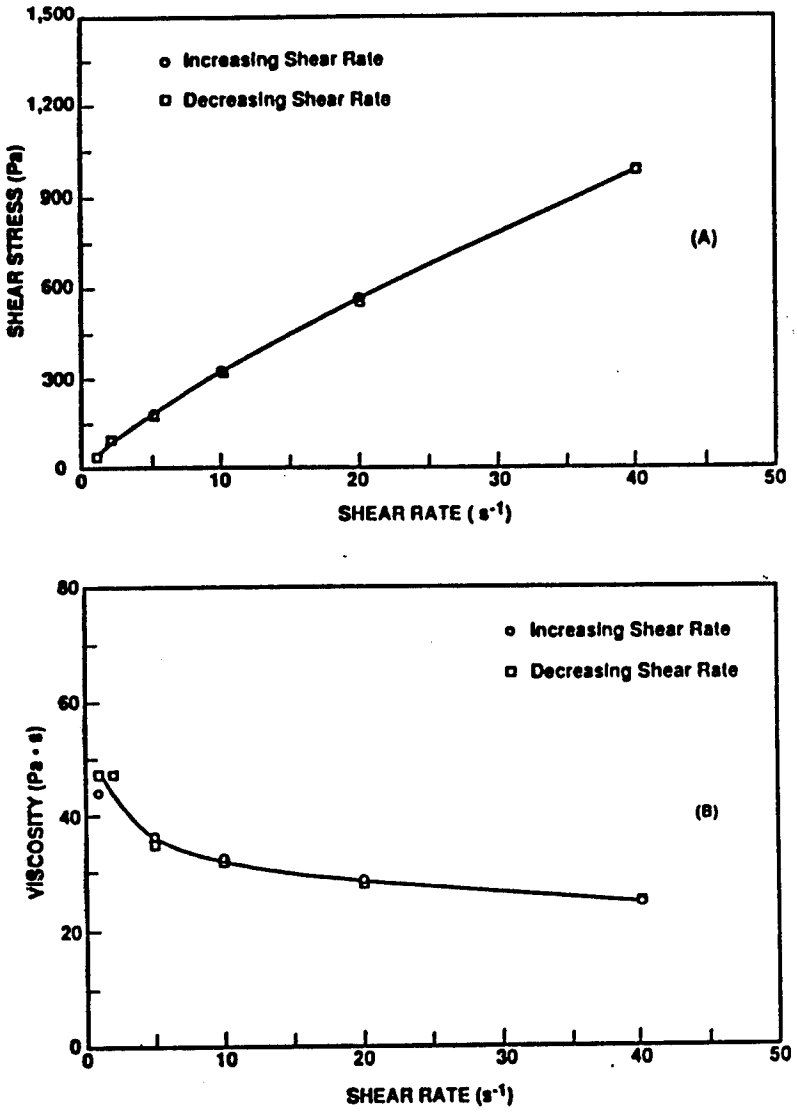

Fig. 1. Plots of (A) shear stress versus shear rate and (B) viscosity versus shear rate for a typical UF fiber spinning solution.

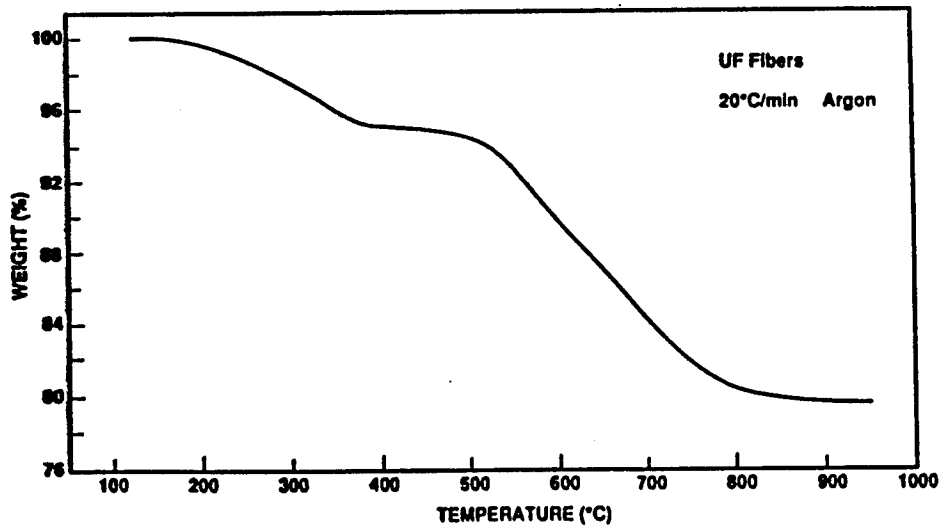

Fig. 2. TGA plot for 'green' (as-spun) UF fibers heated in argon to 950°C at 20°C/min.

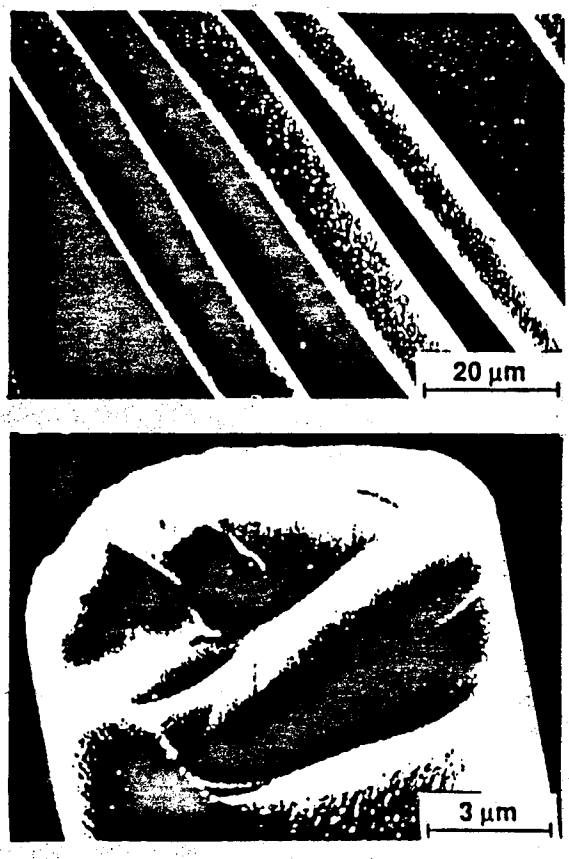

Fig. 3. Scanning electron micrographs of 1000°C-pyrolyzed UF fibers.

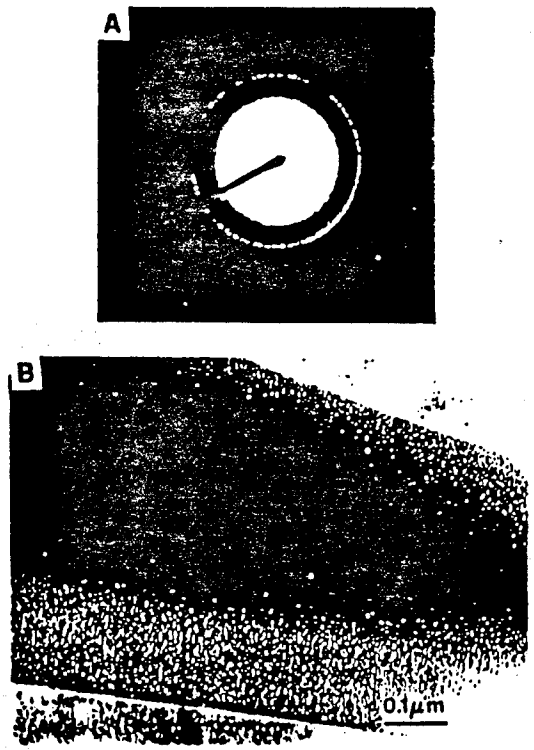

Fig. 4. (A) TEM electron diffraction pattern and (B) TEM bright field image of 1200°C-pyrolyzed UF fibers.

μm had average tensile strengths ≈3 GPa. (Individual fiber strengths exceeding 5 GPa were obtained in a few cases.) Figure 5 also shows tensile strengths for Nicalon fibers (reported by the manufacturer and measured at UF (see note 3)). Data reported by Yajima *et al.* on Nicalon-type fibers are also included.[1,37] It is evident from Fig. 5 that the 1000°C-pyrolyzed UF fibers and Nicalon fibers have very similar tensile strengths at room temperature. Some of the scatter in the tensile strengths for UF fibers may be attributed to the fact that experimental conditions were deliberately varied during the development of the process (e.g. polymer molecular weight, spinning solution viscosity, solution filtration procedure, gas pressure and winding speed during fiber fabrication, etc.) The variations in strength may also reflect the difficulty in rigorously controlling processing conditions because of the small batch sizes (i.e. a few grams) used in most experiments.

Figure 6 shows a comparison of TGA data obtained for Nicalon fibers and UF fibers. The UF fibers used in this experiment were initially pyrolyzed (from the green state) at 750°C for 1 h in nitrogen. As-received Nicalon fibers were given the same heat treatment prior to the TGA experiment. The weight loss was then monitored (Fig. 6) as the fibers were heated in argon at 10°C/min to 1550°C and then held for 1 h at temperature. UF fibers lost only ~3 wt% during this treatment, while the Nicalon fiber lost ~25 wt%. (The latter value is consistent with the weight loss reported for Nicalon in other studies.[11,21]) As discussed earlier, the large weight loss in Nicalon is associated with the high oxygen content of the fiber, as siliceous material reacts with excess carbon to form oxygen-containing volatile products (primarily CO and SiO). In contrast, the relatively low weight loss observed for the UF fibers can be attributed to the absence of such reactions due to the low oxygen content (i.e. since fibers were prepared without an oxidative cross-linking step).

The low oxygen content of UF fibers was confirmed by neutron activation analysis (NAA). Table 1 shows that UF fibers have been produced with oxygen contents in the range ~1.1–2.6 wt%, while Nicalon fibers have oxygen contents in the range of 10–15 wt% (see note 4). (The range of oxygen contents listed in Table 1 for the UF fibers represents analyses on 12 separate batches which were pyrolyzed at 1000°C. Nine of these batches had oxygen contents ≤1.9 wt%.) Other elemental analyses (Table 1) show that UF and Nicalon fibers have similar Si, N, and H contents. These results indicate that the UF fiber has an excess of carbon, i.e. in comparison to both Nicalon fibers and stoichiometric SiC (see note 5).

It should be emphasized that the oxygen present in UF fibers is *not* deliberately incorporated (i.e. to effect polymer cross-linking), but results from unintentional

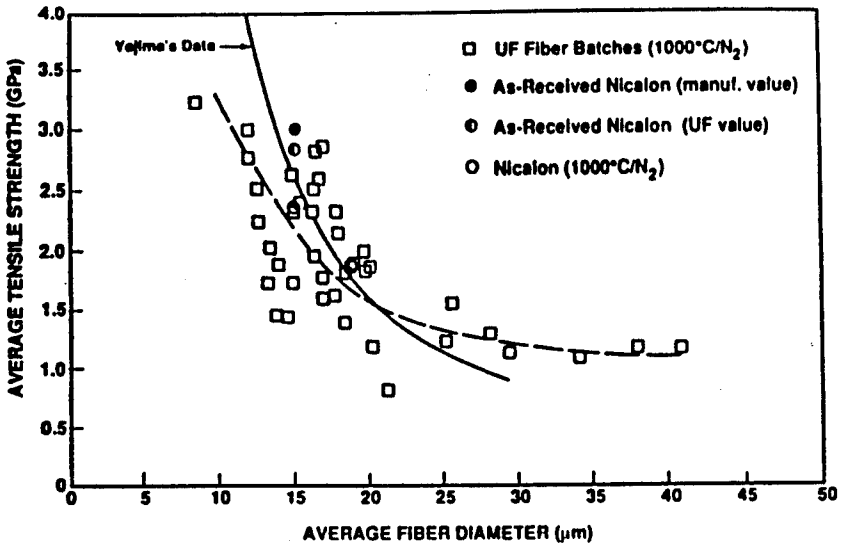

Fig. 5. Plots of average tensile strength versus fiber diameter for different batches of UF fibers. Data are also shown for Nicalon fibers.

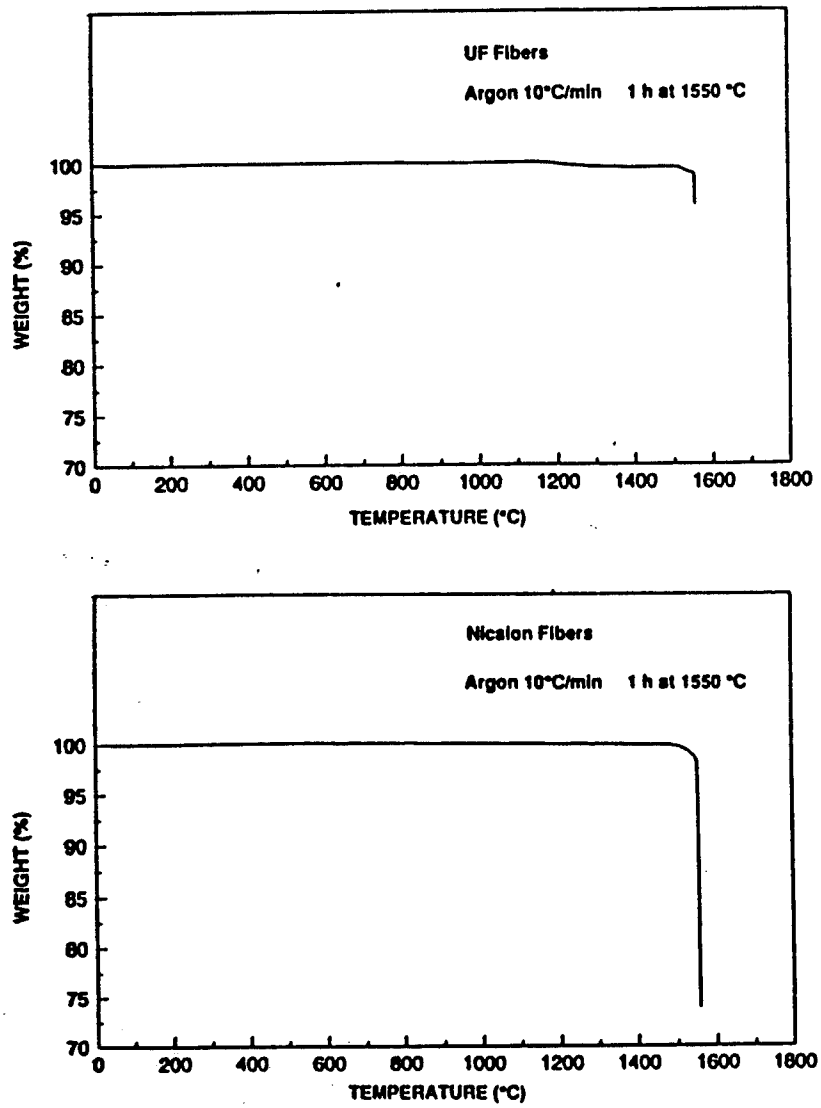

Fig. 6. Weight loss behavior for UF fibers (top) and Nicalon fibers (bottom) heated in argon to 1550°C at 10°C/min and then held for 1 h at temperature.

Table 1. Elemental analysis

Sample	O (wt%)	Si (wt%)	C (wt%)	N (wt%)	H (wt%)
UF fiber	1·1–2·6[a]	55[a,b]	42[c]	1–2[a,d]	<0·5[d]
Nicalon	13·5–15[a]	55[b]	29[d]	<0·5[d]	<0·5[d]
Nicalon[e]	10	58	31		

[a] Determined by neutron activation analysis; [b] determined by atomic absorption; [c] determined by difference; [d] determined by LECO combustion method; [e] reported by manufacturer.

contamination during processing. NAA showed that the starting material for polymer synthesis (i.e. polydimethylsilane) contained only ~0.3–0.4 wt% oxygen. However, analysis of several PC batches showed that oxygen contents increased to levels in the range ~0.3–1.3 wt%, presumably due to exposure to ambient air during the synthesis and purification steps and during storage. Oxygen contamination also occurred during fiber spinning and pyrolysis because most fiber batches were (i) spun and wound in the ambient air atmosphere and (ii) pyrolyzed in an ungettered furnace using standard-grade nitrogen or argon (> 99.995% purity, ~5–20 ppm O_2). Due to the large amount of surface area created when fine-diameter fibers are formed, the oxygen contamination picked up during spinning, winding, and pyrolysis is concentrated near the surfaces of the fibers. This was shown by scanning Auger microprobe (SAM) depth profiling analysis on 1000°C-pyrolyzed UF fibers with relatively low overall oxygen content (~1.9 wt% as determined by NAA). Figure 7 shows survey scans obtained from the fiber surface (i.e. before sputtering) and fiber interior (i.e. after sputtering to a depth of approximately 180 nm). The results show that there is a very large oxygen content at the fiber surface (Fig. 7(A)), while no oxygen signal is observed in the spectrum from the fiber interior (Fig. 7(B)). The atomic concentration depth profiles of Si, C, and O for this fiber are given in Fig. 8 (see note 6). It is evident that the oxygen content is significantly higher in the outer several hundred angstroms of the fiber.

At high levels of surface oxygen contamination, UF fibers undergo the same type of carbothermal reduction reactions observed in Nicalon, i.e. reactions occur between excess carbon and siliceous (Si–O-containing) material near the fiber surface. Figure 9

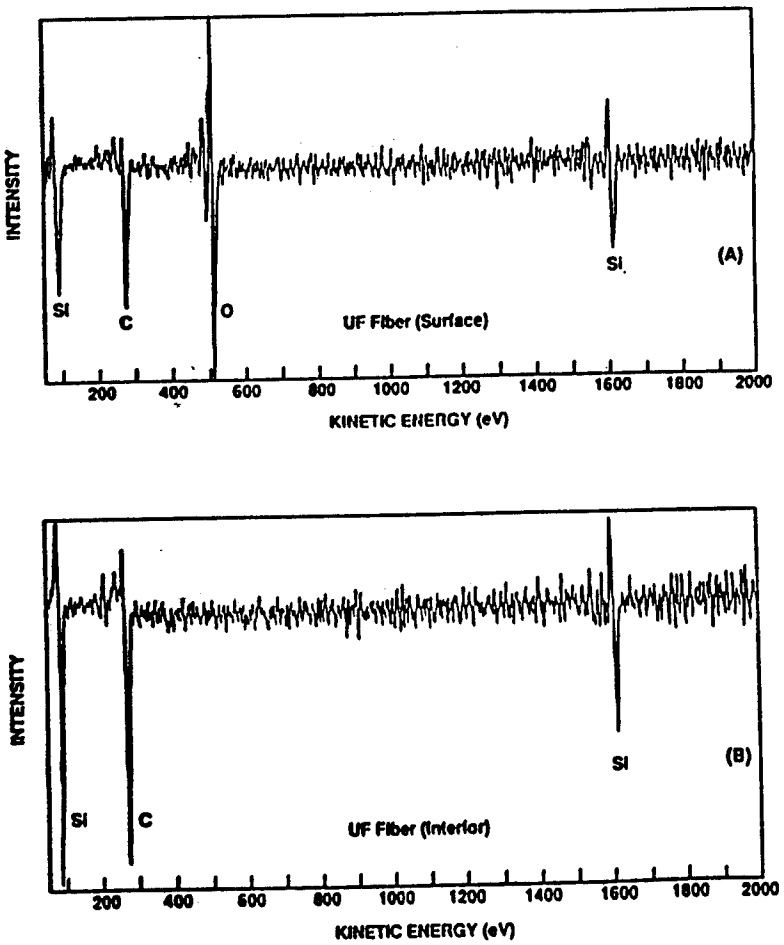

Fig. 7. Scanning Auger microprobe survey scans at the (A) surface and (B) interior of a 1000°C-pyrolyzed UF fiber.

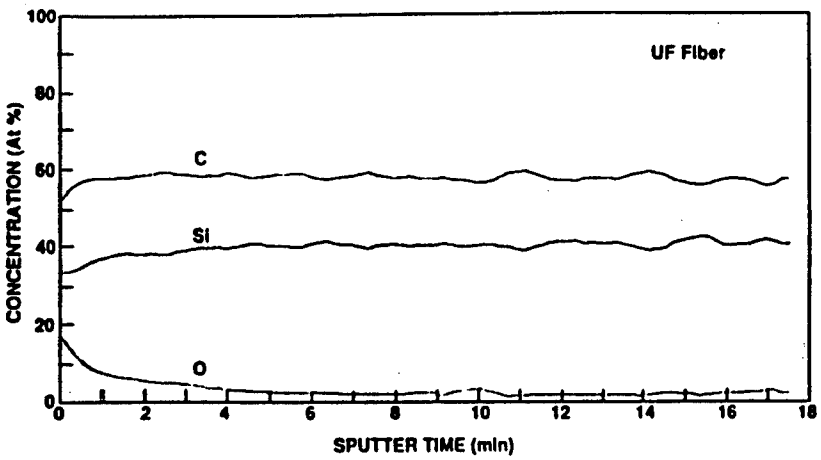

Fig. 8. Scanning Auger microprobe depth profiles of the O, Si, and C atomic concentrations for the same fiber as in Fig. 7.

shows SEM micrographs of an oxygen-contaminated UF fiber sample which was initially pyrolyzed in a nitrogen atmosphere (ungettered furnace) to 1000°C and subsequently heat treated to 1500°C in argon. Growth of some large grains and roughening of the surface is evident. This type of degradation can be avoided by exercising greater control over the spinning and pyrolysis atmospheres so that less exposure to oxygen and water vapor occurs during processing. For example, in order to lower the oxygen partial pressure during pyrolysis, heat treatment was carried out in an argon/1–2% hydrogen atmosphere in some experiments. Figure 10 shows SEM micrographs of a sample pyrolyzed to 1200°C (for 1 h) in argon/1–2% hydrogen and subsequently heated to 1600°C (for 1 h) in argon. The fibers show no evidence of degradation reactions, as their appearance is similar to the 1000°C-pyrolyzed sample shown in Fig. 3. This can be contrasted to the appearance of Nicalon fibers which degrade extensively after heat treatment at 1600°C in argon (Fig. 11).

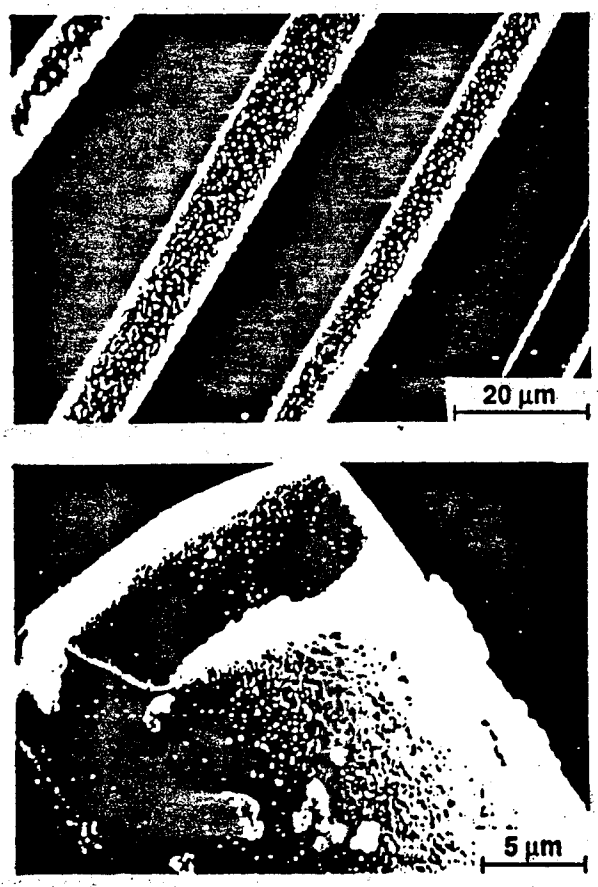

Fig. 9. Scanning electron micrographs of UF fibers with relatively high surface oxygen contamination after heat treatment at 1500°C for 1 h in argon. Growth of large grains and degradation reactions occur at the fiber surface.

Even in samples with high levels of oxygen contamination, degradation of UF fibers is confined to a region near the surface (i.e. the region with more than a few percent oxygen). This was evident from SEM observations of the fiber interior (e.g. see Fig. 9(B)). It was also illustrated using gas adsorption surface area measurements. When degradation reactions occur (and volatile reaction products are eliminated), the fibers develop porosity and the specific surface area increases. If the degradation is limited to a surface region, only moderate increases in specific surface area are observed. Figure 12 shows plots of specific surface area as a function of heat treatment temperature for Nicalon and UF fibers. Nicalon fibers show a sharp increase in specific surface area above 1200°C, reaching ~25 m^2/g at 1600°C. This is consistent with the microstructural observations shown in Fig. 11 and the large weight loss observed by TGA (Fig. 6). In contrast, UF fibers show more gradual increases in specific surface area. For a fiber batch (UF-94) with high oxygen contamination at the surface, the specific surface area increased from ~0.2 m^2/g after pyrolysis at 1000°C in nitrogen to ~2.5 m^2 after subsequent heat treatment at 1600°C in argon.

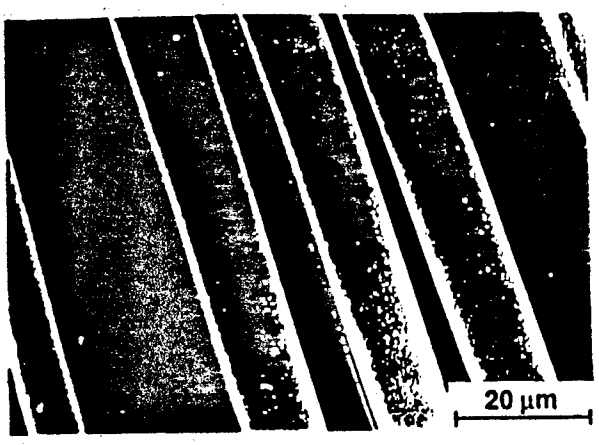

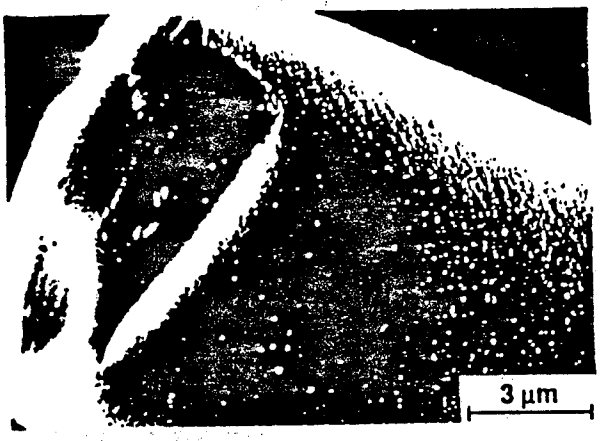

Fig. 10. Scanning electron micrographs of UF fibers with relatively low surface oxygen contamination after heat treatment at 1600°C for 1 h in argon. The fibers have a similar appearance to the 1000°C-pyrolyzed fibers shown in Fig. 3.

However, a fiber batch (UF-127) with lower surface oxygen contamination shows almost no change in specific surface area during heat treatment, i.e. the values were ~0.5 m^2/g after pyrolysis in argon/1–2% hydrogen at 1000°C and ~0.8 m^2/g after further heat treatment in argon at 1600°C (see note 7).

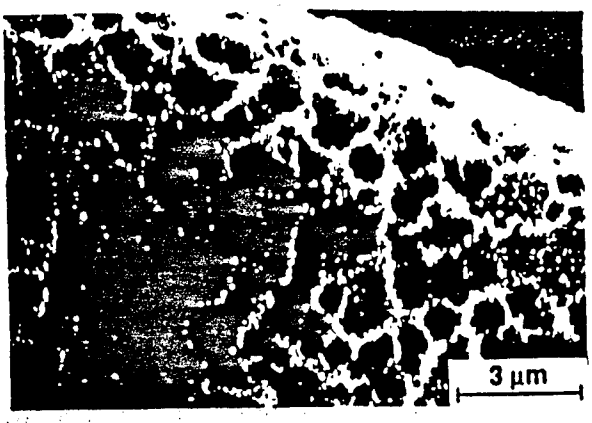

Fig. 11. Scanning electron micrograph of Nicalon fiber after heat treatment at 1600°C for 1 h in argon.

Based on the TGA (Fig. 6), SEM (Figs 9–11), and specific surface area (Fig. 12) results, it is not surprising that UF fibers showed superior thermomechanical properties compared to Nicalon fibers. Figure 13 shows average tensile strength values for UF and Nicalon fibers that were heat treated in the range 1000–1700°C in an argon atmosphere (see note 8). The data labeled 'UF-80' were collected from a single lot of fibers. The results are considered representative of some of the first UF fiber batches that were prepared with low overall oxygen content (~2 wt%), but *without* taking steps to control surface oxygen contamination. In comparison with Nicalon, UF-80 fibers show considerably higher strengths at heat treatment temperatures above 1300°C. For example, after 1.0 h at 1400°C, UF-80 fibers have an average tensile strength of ~1.2 GPa compared to only ~0.3 GPa for Nicalon (see note 9). Furthermore, the UF-80 fibers retained substantial strength (~0.9 GPa) after

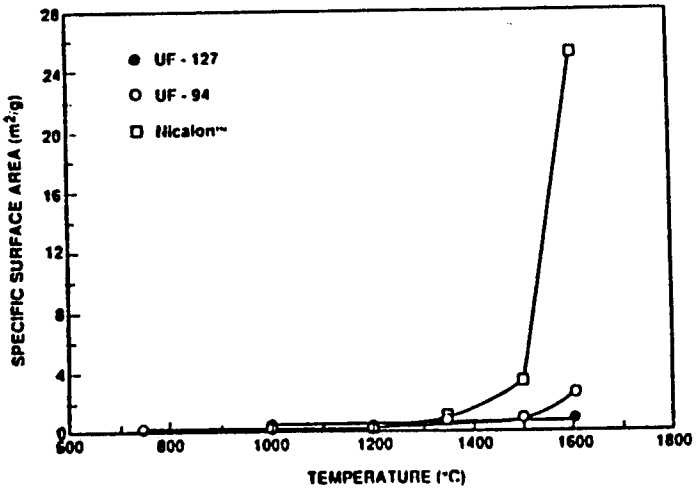

Fig. 12. Plot of specific surface area versus heat treatment temperature for UF fibers and Nicalon fibers. Values are given for UF-127 fibers (lower surface oxygen contamination) and UF-94 fibers (higher surface oxygen contamination).

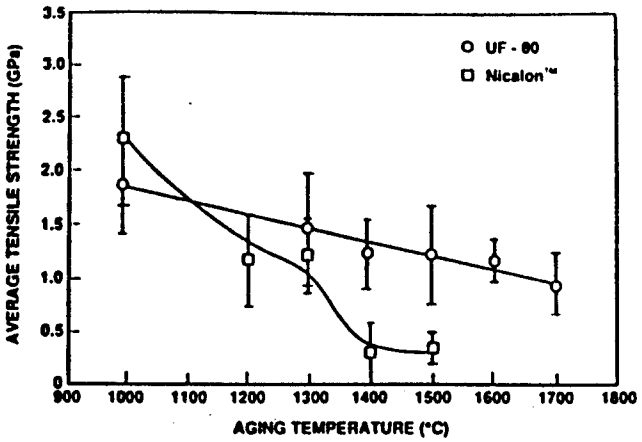

Fig. 13. Plots of average tensile strength versus heat treatment temperature for UF-80 fibers and Nicalon fibers.

heat treatment at 1700°C (1.0 h), while the Nicalon fibers were too weak to be tested.

Figure 14 shows a comparison of average tensile strengths for batch UF-80 with data obtained on a more recently prepared batch (UF-127). Figure 14 also shows data for samples designated 'UF-highest strength.' These data represent the highest *average* strength values obtained from ~15 fiber lots that were processed between lots UF-80 and UF-127. Significant improvements in average strength values are noted in batches prepared more recently. The maximum average strengths were ~3.3 GPa and ~2.2 GPa for 1000 and 1500°C heat-treated fibers, respectively. (The maximum strengths for individuals fibers in these batches exceeded 5 and 3.5 GPa, respectively.)

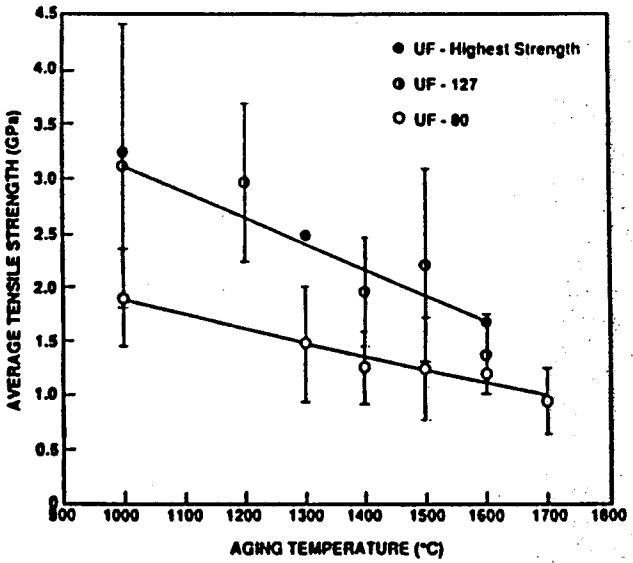

Fig. 14. Plots of average tensile strength versus heat treatment temperature for UF-80 and UF-127 fibers and for UF fiber batches with the highest average strengths. For clarity, the error bars (±1 SD (standard deviation)) are not included for the highest strength data points.

The precise reason(s) for the increased tensile strengths in more recent UF fiber batches are not known. However, there are two factors which may be responsible, at least in part, for the effect:

(1) The procedure for filtering the spinning solutions was improved. The polymer solution used to prepare UF-80 was passed only through a 2–4 μm glass filter, while the solutions used to prepare fiber batches with highest strength (including UF-127) were also filtered through 0.1 μm PTFE. Therefore, the size and concentration of strength-limiting defects in the latter fiber batches were probably reduced due to more effective removal of impurity particles, polymer 'microgel' particles, etc. from the spinning solutions.

(2) The partial pressure of oxygen used during pyrolysis of the high strength batches (including UF-127 fibers) was lower, so the fibers probably had less surface oxygen contamination. Based on the SEM (Figs 9 and 10) and specific surface area (Fig. 12) results described earlier, this should lead to improved strength retention after heat treatment (especially at temperatures ≥ 1400°C).

There are probably other factors which contribute to the observed variations in tensile strength values, including batch-to-batch variations in the characteristics of the polymer (e.g. molecular weight distribution) and the spinning solution (e.g. polymer concentration, rheological properties, etc.). As noted earlier, it was difficult to rigorously control these variables because of the small batch sizes (i.e. typically a few grams) prepared in this study.

Rupture strains and elastic modulus values were also determined from the stress–strain measurements on pyrolyzed and heat-treated fibers. Figure 15 shows average rupture strains as a function of heat treatment temperature for Nicalon and UF fibers (batches 80 and 127). Nicalon and UF fibers heated at 1000°C show similar rupture strains (~1.5%). This result suggests that UF fibers would have good weavability (i.e. comparable to Nicalon) since the fibers also have high tensile strength and fine diameter.

At higher heat treatment temperatures, Nicalon fibers showed a more rapid decrease in rupture strains compared to UF fibers (Fig. 15). This is not surprising considering the large decrease in tensile strength for Nicalon above 1300°C (Fig. 13). Figure 15 also shows that UF-80 and UF-127 fibers have similar rupture strains despite significant differences in tensile strength. This can be attributed to the higher elastic modulus of UF-127 fibers, as shown in Fig. 16.

Figure 16 shows plots of elastic modulus versus heat treatment temperature for Nicalon and UF fibers.

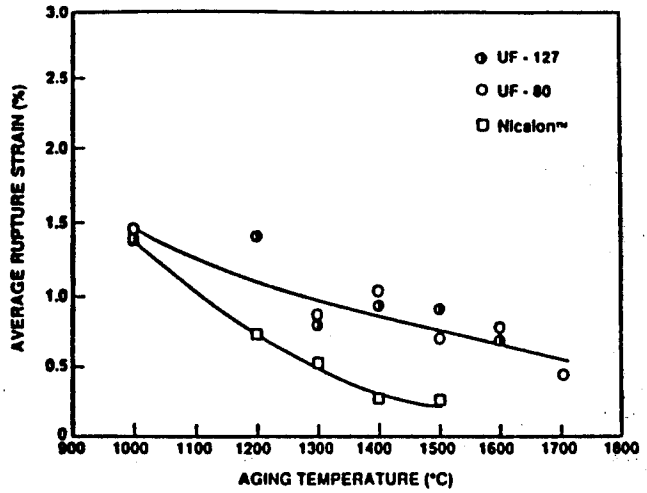

Fig. 15. Plots of average rupture strain versus heat treatment temperature for UF fibers and Nicalon fibers. Values for UF fibers are given for batch nos 80 and 127.

Data are included for the UF-80 and UF-127 fibers, as well as the UF fiber batches having the highest *average* elastic modulus values. Nicalon fibers show a large decrease in modulus after heat treatment above 1300°C. This presumably reflects the formation of porosity in the fibers as weight loss occurs at high temperatures. In contrast, UF fibers show either small increases (UF-80) or nearly constant (UF-127) modulus values with increasing heat treatment temperature, reflecting the improved thermal stability compared to Nicalon.

The reason(s) for the large differences in modulus between the various UF fiber batches are not known. XRD analysis did not reveal any significant differences in the degree of crystallization (i.e. amount of β-SiC). (XRD patterns were virtually identical for UF-80 and UF-127 samples heated to 1600°C.) Preliminary analysis by SAM depth profiling indicates that the carbon content may be somewhat lower for batch UF-127, but more data (quantitative elemental analysis) are needed to confirm this.

It should be noted that both Nicalon and UF fibers have relatively low elastic modulus values compared to stoichiometric polycrystalline SiC. As discussed earlier in regards to Fig. 4, PC-derived fibers develop an amorphous, carbon-rich structure after low temperature pyrolysis.[8,9,15] The fibers retain a substantial amount of amorphous carbon during heat treatment at higher temperatures in inert atmospheres. Phase development in UF fibers is similar to that observed in Nicalon. Figure 17 shows typical XRD diffraction patterns for UF fibers after pyrolysis at 750°C and after subsequent heat treatments in the range 1000–1600°C. The patterns are very similar to results reported for Nicalon-type fibers, except that peaks associated with silica are absent in UF fibers due to their low oxygen content.[8,9,15] The β-SiC peaks

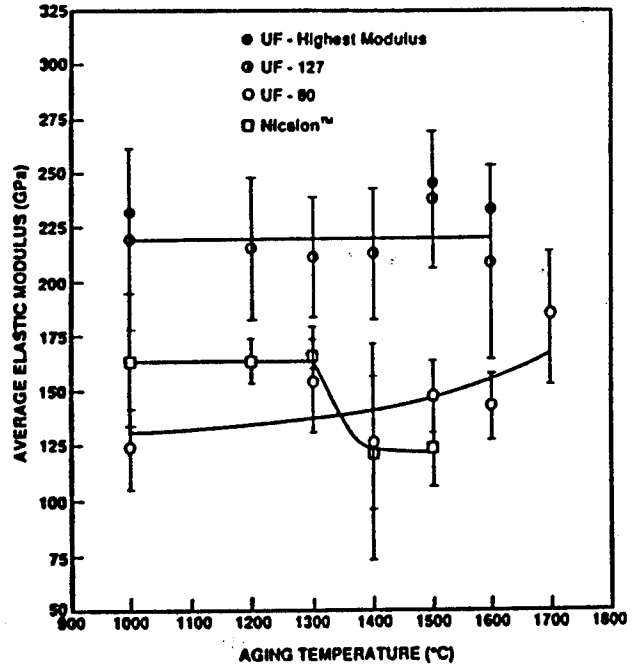

Fig. 16. Plots of average elastic modulus versus heat treatment temperature for UF fibers and Nicalon fibers. Values for UF fibers are given for batch nos 80 and 127 and for the batches with the highest average elastic moduli. For clarity, the error bars (±1 SD) are not included for the highest modulus data points.

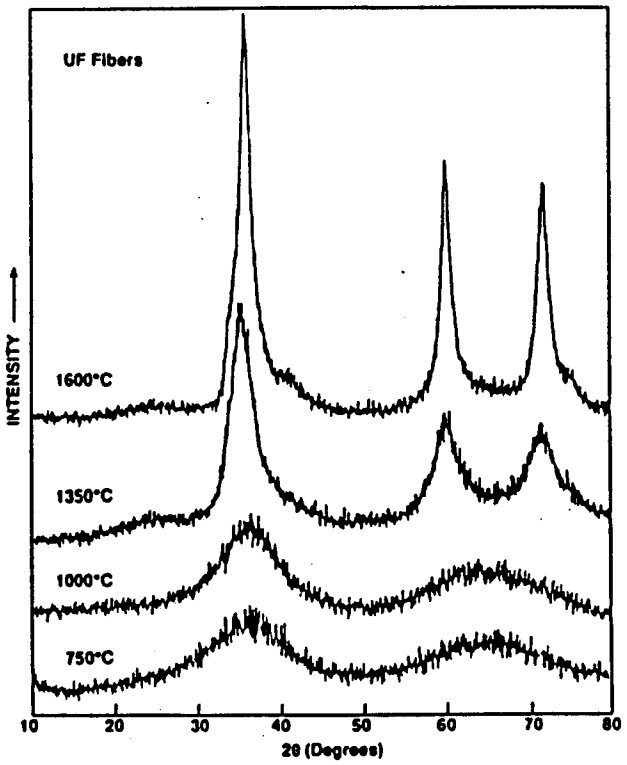

Fig. 17. X-ray diffraction patterns for UF fibers after heat treatment at the indicated temperatures.

progressively narrow and increase in intensity as the heat treatment temperature is increased. TEM results are consistent with the XRD data in that the size of the β-SiC grains was observed to increase with increasing temperature. However, it is unclear if the amount of crystalline SiC is also increasing (i.e. relative to amorphous, carbon-rich material). It was originally believed that the small increase in elastic modulus for UF-80 fibers indicated an increase in the amount of crystalline SiC (see note 10). However, UF-127 fibers show similar changes in the XRD patterns (i.e. increased β-SiC peak intensities), yet no increase in elastic modulus is observed with increasing heat treatment temperature (Fig. 16). (As noted earlier, UF-80 and UF-127 fibers heat treated at 1600°C in argon show essentially identical XRD patterns.)

Despite the high content of amorphous carbon-rich material, UF fibers have relatively good thermomechanical stability in an air atmosphere. For example, after 1.0 h heat treatments in air at 1400 and 1500°C, the average tensile strengths (at room temperature) for three different lots of UF fibers were in the range of ~1.3–1.7 GPa and ~1.2–1.4 GPa, respectively. In addition, a UF fiber batch (see note 11) tested at 1400°C in air had an average tensile strength of ~1.1 GPa (178 mm gage length). In contrast, Nicalon fibers tested under identical conditions had a strength of only ~0.7 GPa.

A TGA experiment showed that UF fibers (initially pyrolyzed at 1000°C) gained ~1.5 wt% when heated in air at 10°C/min to 1550°C and subsequently held for 1 h at temperature. NAA showed that the oxygen content in this particular sample increased from ~2.6 wt% (as-pyrolyzed) to ~5.5 wt% (after oxidation treatment). It is presumed that the oxygen weight gain is greater than the overall weight gain due to an oxidation reaction that forms silicon dioxide (non-volatile) and carbon monoxide (volatile), i.e. a reaction such as:

$$SiC_x(s) + \left(1 + \frac{x}{2}\right)O_2(g) \Rightarrow SiO_2(s) + xCO(g)\uparrow$$

Characterization of the fibers by electron microscopy and SAM depth profiling would be helpful in understanding the oxidation mechanism. A more detailed investigation of the thermochemical and thermomechanical stability of UF fibers in highly oxidizing environments is planned.

CONCLUSION

Continuous silicon carbide fibers (UF fibers) with low oxygen contents (~1–2 wt%), small diameters, and high tensile strengths were prepared by dry spinning of novel organosilicon polymer solutions and subsequent pyrolysis of the as-spun fibers. By controlling several key polymer and solution characteristics, a process with the following advantages was developed: (1) fiberizing solutions had excellent spinnability; (2) green and partially pyrolyzed fibers had good mechanical properties; (3) green fibers could be directly pyrolyzed to a ceramic without melting, i.e. the process was carried out without an oxidative or irradiative cross-linking step; (4) a high ceramic yield was obtained after pyrolysis; and (5) fibers with smooth surfaces and round cross-sections could be produced with a range of diameters (~8–50 μm).

UF fibers showed excellent thermomechanical stability in comparison to commercially available Nicalon fibers, as indicated by lower weight losses, lower specific surface areas, and improved strength retention after heat treatment at elevated temperatures. This was attributed to the relatively low oxygen content for UF fibers (i.e. compared to Nicalon). Scanning Auger microprobe analysis showed that the residual oxygen in UF fibers was concentrated near the fiber surfaces, apparently due to contamination from atmospheric oxygen and water vapor during the spinning and pyrolysis operations. In samples with high levels of surface oxygen contamination, reaction between siliceous (Si–O-containing) and carbon-rich materials resulted in some surface degradation of the fibers after high-temperature ($\geq$1500°C) heat treatment. Fibers with improved thermomechanical stability were produced by reducing the partial pressure of oxygen during pyrolysis. SEM observations and specific surface area measurements showed that surface degradation reactions were greatly inhibited in fibers with lower oxygen contamination.

As observed in other PC-derived ceramics, heat-treated UF fibers have a carbon-rich, weakly crystalline structure. This resulted in relatively low elastic modulus, even after heat treatment at temperatures up to 1700°C. Ongoing investigations are being directed toward the development of fully crystalline, stoichiometric silicon carbide fibers with higher elastic modulus, while still retaining high tensile strength and excellent thermomechanical stability.

ACKNOWLEDGEMENTS

The authors gratefully acknowledge B.J. Madana and E.J. Serrano of the University of Florida (UF) for assistance in room temperature mechanical property measurements, E. Lambers of UF for assistance in the SAM measurements, and M. Jenkins of Oak Ridge National Laboratory for assistance in high temperature strength measurements. This work was supported by the Defense Advanced Research Projects Agency under Contract Nos MDA 972-88-J-1006 and N00014-91-J-4075.

NOTES

1. Molecular weight distributions were determined by size exclusion chromatography with UV detection at 254 nm. Measurements were carried out using 500 and 5000 Å Phenogel™ columns (Phenomenex, Torrance, CA), polystyrene standards, and THF as the solvent.

2. These results were obtained on fibers with sufficient handling strength to be tested. However, many fibers failed during preparation for testing, so the reported values may not be representative of the true average mechanical properties.

3. Lot No. AP-018001, Ceramic Grade, Nippon Carbon Co., Tokyo, Japan.

4. According to the manufacturer (see Table 1), Ceramic Grade (CG) Nicalon fibers have ~10 wt% oxygen. In this study, however, the NAA analysis on two lots (AP-018001 and 093) gave oxygen contents of 15 and 13.5 wt%, respectively.

5. The carbon content (~42 wt%) listed in Table 1 for UF fibers was determined by difference, i.e. 100% minus the combined concentrations for Si, O, N, and H. Combustion analysis (LECO method) on UF fibers consistently gave lower carbon contents (~37 wt%) than the value listed in Table 1. However, these results were considered unreliable since oxidative combustion of the UF fibers was probably incomplete under the experimental conditions used in the measurements. In contrast, analysis of the carbon content by the combustion method is considered reliable for Nicalon because the fibers degrade more rapidly at elevated temperatures. The development of porosity and high specific surface area in heat-treated Nicalon fibers (see Figs 11 and 12) is expected to accelerate the oxidative combustion reaction rate. In fact, the carbon content determined by the LECO method is in good agreement with the value reported by the manufacturer. Furthermore, the concentrations of Si, C, O, N, and H total to ~100% for the Nicalon fibers.

6. Based on the atomic sensitivities, magnitude of the C and Si signals, and signal-to-noise ratio, it is estimated that the limit of detection for oxygen for the survey scan shown in Fig. 7(B) is ~1 at%. The apparently high oxygen levels (~3 at%) in the fiber interior in Fig. 8 are attributed to higher background noise (i.e. lower oxygen signal-to-noise ratios), as data were collected for shorter scanning times compared to the survey scan. Thus, the oxygen levels in Fig. 8 should not be taken as precise quantitative measurements.

7. The initial surface area (1000°C-pyrolyzed sample) for the fiber with lower surface oxygen contamination is probably larger than the corresponding sample with higher surface oxygen contamination (~0.5 versus ~0.2 m^2/g) because the fiber diameter is smaller (i.e. ~11 versus ~23 μm).

8. Heat treatment times were 1.0 h except that the 1300°C Nicalon sample was heated for 2.0 h and the 1500°C UF-80 and Nicalon samples were heated for 0.5 h.

9. The results in Fig. 13 for Nicalon fibers heated to high temperatures (e.g. ≥ 1400°C) are probably not representative of the true average strengths because the values reported were determined on fibers that had sufficient handling strength to be tested. However, many fibers failed during preparation for testing. Thus, true average strengths for the Nicalon fibers are probably less than indicated in Fig. 13.

10. The largest elastic modulus for UF-80 fibers is observed in the 1700°C-heat-treated sample. This may be due to the increased importance of the reaction between carbon and siliceous (Si–O-containing) material at higher temperatures. In this case, the volume fraction of SiC would increase as oxygen and excess carbon are eliminated (i.e. as volatile species such as CO and SiO).

11. This batch was initially pyrolyzed at 1250°C in nitrogen, i.e. prior to testing at high temperature.

REFERENCES

1. Yajima, S., Hayashi, J., Omori, M. & Okamura, K. Development of a silicon carbide fiber with high tensile strength. *Nature*, 261 (1976) 683–5.
2. Yajima, S., Okamura, K., Hayashi, J. & Omori, M., Synthesis of continuous SiC fibers with high tensile strength. *J. Am. Ceram. Soc.*, 59 (1976) 324–7.
3. Prewo, K., & Brennan, J., High-strength silicon carbide-fiber-reinforced glass matrix composites. *J. Mater. Sci.*, 15 (1980) 463–8.
4. Brennan, J. and Prewo, K., Silicon carbide fiber reinforced glass-ceramic matrix composites exhibiting high strength and toughness. *J. Mater. Sci.*, 17 (1982) 2371–83.
5. Prewo, K.M., Brennan, J.J. & Layden, G.K., Fiber reinforced glasses and glass-ceramics for high performance applications. *Am. Ceram. Soc. Bull.*, 65 (1986) 305–13, 322.
6. Lamicq, P.J., Bernhart, G.A., Dauchier, M.M. & Mace, J.G., SiC/SiC composite ceramics. *Am. Ceram. Soc. Bull.*, 65 (1986) 336–8.
7. Mazdiyasni, K.S. (ed.), *Fiber Reinforced Ceramic Composites: Materials, Processing, and Technology*. Noyes Publications, Park Ridge, NJ, 1990.
8. Mah, T. *et al.*, Thermal stability of SiC fibres (Nicalon). *J. Mater. Sci.*, 19 (1984) 1191–201.
9. Simon, G. & Bunsell, A.R., Mechanical and structural characterization of the Nicalon silicon carbide fibre. *J. Mater. Sci.*, 19 (1984) 3649–57.
10. Clark, T.J., Arons, R.M., Stamatoff, J.B. & Rabe, J., Thermal degradation of Nicalon SiC fiber. *Ceram. Eng. Sci. Proc.*, 6 (1985) 576–8.
11. Jaskowiak, M.H. & DiCarlo, J.A., Pressure effects on the thermal stability of silicon carbide fibers. *J. Am. Ceram. Soc.*, 72 (1989) 192–7.
12. Pysher, D.J., Goretta, K.C., Hodder Jr, R.S. & Tressler, R.E., Strengths of ceramic fibers at elevated temperatures. *J. Am. Ceram. Soc.*, 72 (1989) 284–8.

13. Bender, B.A., Wallace, J.S. & Schrodt, D.J., Effect of thermochemical treatments on the strength and microstructure of SiC fibers. *J. Mater. Sci.*, 26 (1991) 970–6.
14. Johnson, S.M., Brittain, R.D., Lamoreaux, R.H. & Rowcliffe, D.J., Degradation mechanisms of silicon carbide fibers. *Comm. Am. Ceram. Soc.*, 71 (1988) C-132–C-135.
15. Hasegawa, Y., Synthesis of continuous silicon carbide fibre. Part 6. Pyrolysis process of cured polycarbosilane fibre and structure of SiC fibre. *J. Mater. Sci.*, 24 (1989) 1177–90.
16. Frechette, F., Dover, B., Venkateswaran, V. & Kim, J., High temperature continuous sintered SiC fiber for composite applications. *Ceram. Eng. Sci. Proc.*, 12 (1991) 992–1006.
17. Silverman, L.A., Hewett Jr, W.D., Blatchford, T.P. & Beeler, A.J., Silicon carbide fibers from slurry spinning. *J. Appl. Polymer Sci.: Appl. Polymer Symp.*, 47 (1991) 99–109.
18. Lipowitz, J., Rabe, J.A. & Zank, G.A., Polycrystalline SiC fibers from organosilicon polymers. *Ceram. Eng. Sci. Proc.*, 12 (1991) 1819–31.
19. Lipowitz, J., Rabe, J.A. & Zank, G.A., Crystalline SiC fibers from organosilicon polymers. In *Proc. HITEMP REVIEW* 1991. NASA Lewis Research Center, Cleveland, OH, 1991, pp. 48-1–48-11.
20. Takeda, M., Imai, Y., Ichikawa, H. & Ishikawa, T., Properties of the low oxygen content SiC fiber on high temperature heat treatment. *Ceram. Eng. Sci. Proc.*, 12 (1991) 1007–18.
21. Takeda, M. *et al.*, Thermal stability of the low oxygen content silicon carbide fibers derived from polycarbosilane. *Ceram. Eng. Sci. Proc.*, 13 (1992) 209–17.
22. Toreki, Wm., Choi, G.J., Batich, C.D., Sacks, M.D. & Saleem, M., Polymer-derived silicon carbide fibers with low oxygen content. *Ceram. Eng. Sci. Proc.*, 13 (1992) 198–208.
23. Toreki, Wm., Batich, C.D., Sacks, M.D. & Morrone, A.A., Synthesis and applications of a vinylsilazane preceramic polymer. *Ceram. Eng. Sci. Proc.*, 11 (1990) 1371–86.
24. *Test Method for Tensile Strength and Young's Modulus for High Modulus Single Filament Materials*. ASTM D3379. American Society for Testing and Materials, Philadelphia, PA.
25. New product information—Polycarbosilane. Product bulletin, Dow Corning Corp., Midland, MI, 1989.
26. Hasegawa, Y., Iimura, M. & Yajima, S., Synthesis of continuous silicon carbide fibre. Part 2. Conversion of polycarbosilane fibre into silicon carbide fibres. *J. Mater. Sci.*, 15 (1990) 720–8.
27. Wynne, K.J. & Rice, R.W., Ceramics via polymer pyrolysis. *Ann. Rev. Mater. Sci.*, 14 (1987) 297–324.

BOOK I

Section 2

Processing

of

Mullite Composite Fibers

Principal Investigators: J.J. Simmons
M.D. Sacks
A.B. Brennan

PROCESSING OF MULLITE COMPOSITE FIBERS

Investigators:
Faculty: J. H. Simmons, M. D. Sacks and A. B. Brennan
Students: S. Al-Assafi, T. Cruse

July 15, 1994.

Objectives

(1) To develop a sol-gel process for the continuous extrusion of high performance mullite fibers with improved thermomechanical properties compared to commercially available mullite fibers.

(2) To optimize the mullite formation process for improved retention of high temperature strength through the control of composition and microstructure.

Research Summary

University of Florida (UF) researchers have developed a mullite fiber formation process which essentially meets the objectives of the research effort. The process is novel and has produced continuous mullite fibers with excellent phase composition and reasonable room temperature strength. These results have been reported in two oral presentations at the Engineered Materials Composite Symposium in Cocoa Beach, FL, January 1994 and at the Annual Meeting of the American Ceramic Society, Symposium on Ceramic-Matrix Composites in Indianapolis, IN, May 1994. Both presentations will be published in Transactions of the American Ceramic Society. A journal article is in preparation for submission to the Journal of the American ceramic Society. Below is a list of achievements.

- A sol-gel based process was developed for the formation of mullite fibers.
- The process allows continuous spinning of fibers.
- The process includes novel precursor solvents.
- The process involves a novel and critical ageing (hydration) step, which controls the mullite grain size and the temperature of mullite transformation.
- The ageing step can be conducted on-line, during fiber spinning.
- All steps of the process have been streamlined to be conducted on-line during fiber spinning.
- The fibers exhibit
  - single-phase mullite composition
  - submicron grain sizes
  - no intergranular glass phase
  - density values of mullite
  - 1.45 GPa bend strength at room temperature
- When exposed to an HF acid wash, designed to dissolve the intergranular glass phase, the UF mullite fibers exhibit no apparent change in microstructure, while the commercially available Nextel fibers all exhibit significant structural degradation.

These results are discussed in the attached papers submitted as appendices.

The first paper describes the results of last years' work with triethanolamine (TEA) chelating agent and discusses:

(a) the viscosity considerations developed to obtain spinnability of a sol-gel precursor solution, including the role of non-Newtonian viscosity behavior.
(b) the development of a novel ageing process in which fiber hydration is encouraged to remove alkoxide from the fiber structure. This step is critical to alkoxide removal and resolves the problem of excessive burn out during sintering.
(c) densification studies which demonstrate full densification below 1400°C.
(d) complete and single-phase mullite formation, confirmed by XRD patterns.
(e) comparisons of resistance to HF acid exposure between UF fibers and commercial Nextel fibers. The UF fibers show no sign of degradation while the Nextel fibers exhibit extreme structural degradation.

The second paper describes the results of recent developments in process optimization which have discovered process improvements with the use of acetylacetonate chelating agent instead of triethanolamine, and discusses:

(a) the novel experimental procedure.
(b) the dependence of sol spinnability on chelating agent concentration and the resulting production of high quality continuous green fibers using acetylacetonate (AcAc).
(c) the reduction of the ageing step to a short time exposure at 100°C, making this step integrable into a continuous spinning process.
(d) improved solvent removal and mullite crystallization by the new process.
(e) micrographs showing the formation of submicron grains by the new process.
(f) the production of fibers with >98% theoretical density by the new process.

Results not yet reported include:

(a) a high resolution TEM study to examine the intergranular glass phase in fabricated fibers which demonstrates clearly the absence of any glass phase in the grain boundary region and at 3-grain intersections. (See Figure 1.) This has never been achieved commercially before.
(b) a micrograph (Figure 2) showing that the AcAc produced fibers resist HF acid treatment as well as TEA fibers, and far better than all mullite Nextel fibers.
(c) the effect of ageing treatment on mullite grain size after densification which shows a strong dependence on ageing treatment time and temperature. See for example the difference in grain size between samples treated at 80°C (Figure 3) and samples treated at 100°C (Figure 4). The 80°C samples exhibit grains of the order of 1 μm in size, while the average grain size of 100°C samples is about 200 nm.
(d) the results of strength measurements which showed bend strengths of 1.45 MPa at room temperature on sintered fibers. Measurements of tensile strength on 1" gage length fibers were inconclusive due to premature fiber failure at the epoxy joints involved in attaching the fibers to the tensile test apparatus. Work is still on-going to determine a more suitable test configuration.

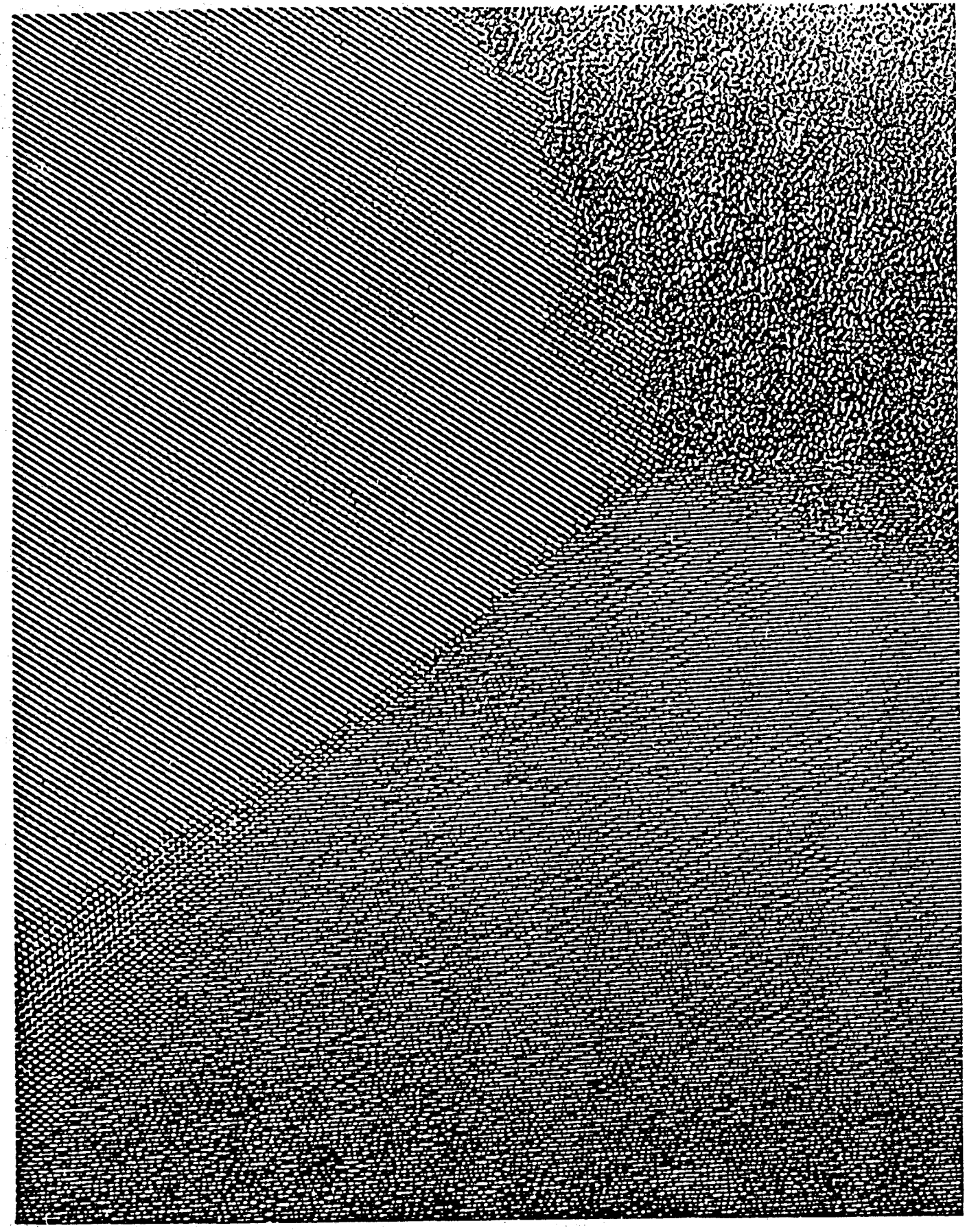

Figure 1 - High Resolution TEM of Mullite fiber showing glass-free intergranular boundaries

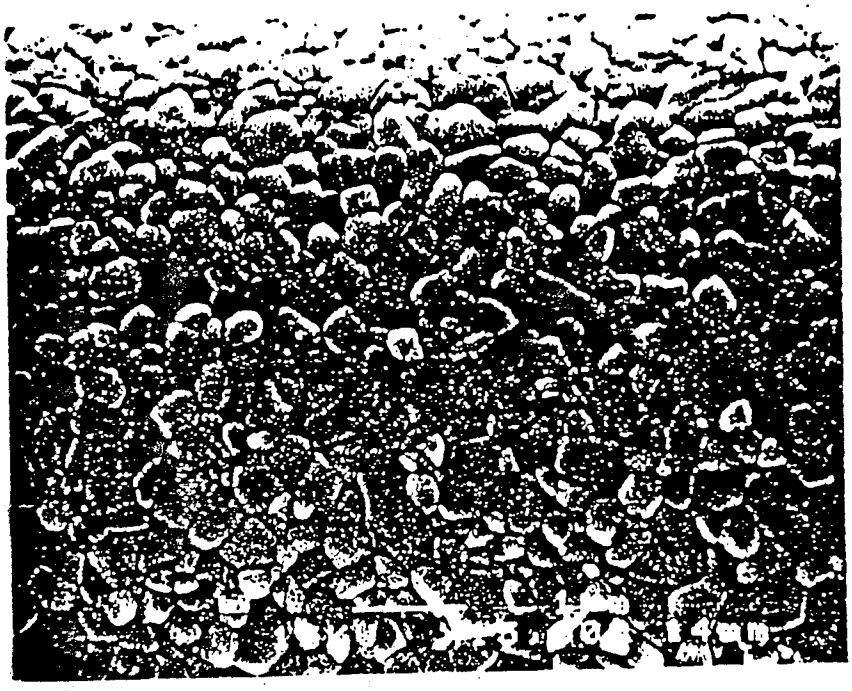

Figure 2 - Mullite fiber produced with the AcAc chelating agent, after exposure to HF acid treatment.

Figure 3 - Mullite fiber produced by 80°C ageing treatment.

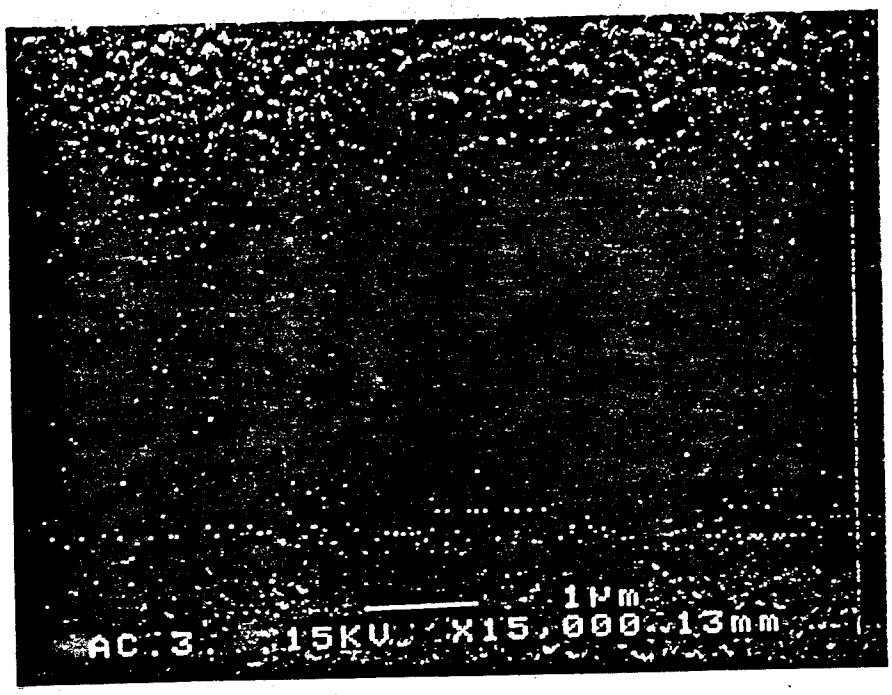

Figure 4 - Mullite fiber produced by 100°C ageing treatment.

PROCESSING OF FINE-DIAMETER CONTINUOUS MULLITE FIBERS

S. Al-Assafi, T. Cruse, J.H. Simmons, A.B. Brennan, and M.D. Sacks, Department of Materials Science and Engineering, University of Florida, Gainesville, FL 32611.

ABSTRACT

Fine-diameter, continuous mullite fibers were fabricated by sol-gel processing using two different chelating agents. The effect of chelating agent on weight loss behavior, mullite formation, and sintered fiber microstructure was examined. The molar ratio, R, of chelating agent to alumina precursor on sol was varied in order to optimize continuous spinning conditions. The importance of aging conditions on the sintered fiber density was demonstrated.

INTRODUCTION

Mullite has excellent creep resistance and strength retention at high temperatures, as well as good chemical stability [1]. Thus, fine-diameter, continuous mullite fibers are of interest for the development of ceramic fiber-reinforced composites with improved high temperature properties in oxidizing atmospheres.

Mullite fibers are usually fabricated by sol-gel methods [2-6]. These processing routes allow for good control over sol rheological properties. Hence, sols with good spinnability and fibers with fine diameter are readily produced. Furthermore, the molecular or near-molecular scale of mixing of alumina and silica precursors results in mullite formation and fiber densification at relatively low temperatures [2,6]. The mullite transformation temperature is dependent on the type of sol-gel precursor. Single-phase precursors, which exhibit a nucleation-controlled transformation mechanism, form mullite at temperatures below 1000°C [7]. In contrast, diphasic precursors transform to mullite at higher temperatures (typically at or above 1200°C) by a diffusion-controlled transformation mechanism [8].

Glass-free mullite fibers have been prepared from diphasic sols by Venkatachari

et al. [2]. Aluminum formoacetate and aluminum hydroxychloride hydrate were used as alumina precursors and LUDOX® colloidal silica sols were used as silica precursors. Fibers were produced with fine-diameter, low porosity, and fine-grain size after heat treatment at temperatures up to 1500°C. However, fibers were limited to short lengths, as continuous spinning was not carried out. Tucker et al. used single-phase sols to fabricate continuous mullite fibers [3]. The silica and alumina precursors were tetraethyl orthosilicate and aluminum diisopropoxide acetoacetic ester chelate, respectively. The sintered fibers were extremely brittle and microstructure observations showed extensive porosity and microcracks. This was attributed to difficulties in removing volatiles during heat treatment of the large-diameter fibers ($\sim 110\ \mu m$ after sintering).

In this study, sols prepared with two different chelating agents were used to produce continuous single-phase mullite fibers with diameters of $\sim$ 10-25 μm. The effects of chelating agent and aging conditions on the processing and properties of fibers were investigated.

EXPERIMENTAL PROCEDURE

Silica sols were prepared by mixing tetraethyl orthosilicate (TEOS) with ethanol and subsequently carrying out partial hydrolysis with water additions (i.e., 1:2 molar ratio of TEOS:water). In method I, the silica sol was added slowly to an unhydrolyzed solution of aluminum-sec-butoxide (ASB) and triethanolamine, TEA, (i.e., the chelating agent). The TEA/ASB molar ratio was 0.3. The TEOS/ASB ratio was selected to yield a composition of $\sim$ 72 wt% alumina/28 wt% silica after heat treatment. In method II, the same procedure was followed except that the TEA was replaced by acetylacetone (AcAc), another chelating agent. The purpose of using chelated aluminum alkoxides is to reduce the hydrolysis/condensation rate and thereby prevent local precipitation of aluminum hydroxide in the mixed sol [9].

After mixing of components, the sol was concentrated until the rheological conditions for continuous spinning were achieved. The sol was then extruded through a spinneret with 40 μm hole diameter and continuous fibers were collected by winding on a rotating drum. The fibers formed with TEA were aged at room temperature for 24 hours inside a chamber at relative humidity of 100%. In contrast, more rapid aging was carried out for fibers prepared with AcAc. The as-spun fibers were heated in the humidity chamber at $\sim$ 0.7°C/min to temperatures up to 100°C and then cooled immediately to room temperature. In each method, aged fibers were subsequently sintered at 1500°C for 10 min.

Rheological measurements, thermal gravimetric analysis/differential thermal analysis (TGA/DTA), sink-float apparent density measurements [10], and scanning electron microscopy (SEM) were used to study the effects of the chelating agent and the aging conditions on fiber processing and structure.

RESULTS AND DISCUSSION

The effect of molar ratio, R, of AcAc/ASB on the sol rheological behavior was investigated (Fig. 1). Low values of R (<0.3) resulted in thixotropic sols which gelled readily when exposed to air. In contrast, high values of R (>0.5) resulted in approximately Newtonian flow behavior. In addition, precipitate formation was observed in these sols. The optimum R value for good spinning behavior and good stability of the sol was ≈ 0.3. As shown in Fig. 1, sols with this R value have slightly shear thinning flow behavior. As reported previously [6], the optimum spinning behavior for method I (TEA) fibers is also obtained when sols are slightly shear thinning.

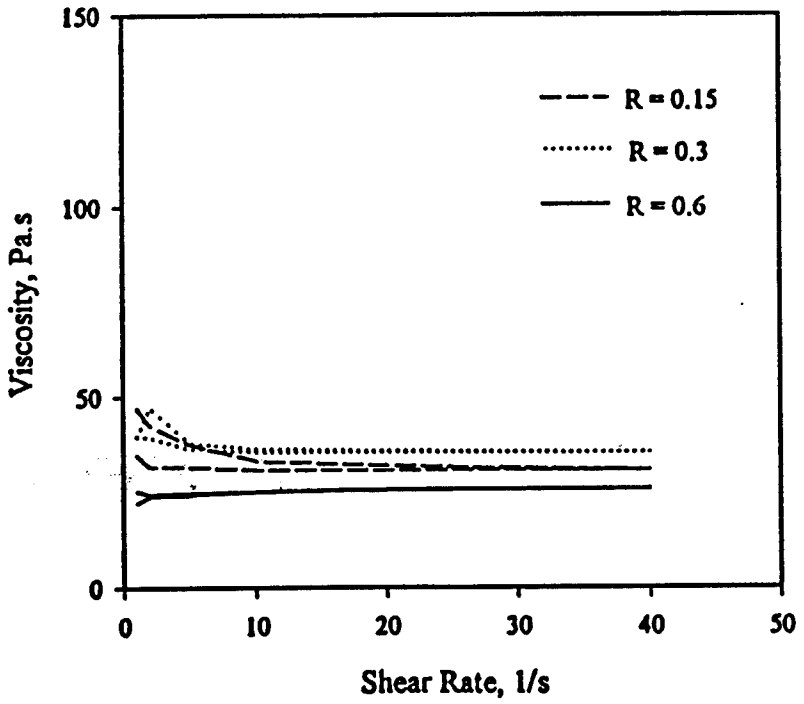

Figure 1. Plots of viscosity vs. shear rate for sols with different molar ratios, R, of AcAc/ASB.

Although good spinnability could be obtained for both method I and II sols, subsequent processing of green fibers was carried out much more easily using method II (AcAc). First, it was very difficult to avoid inter-filament sticking of green and sintered fibers prepared by method I. This was not a problem for method II fibers. Second, qualitative observations based on routine handling of the as-spun and aged fibers, indicated that the method II fibers had much better strength and flexibility. Third, it was easier to obtain fibers with circular cross-sections using method II.

The effect of the type of the chelating agent on the removal of volatile components was determined by TGA. Figure 2 shows plots of weight loss vs. temperature (heating rate 10°C/min) for fibers made with AcAc and TEA. Both samples were aged for 24 hours at room temperature in a humidity chamber prior to analysis. The data show that volatiles are removed at a lower temperature for fibers prepared with AcAc. This may be helpful in avoiding gas entrapment in the fibers when the pores close during sintering.

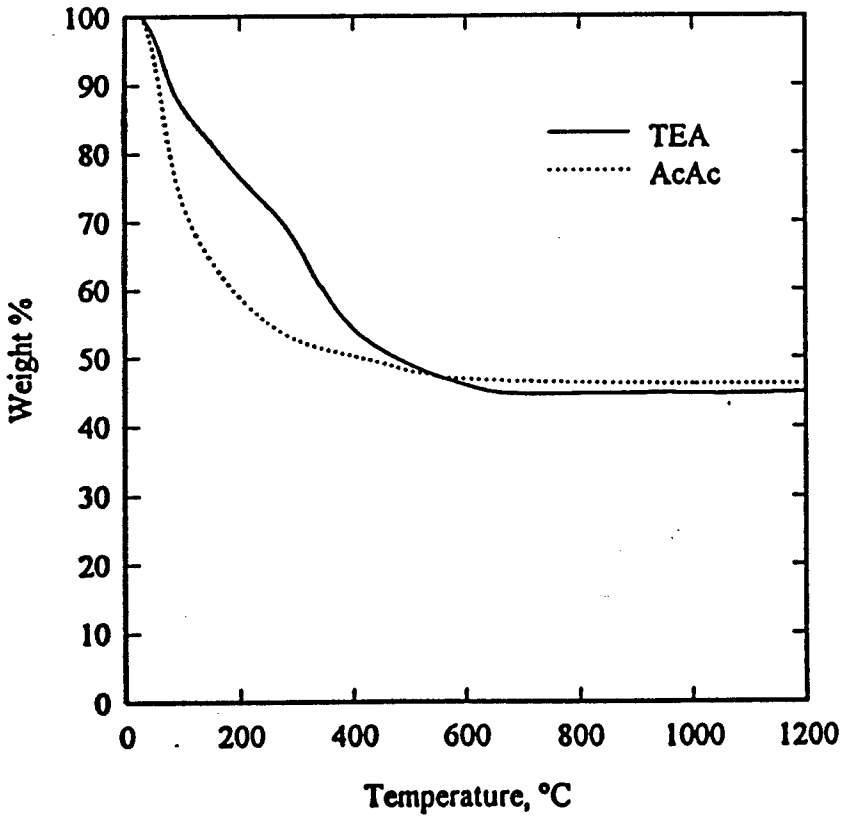

Figure 2. TGA plots for fibers prepared with TEA and AcAc.

Figure 3 shows the results of differential thermal analysis for fibers prepared with AcAc and TEA. Both fibers show an exotherm at ~980°C, although the peak is much stronger for the sample prepared with AcAc. These results indicate a significant enhancement in mullite formation in the method II (AcAc) fibers and suggests that more uniform (i.e., molecular-scale) mixing is achieved during sol-gel processing.

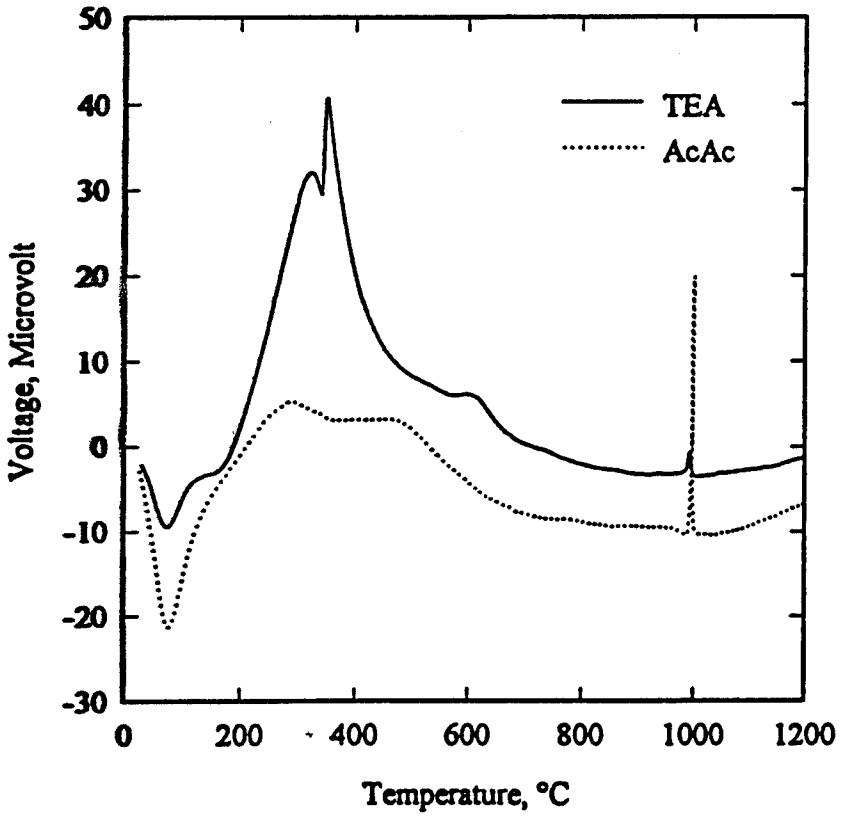

Figure 3. DTA for fibers aged for 24 hr at room temperature.

Sintered fibers with high relative density (low porosity) were prepared by method II (AcAc) by utilizing a high temperature aging step. The final apparent density (determined by the sink-float method) depended upon the aging temperature. Fibers aged at 80°C and 100°C had apparent densities of ~2.9 and ~3.1 g/cm^3, respectively, after sintering at 1500°C for 10 min. In contrast, method I (TEA) fibers had considerably lower density (~2.7 g/cm^3) if aging was carried out rapidly (at 100°C).

The type of chelating agent used had a significant effect on the fiber microstructure after sintering at 1500°C. Fibers prepared with TEA (method I) had grain sizes > 1 μm, as shown in Figure 4. In contrast, fibers prepared with AcAc (method II) had substantially smaller grain sizes, as shown in Figure 5.

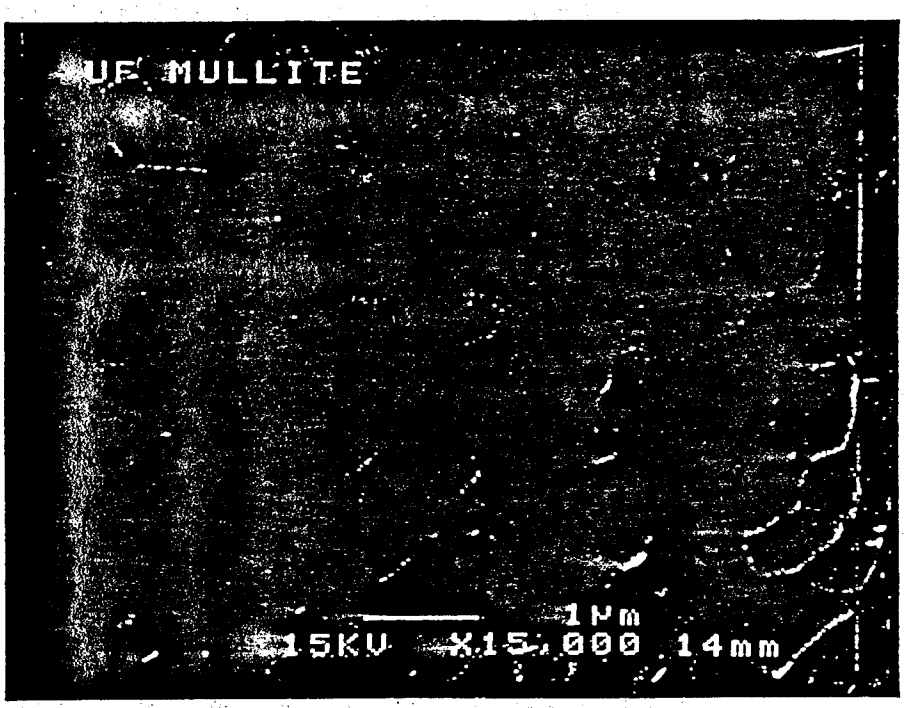

Figure 4. SEM micrograph for a fiber from method I fired at 1500°C for 10 min.

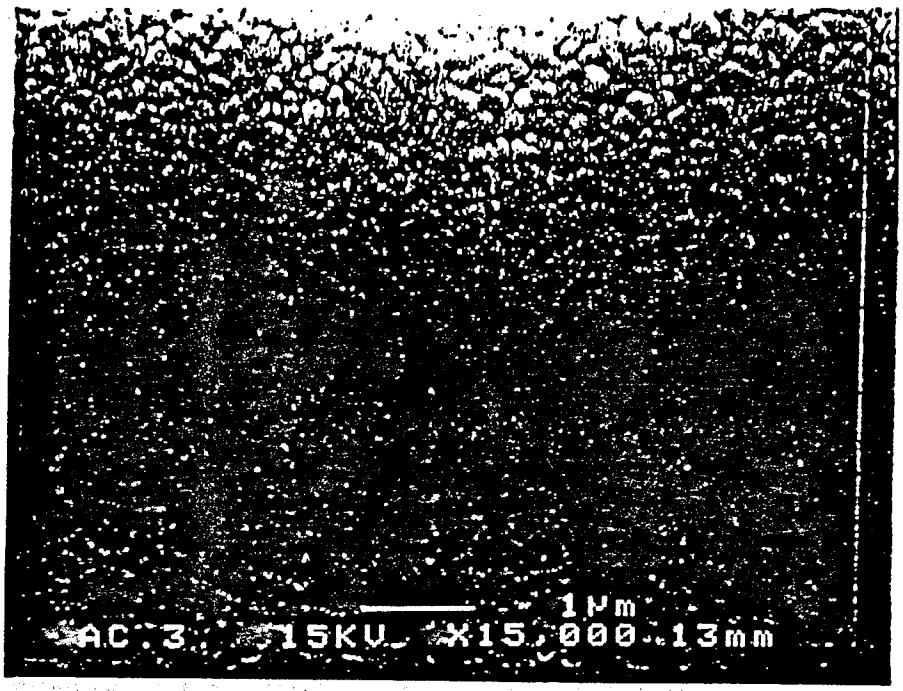

Figure 5. SEM micrograph for a fiber from method II fired at 1500°C for 10 min.

SUMMARY

Continuous mullite fibers were prepared using acetylacetone (AcAc) and triethylamine (TEA) as sol-gel processing additives. The use of AcAc in optimum concentration provided the following advantages: (i) enhanced sol stability, (ii) excellent spinnability, (iii) improved green fiber handling capability, (iv) reduced temperature for removal of volatile components, (v) enhanced mullite formation at low temperature (~980°C), and (vi) the development of sintered fibers with high relative density (≥98% of the theoretical value for mullite) and the retention of submicrometer grain size after heat treatment at 1500°C.

ACKNOWLEDGMENTS

This work was supported by DARPA under Grant No. N00014-91-J-4075. The authors gratefully acknowledge the assistance of R. Crockett and G. W. Scheiffele.

REFERENCES

[1] I. A. Aksay, D. M. Dabbs, and M. Sarikaya, "Mullite for Structural, Electronic, and Optical Applications," J. Am. Ceram. Soc., 74 [10] 2343-2358 (1991).

[2] K. R. Venkatachari, L. T. Moeti, M. D. Sacks, and J. H. Simmons, "Preparation of Mullite-Based Fibers by Sol-Gel Processing," Ceram. Eng. Sci. Proc., 11 [9-10] 1512 (1990).

[3] D. S. Tucker, J. S. Sparks, and D. C. Esker,"Production of Continuous Mullite Fiber via Sol-Gel Processing," Am. Ceram. Soc. Bull., 69 [12] 1971-1974 (1990).

[4] G. Kim, D. Lee, H. Lee, and S. Yoon,"A Study on the Development of Mullite Fibers Using the Sol-Gel Process," Materials Science and Engineering A:Structural Materials: Properties, Microstructure and Processing, 167 [1-2] 171-178 (1993).

[5] E. A. Richards, C. J. Goodbrake, and H. G. Sowman,"Reactions and Development in Mullite Fibers," J. Am. Ceram. Soc., 74 [10] 2404-2409 (1991).

[6] S. Al-Assafi, T. Cruse, J. H. Simmons, A. B. Brennan, and M. D. Sacks,"Processing of Sol-Gel Derived Continuous Mullite Fibers via Sol-Gel," Proceedings of the 18thAnnual Conference on Composites and Advanced Ceramics, Cocoa Beach 1994.

[7] D. X. Li, and W. J. Thompson, "Mullite Formation Kinetics of a Single-Phase Gel," J. Am. Ceram. Soc., 73 [4] 964 (1990).

[8] D. X. Li, and W. J. Thompson, "Kinetic Mechanisms for Mullite Formation from Sol-Gel Precursors," J. Mat. Res., 5 [9] 1963 (1990).

[9] T. Heinrich, F. Raether, H. Marsmann,"Growth and Structure of Single Phase Mullite Gels from Chelated Aluminum Alkoxides and Alkoxysilanes," J. N. Cryst. Sol., 168 14-22 (1994).

[10] ASTM Test Method D 3800, Procedure B,"Sink-Float Technique," American Society for Testing and Materials, Philadelphia, PA.

SOL-GEL PROCESSING OF CONTINUOUS MULLITE FIBERS

S. Al-Assafi, T. Cruse, J. H. Simmons, A. B. Brennan, and M. D. Sacks, Department of Materials Science and Engineering, University of Florida, Gainesville, FL 32611.

ABSTRACT

A sol-gel process was developed to produce continuous mullite fibers. Spinnability of the sol was achieved by controlling hydrolysis and polycondensation conditions. The rheological properties needed for continuous fiber spinning were determined. The effect of aging of spun fibers on mullite formation was determined. Under optimum processing conditions, mullite formation was observed at ~1000°C and theoretical density was approached at ~1300°C. Fibers heat treated at 1500°C showed approximately 1 μm grain sizes. Exposure to a concentrated HF solution had no discernable effect on the fibers which suggested that little or no siliceous glass was present.

INTRODUCTION

Continuous mullite fibers are of interest for the development of ceramic fiber-reinforced composites for high temperature applications. Bulk mullite ($3Al_2O_3 \cdot 2SiO_2$) is known to have excellent creep resistance and strength retention at elevated temperatures, as well as good thermal shock resistance and chemical stability.[1] However, commercially-available aluminum silicate and mullite-based fibers do not show comparable high temperature mechanical properties.[2] One possible reason for this behavior is that commercial fibers contain secondary phases which are less refractory than mullite. Therefore, it is of interest to fabricate high-purity, single-phase, continuous mullite fibers.

Mullite fibers are usually prepared by sol-gel processing.[3-6] Commercially-available mullite fibers (i.e., Nextel 480) are processed with boria additions.[4] In contrast, Venkatachari et al. [5] reported fabrication of mullite fibers without using inorganic additives. Aluminum formoacetate and aluminum hydroxychloride hydrate were used as alumina precursors and LUDOX® colloidal silica sols were used as silica precursors. Fine diameter (~5-20 μm), single-phase mullite fibers were produced with high relative density (low porosity) and fine-grain size after heat treatment at temperatures in the range ~1200-1500°C. However, continuous spinning was not carried out and spun fibers were limited to short lengths. Tucker et al. [6] reported fabrication of continuous mullite fibers using sols prepared with tetraethyl orthosilicate as the silica precursor and aluminum diisopropoxide acetoacetic ester chelate as the alumina precursor. Fibers sintered at 1300°C were reported to be pure mullite. However, fibers were extremely brittle and microstructure observations showed that extensive porosity and microcracks were present. This was attributed to difficulties in removal volatiles during heat treatment of the large-diameter fibers

(i.e., ~150 μm after spinning and ~110 μm after sintering).

In the present study, a method was developed to fabricate fine-diameter (<25 μm), single-phase mullite fibers. The rheological conditions for continuous spinning were determined. The effects of aging and heat treatment on phase development and fiber density were investigated.

EXPERIMENTAL PROCEDURE

Tetraethyl orthosilicate (TEOS) was used as a silica precursor. TEOS was mixed with ethanol and partially hydrolyzed with water. The silica sol was added slowly to an unhydrolyzed solution of aluminum-sec-butoxide, sec-butanol, and triethylamine. The solution concentrations were selected to yield an ~72 wt% alumina/28 wt% silica composition after heat treatment. The mixture was stirred vigorously to ensure homogeneity. The sol was then concentrated until the rheological conditions for continuous spinning were achieved. Fibers were formed by extruding the concentrated sol through a 40 μm one-hole spinneret using nitrogen gas pressure. Continuous fibers were collected by winding on a rotating drum. The fibers were then aged to complete hydrolysis and polycondensation reactions. Following aging, the fibers were heat treated in air at temperatures up to 1500°C. Thermal gravimetric analysis/differential thermal analysis (TGA/DTA), sink-float apparent density measurements [7], X-ray diffraction (XRD) analysis, and scanning electron microscopy (SEM) were used to analyze the effect of heat treatment on the fiber structure and properties.

RESULTS AND DISCUSSION

The conditions for continuous spinning were determined through rheological measurements. Figure 1 shows plots of shear stress vs. shear rate and viscosity vs. shear rate for both spinnable and unspinnable sols. Sols with slightly shear thinning behavior were required in order to achieve continuous fiber spinning. In contrast, sols exhibiting thixotropic flow behavior were not spinnable. Thixotropy is characteristic of highly structured systems (i.e., three-dimensional networks), so the latter sol was apparently too elastic for fiber spinning. These results are consistent with previous observations for TEOS-derived silica sols.[8]

DTA and TGA measurements were used to investigate the effect of aging prior to fiber heat treatment. TGA data generally showed that increases in aging time resulted in decreases in the temperature needed to complete weight loss processes (i.e., solvent removal, dehydroxylation, etc.). DTA results (Fig. 2) indicated that low temperature (~1000°C) mullite formation was enhanced with longer aging time. This was suggested by the increased intensity of the DTA exotherm in Fig. 2 for the sample aged for 24 hours. A small, but noticeable, peak shift to lower temperatures was also observed with increasing aging time.

Figure 3 shows a plot of apparent density vs. heat treatment temperature for fibers aged 24 hours. The sharp increase in the density at about 800°C presumably indicates the onset of sintering. Densities close to the theoretical value for stoichiometric mullite (~3.17 g/cm^3) were approached at ~1300°C. The sintering temperatures were similar to those observed for other sol-gel processed mullite fibers.[3,5,6]

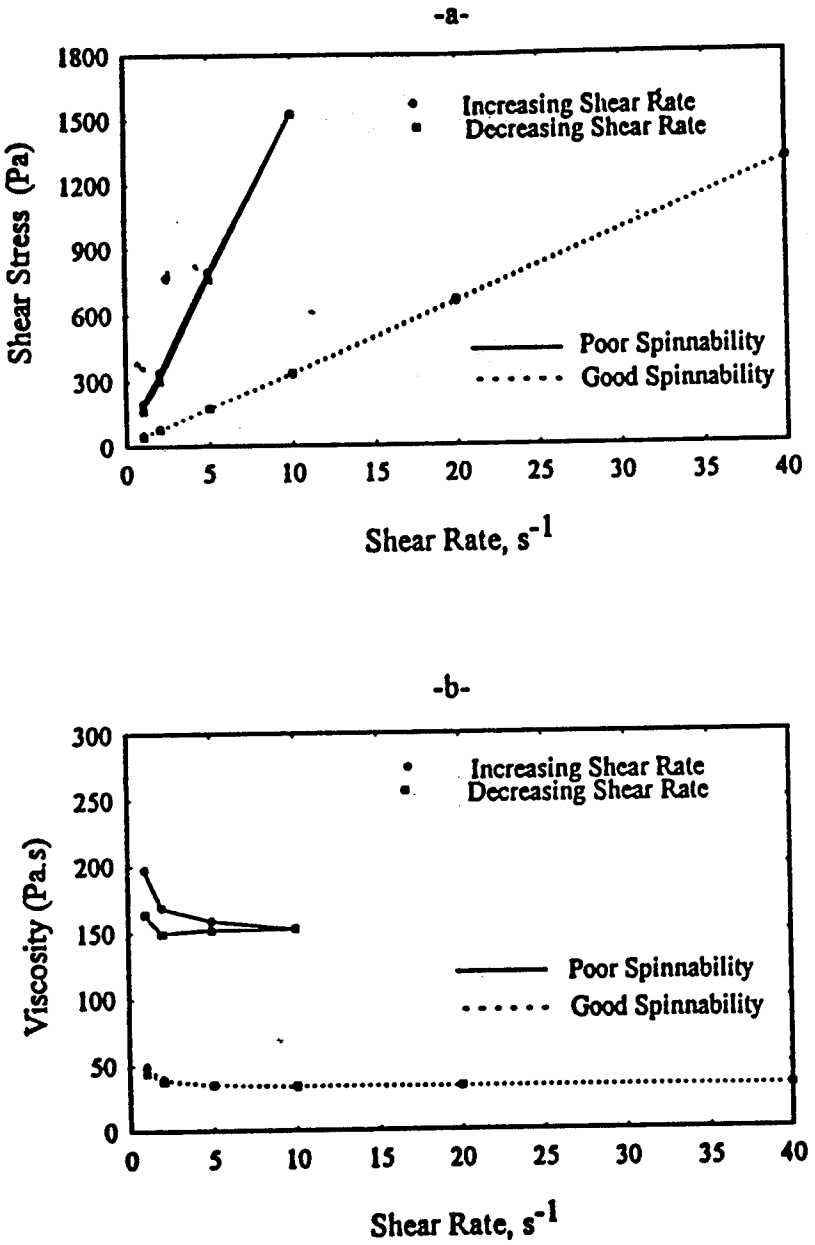

Figure 1 Plots of (a) shear stress with shear rate and (b) viscosity vs. shear rate for two different mullite sols.

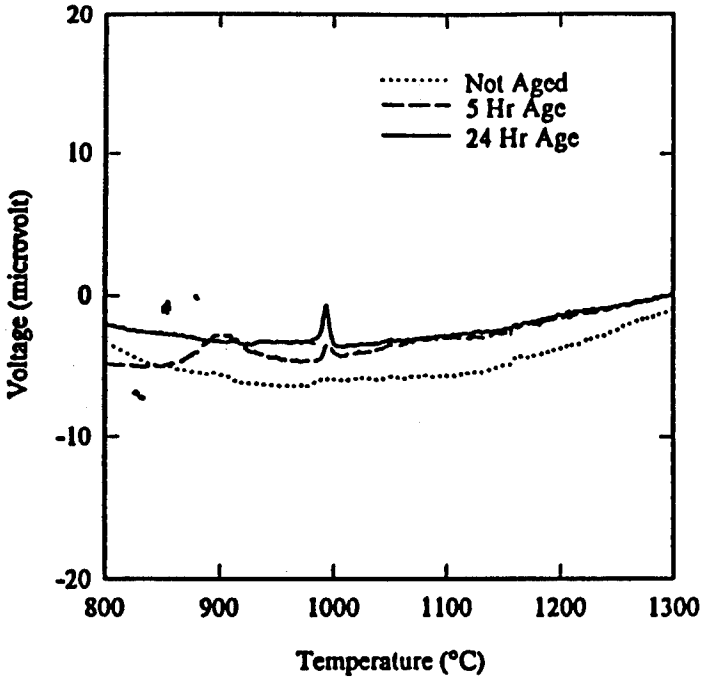

Figure 2 DTA curves for fibers with different aging times.

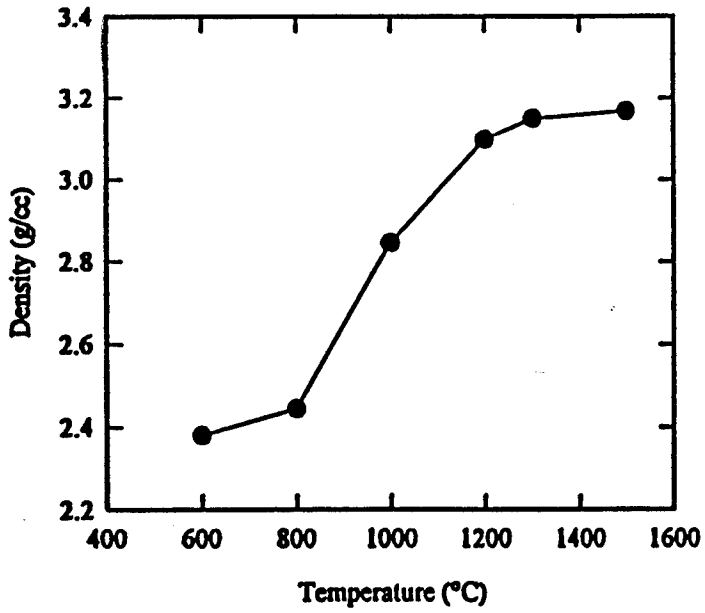

Figure 3 Plot of apparent density vs. heat treatment temperature fibers aged for 24 hours.

Figure 4 shows an SEM micrograph for a fiber sintered at 1500°C for 10 min. Typical diameters of the sintered fibers were in the range of ~ 10-25 μm. The grain sizes were approximately 1 μm.

XRD analysis (Fig.5) showed that mullite was the only crystalline phase present. Fibers were exposed to a concentrated HF solution in order to determine if siliceous glass was present. (Silica dissolves at much higher rate than mullite in HF solutions.[9]) Figure 6 shows an SEM micrograph of a fiber immersed in a 52% HF solution for 15 min. No noticeable difference is observed compared to fibers which were not exposed to an HF solution (e.g., Fig. 4). In contrast, commercial Nextel 480 fibers show obvious degradation after HF treatment (Fig. 7).

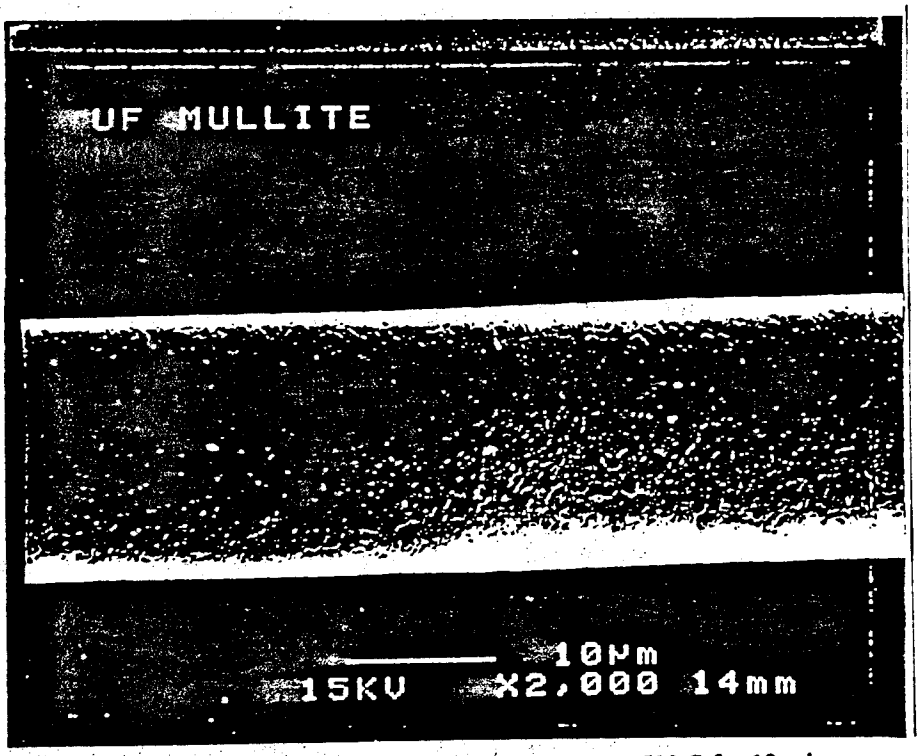

Figure 4 SEM micrograph of mullite fiber sintered at 1500°C for 10 min.

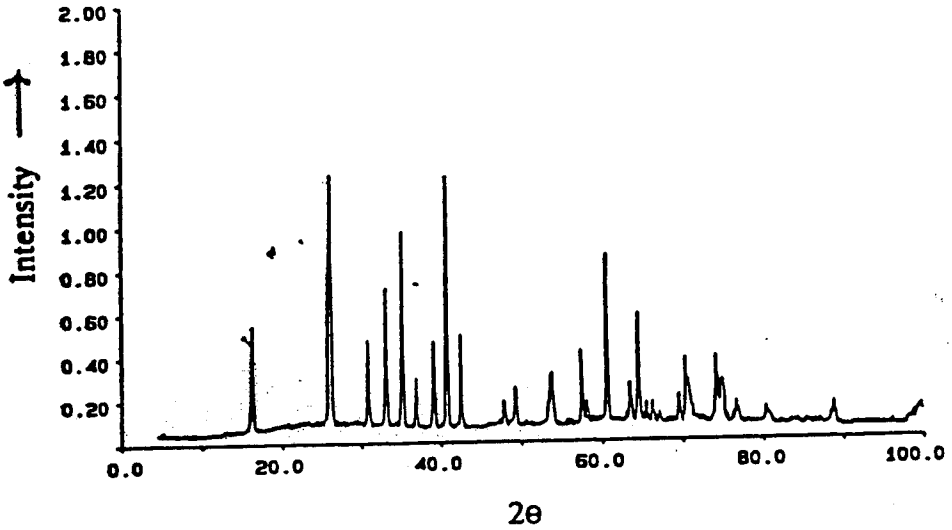

Figure 5 XRD pattern of mullite fibers sintered at 1500°C for 10 min.

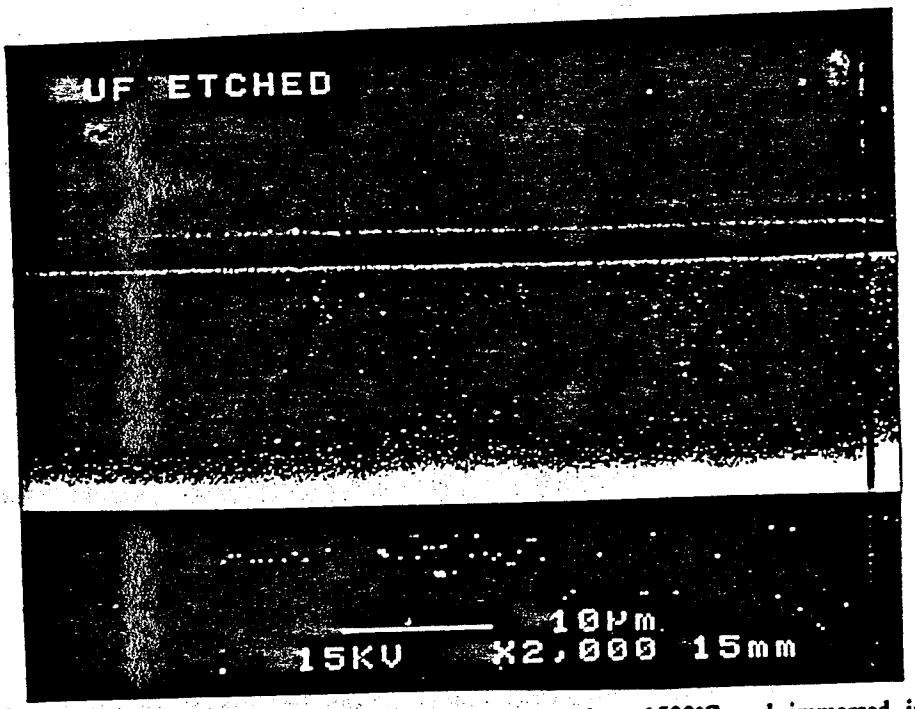

Figure 6 SEM micrograph of mullite fiber sintered at 1500°C and immersed in a concentrated HF solution for 15 min.

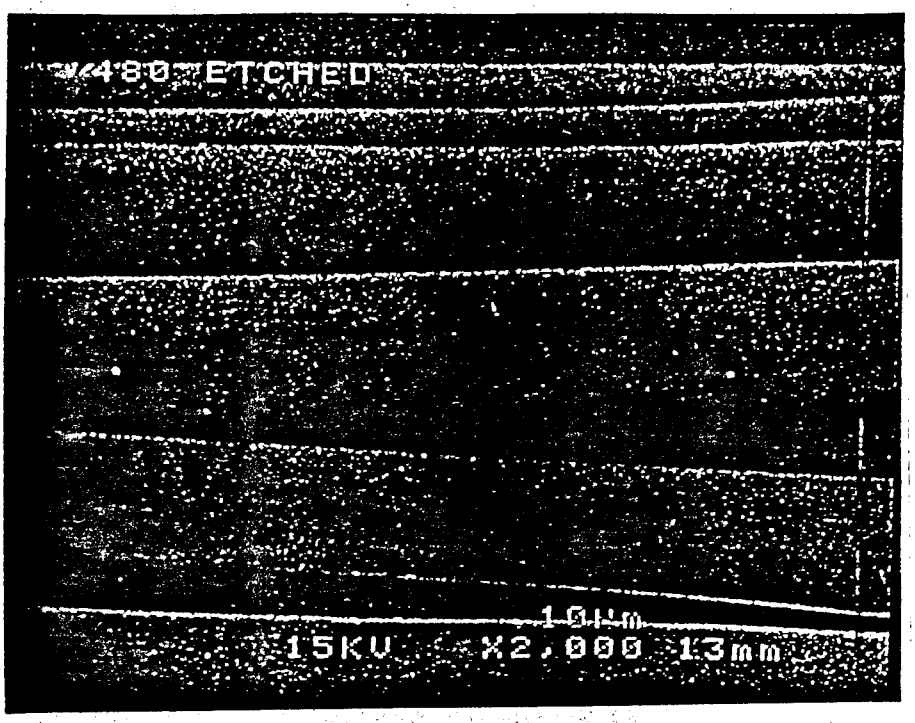

Figure 7 SEM micrograph of Nextel 480 fibers etched in a concentrated HF solution for 15 min.

CONCLUSION

Mullite fibers were prepared by sol-gel processing. The sol was prepared under conditions such that the hydrolysis/condensation reactions were only partially completed prior to fiber spinning. The rheological properties needed for continuous spinning were determined. An aging step was utilized to complete the hydrolysis/condensation reactions and to enhance mullite formation. Mullite formation was observed at ~1000°C and theoretical density was approached at ~1300°C. Fibers with diameters in the range ~10-25 μm were produced. Fibers were resistant to etching by concentrated HF solutions.

ACKNOWLEDGMENTS

This work was supported by the DARPA under Contract No. N00014-91-J-4075. The authors gratefully acknowledge the assistance of A. Marrone, G. LaTorre, R. Crockett, D. Folz, G. W. Scheiffele, C. Simmons, M. Saleem, and R. Raghunathan.

REFERENCES

[1] E. A. Richards, C. J. Goodbrake, and H. G. Sowman, "Reactions and Microstructure Development in Mullite Fibers," J. Am. Ceram. Soc., 74 [10] 2404-2409 (1991).

[2] D.D. Johnson, A.R. Holtz, and M.F. Grether, "Properties of Nextel 480 Ceramic Fibers," Ceram. Eng. Sci. Proc., 8 (7-8) 744-754 (1987).

[3] K. Karst and H.G. Sowman, "Non-Frangible Alumina-Silica Fibers," U.S. Pat. No. 4,047,965 (1977).

[4] H. G. Sowman,"A New Era in Ceramic Fibers Via Sol-Gel Technology," Am. Ceram. Soc. Bull., 67 [12] 1911-1916 (1988).

[5] K. R. Venkatachari, L. T. Moeti, M. D. Sacks, and J. H. Simmons,"Preparation of Mullite-Based Fibers by So-Gel Processing," Ceram. Eng. Sci. Proc., 11 [9-10] 1512 (1990).

[6] D. S. Tucker, J. S. Sparks, and D. C. Esker,"Production of Continuous Mullite Fiber Via Sol-Gel Processing," Am. Ceram. Soc. Bull., 69 [12] 1971-1974 (1990).

[7] ASTM Test Method D 3800, Procedure B, Sink-Float Technique. American Society for Testing and Materials, Philadelphia, PA.

[8] M.D. Sacks and R.-S. Sheu, "Rheological Properties of Silica Sol-Gel Materials," J. Non-Crystalline Solids, 92 383-396, 1987.]

[9] M.D. Sacks, R.B. Langston, S.T. Tso, and J.A. Pask, "Corrosion and Mechanical Behavior Correlations with Composition and Microstructure of Aluminum Silicate Refractories," Am. Ceram. Soc. Bull., 58 [7] 691-697 (1979).

BOOK I

Section 3

Chemical Vapor Deposition (CVD)

and

Chemical Vapor Infiltration (CVI)

Principal Investigator: **T.J. Anderson**

Chemical Vapor Deposition (CVD) and Chemical Vapor Infiltration (CVI)

Principal Investigator: T. Anderson

Objectives

The study of the process of Chemical Vapor Deposition (CVD) in this project has pursued two major objectives.

(1) The investigation of Chemical Infiltration (CVI) in the densification of fibrous Nicalon preforms with a TiC matrix.

(2) The modification of the properties of the resulting composite via variation of the interfacial interaction between the fibers and matrix. To achieve this goal, Atomic Layer Deposition (ALD) has been proposed to precoat or "treat" the fibers with thin coatings of BN.

Research Summary

In route to the first goal, the project's first step was to obtain a quantitative understanding and to characterize the growth process of TiC on flat substrates [1,2,3]. The focus of these studies involved the determination of growth conditions leading to reaction-limited deposition, and the subsequent measurement of the process kinetics under these conditions. These results would later be used in selecting suitable operating parameters for CVI.

Although, some CVI experiments have been performed, it became clear at the beginning of this year that the requirements of the proposed goals had outgrown the existing equipment capabilities [2]. As a result, a new 4-gas, 3-bubbler CVD system was designed and constructed. This system is capable of depositing a number of carbide, nitride, boride and silicide chemistries which have already been demonstrated. The system features computer operated mass flow controllers, pressure control and a rapid reactant switching run-vent manifold. These features will allow the investigation of mixed chemistries, compositionally graded coating, multilayer structures, chloride etching effects and extended time ALE.

In our initial CVI work, we have used the forced-flow, temperature-gradient (FCVI) scheme developed by ORNL. However, as part of our CVI objectives, we have proposed a novel CVI scheme which supplements the ORNL technique with the addition of HC1 to the gaseous feed. The addition of HC1 is meant to provide a control parameter for the densification process. In the traditional FCVI scheme, infiltration occurs faster on one side of the fibrous preform due to the temperature gradient. Unfortunately, reaction still occurs

in intermediate (colder) zones because the temperature is high enough for the deposition to be allowed thermodynamically. Under ideal infiltration conditions, densification should begin at the hotter side of the preform and be restricted to a narrow thickness of the preform (reaction plane). After densification in this zone, the process should proceed by slow displacement of the reaction plane throughout the preform. In theory, the addition of HCl should produce this effect. T prove this, the new scheme was modeled by using a complex multi-species, multi-reaction equilibrium algorithm. The results of these calculations (Figures 1 and 2) demonstrate the existence of an etch-deposition boundary for the equilibrium yield of TiC. In practice, this indicates that there is a critical concentration of HCl under which no TiC will be formed for a given temperature gradient. By gradually lowering the HCl concentration, colder areas of the preform gradually fall on the deposition side of the boundary, thus affording more controlled densification. The next step involved the experimental demonstration of the new scheme using the conditions resulting from the model. However, the current configuration of heating element and sample holder resulted in relatively low temperature gradients, and thus, little densification and long infiltration times, even for the traditional FCVI scheme. This set-up is under current redesign. The short term goal is, ten, to experimentally demonstrate the technique and compare it to ORNL's FCVI process. In addition, since the fast switching manifold of the new system is now available, we have resumed work on the ALD area. Currently, we are trying to deposit several chemistries on flat sapphire substrates. These results will also be available for the annual review.

Publications

(1) R. Aparicio, J.L. Ponthenier, F. Hong and T. Anderson, "Chemical Vapor Deposition on TiC_x on Al_2O_3 Substrates," Ceram. Eng. Sci. Proc., **10** [9-10] pp. 1462-1471 (1989).

(2) M.S. Dariel, R. Aparicio, T.J. Anderson and M.D. Sacks, "CVD if TiC_x on Refractory Materials," Proc. 11th International Conference on Chemical Vapor Deposition, Seattle, WA, 1990.

(3) R. Aparicio, T.J. Anderson and M.D. Sacks, "Chemical Vapor Deposition of TiC_x on Single Crystal Structures," pp. 145-152, Ceramic Transactions, Vol. 19, Advanced Composite Materials. Edited by Michael Sacks. The American Ceramic Society, Westerville, Ohio, 1991.

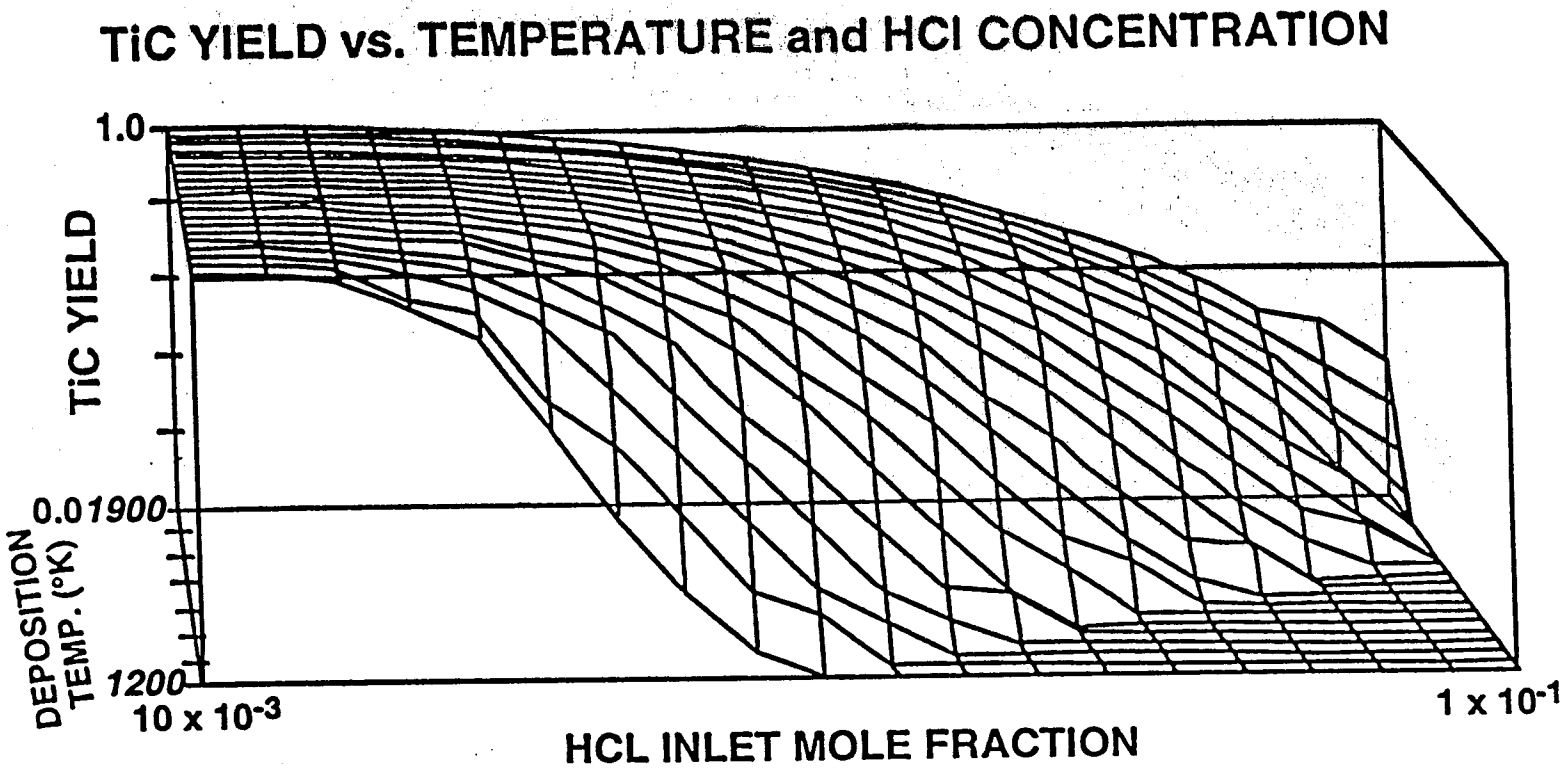

Fig 1. Equilibrium yield of TiC as a function of deposition temperature and HCl inlet concentration. The etch or no-deposition zone lies where the temperature is low and the HCl concentration is high.

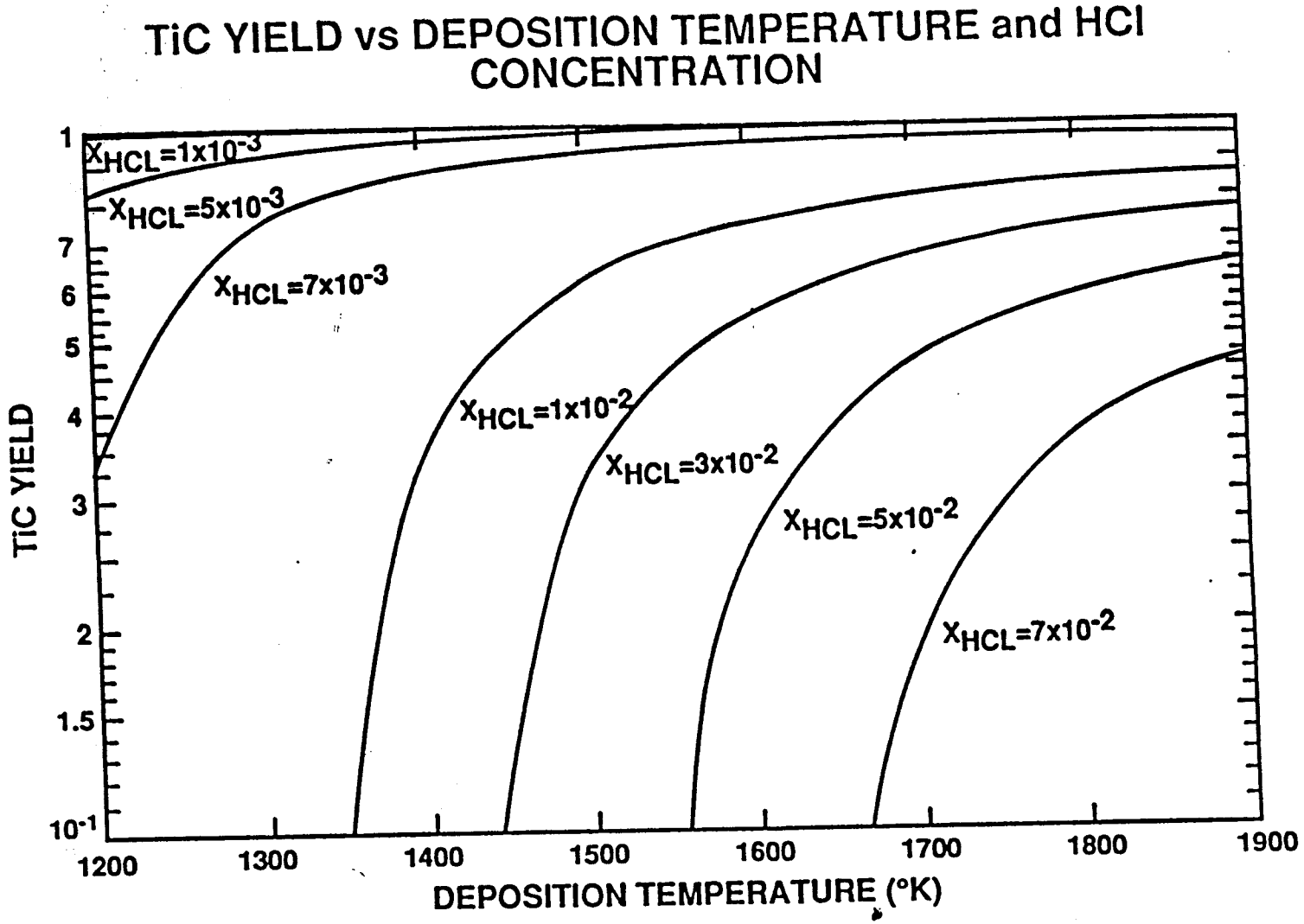

Fig 2. Equilibrium yield of TiC as function of deposition temperature for various HCL inlet concentrations.

Chemical Vapor Deposition of TiC_x on Al_2O_3 Substrates

R. Aparicio, J. L. Pontienier, F. Hong, and T. Anderson

Chemical Engineering Department
University of Florida
Gainesville, FL

M. D. Sacks and G. Johnson

Materials Science and Engineering Department
University of Florida
Gainesville, FL

Deposition of TiC_x films on Al_2O_3 substrates by chemical vapor deposition using $TiCl_4$ and CH_4 sources in H_2 was studied as a function of growth temperature and inlet feed composition. Arrhenius-type behavior was observed with an apparent activation energy of 129.9 kJ/mole. The stoichiometry of the film was measured as a function of inlet composition. The carbon content increased slightly with increasing CH_4 partial pressure, in agreement with equilibrium predictions. The TiC_x grain size increased with deposition rate, and grains were highly oriented.

Introduction

Titanium carbide is an attractive material for many applications because of its high melting temperature (3340 K), high hardness, and excellent strength. As an example, titanium carbide coatings deposited by chemical vapor deposition (CVD) have been widely used to improve the wear resistance of cemented carbide tools. Yang et al.[1] have recently proposed coating Al_2O_3 powders with TiC_x to increase the wetting of alumina by metals in metal-matrix ceramic composites.

Thermal CVD of TiC_x is most commonly performed with a chloride chemistry using $TiCl_4$ and saturated hydrocarbon precursors. Methane is easily transported, available in high purity, and the rate of thermal decomposition is expected to be relatively rapid. This expectation was confirmed by the study of Teyssandier[2] who compared the rate of depositing TiC_x on Mo substrates using either CH_4 or C_3H_8 as the carbon source. The deposition rate using CH_4 was found to be approximately three times that using C_3H_8. Deposition of TiC_x from CH_4-$TiCl_4$-H_2 mixtures on Al_2O_3 has received very little experimental study to date.

Stjernberg et al.[3] measured the influence of inlet $TiCl_4$ and HCl partial pressures on the growth rate of TiC_x at 1000°C. The average growth rate of TiC_x was quite different on Al_2O_3 substrates than on a cemented carbide substrate. More recently, Yang, et al.[1] examined the use of plasma-enhanced CVD to deposit TiC_x on fine Al_2O_3 particles and flat Al_2O_3 substrates.

The overall deposition reaction for formation of TiC_x from $TiCl_4$ and CH_4 is

$$TiCl_4(g) + xCH_4(g) + 2(1-x)H_2(g) = TiC_x + 4HCl(g) \quad (1)$$

Lindstrom and Amberg[4] reported that the deposition rate of TiC_x was independent of the total flow rate, suggesting the deposition reaction is controlled by surface reaction. Titanium tetrachloride decomposition is believed to occur by heterogeneous and parallel disproportionation to form Ti sub-chlorides and HCl. The extensive studies of Stjernberg et al.[3] on deposition of TiC_x by this chemistry suggested that a Langmiur-Henshelwood mechanism is operative and identified adsorption of CH_4 as the rate controlling step. It was also suggested that adsorption of HCl, produced by decomposition of $TiCl_4$ or intentionally added, was competitive with CH_4 adsorption. The purpose of this study was to examine in greater detail the deposition of TiC_x from $TiCl_4$-CH_4-H_2 mixtures on Al_2O_3 substrates. The effect of deposition temperature on growth rate, inlet Ti/C molar ratio on the solid composition, and growth conditions on microstructure were studied.

Experimental Apparatus

A schematic of the experimental CVD system is shown in Fig. 1. The reactor was a vertical pedestal type, heated by a 7.5 kw rf generator. The pedestal susceptor was made of graphite and supported by a closed-one-end alumina tube placed in a centered hole in the susceptor. A Pt/Pt-10% Rh control and measurement thermocouple was placed inside this support tube. The reactor was enclosed by a 76 mm quartz tube, o-ring sealed at both ends by water-cooled flanges.

Reactant and carrier gases were delivered to the reactor by a gas manifold system. Cylinder H_2, CH_4, and Ar were provided along with liquid $TiCl_4$. The $TiCl_4$ was contained in a Pyrex bubbler immersed in a constant temperature bath. Research grade H_2 was bubbled through the $TiCl_4$ source to transport $TiCl_4$. Ar was used as an inert gas to purge the system before opening the reactor to ambient.

The exit gases were first passed through a cold trap to condense $TiCl_x$ species. The remaining exhaust gases were bubbled through an Hg check valve and finally vented to atmosphere. A chemical series mechanical pump could also be connected to the exhaust line to evacuate the system before each run. Stainless steel construction was used in the exhaust system to minimize reaction with deposition reaction products.

Results and Discussion

Over 150 films of TiC_x were deposited on Al_2O_3 substrates. A majority of the alumina substrates were hot pressed pellets, 0.9 cm in diameter and 0.3 cm thick. Several depositions were also performed using high smoothness Al_2O_3 squares, 1 cm^2 in area and 0.1 cm thick. The films were characterized by x-ray diffraction and XPS to verify the deposition of single phase TiC_x.

Several experiments were performed to determine the growth rate as a function of deposition temperature. The growth rate was determined by measuring the weight gain of the substrate after deposition, assuming uniform deposition on all sides. Figure 2 shows the weight gain of the substrate as a function of growth time at three different temperatures. The $CH_4/TiCl_4$ inlet mole ratio was unity and the reactant flow rate was 2% of the total flow rate (500 sccm). The observed rate is a linear function of growth time. The thickness extrapolates to a value of zero at the beginning of growth for each temperature, indicating no significant nucleation limitation. An average growth rate was calculated from the slope of these three lines and plotted vs reciprocal temperature in Fig. 3. Arrhenius-type behavior is clearly illustrated in Fig. 3, with an apparent activation energy of 129.9 kJ/mole TiC_x. A linear regression of the data resulted in the following expression for the growth rate, r

$$\ln (r) = 6.9 \times 10^4 \text{ mg/h} \exp [-1.56 \times 10^4/T(K)] \quad (2)$$

This represents the first report of an activation energy for deposition of TiC_x on alumina. Other substrates have been used in the deposition of TiC_x and the reported activation energies are compared in Table I. The apparent activation energy of this study is the lowest reported using CH_4 as the carbon source. The substrate should influence the nucleation structure of TiC_x and therefore the grain orientation. The samples were found to have a preferred orientation in the <200>. If the process is truly controlled by heterogeneous reaction, the surface orientation will affect the apparent activation energy and may be responsible for the various observed activation energies.

A series of experiments was also performed to determine the effect of reactant inlet composition on the stoichiometry of TiC_x. In initial studies the inlet partial pressure of $TiCl_4$ was maintained constant at a value of 10^{-3} atm and the CH_4 partial pressure was varied at a constant growth temperature of 1500 K and total flow rate of 1000 sccm.

The value of the C/Ti molar ratio was determined from the lattice parameter measured by x-ray diffraction. The results for several runs are shown in Fig. 4. The reproducibility for a given set of operating parameters is seen to be excellent. All films were found to be near the TiC-Ti 2-phase boundary. The carbon content gradually increased with increasing CH_4 partial pressure. This rather flat response to

Table I. Comparison of Activation Energies for Deposition of TiC_x on Various Substrates

Substrate	E (kJ/mole)	Hydrocarbon Source	P (atm)	Reference
WC-Co	351–393	C_3H_8	1	5,6
WC-Co	276	CH_4	1	7
WC-Co	184	CH_4	1	6
WC-Co	372	CH_4	1	4
Graphite	418	CH_4	0.132	8
Graphite	159	Ch_4	1	7
Graphite	84	none	1	9
Graphite	100	none	1	10
Porous Graphite	62	none	1	11
Pseudocrystal Graphite	71	none	1	11
Mo	192	CH_4	1	9
WC-Co	108	none	1	4
Steels	201	CH_4	1	12
Al_2O_3	129.9	CH_4	1	this study

methane partial pressure is consistent with the predictions of thermodynamic analysis,[11,13,14] though the predicted C/Ti molar ratio is slightly higher.

The microstructure of deposited TiC_x was also examined as a function of growth conditions. Shown in Fig. 5(*a–f*) are scanning electron micrographs of TiC_x films deposited on high smoothness Al_2O_3 substrates at various growth conditions. All micrographs are at the same magnification. Figure 5(*a*) shows the clean Al_2O_3 substrate has surface roughness on the order of a few microns. Figures 5(*b–f*) show the microstructure of TiC_x films deposited at a constant pressure of 1 atm and total flow rate of 500 sccm. The effect of deposition temperature is seen by comparing Fig. 5(*b*) (1500 K) and (*d*) (1600 K). The increase in growth rate produces a considerably larger grain size. Very little growth occurred under the growth conditions represented by Fig. 5(*b*). It appears that growth is initiated on the flat portions of the individual Al_2O_3 grains. The influence of $CH_4/TiCl_4$ molar ratio at constant temperature on the microstructure is shown in the series of micrographs (*c–f*). Since growth rate is first order in CH_4 partial pressure, a significant increase in the grain size is produced as the $CH_4/TiCl_4$ molar ratio is increased. It is also observed that the TiC_x grains are highly oriented. A microstructure similar to that shown in Figs. 5(*c*) and (*d*) was reported by Yang et al.[1]

Conclusions

Chemical vapor deposition has been used to grow TiC_x films on both rough and high smoothness Al_2O_3 substrates. The films were confirmed to be single phase TiC_x by both x-ray diffraction and XPS.

The deposition appears to be rate-limited by heterogeneous reaction with a measured apparent activation energy of 129.9 kJ/mole. The stoichiometry of TiC_x was measured as a function Ti/C molar ratio and the results were qualitatively consistent with equilibrium predictions. The deposited films consisted of oriented grains that increase in size as the growth rate increased (i.e., increasing deposition temperature and increasing $CH_4/TiCl_4$ molar ratio).

Acknowledgment

The authors gratefully acknowledge that this work was supported by the Defense Advanced Projects Agency (MDA972-88-J-1006). The authors thank Dr. John Halloran of Ceramics Process Systems for providing the high smoothness of Al_2O_3 substrates.

References

[1]M. Y. Yang, S. P. Kohler, and B. M. Kramer, *Adv. Ceram. Mat.*, 3, 341 (1988).
[2]F. Teyssandier, Ph.D. Thesis, University of Grenoble (1986).
[3]K. G. Stjernberg, *Thin Solid Films*, 40, 81 (1977).
[4]J. N. Lindstrom and S. Amberg, Proc. IV Int. Conf. CVD, 115 (1973).
[5]M. Lee and M. N. Richman, *J. Electrochem. Soc.*, 120, 993 (1978).
[6]J. S. Chun and C. W. Lee, Proc. IX Int. Conf. CVD, 573 (1981).
[7]J. S. Cho and J. S. Chu, Proc. VIII Int. Conf. CVD, 540 (1988).
[8]F. Langlais, R. Naslain, and J. Y. Rossignol, Proc. IX Int. Conf. CVD, 596 (1984).
[9]L. Agour, E. Fitzer, and J. Schlichting, Proc. V Int. Conf. CVD, 600 (1975).
[10]R. S. Ambertsumyan and B. N. Babich, *Akad. Nauk. SSSR. Neorg. Materiali.*, 5, 301 (1969).
[11]C. Vincent, Ph.D. Thesis, University of Lyon (1987).
[12]T. Takalashi, K. Tomita, and K. Sugiyama, *J. Electrochem. Soc.*, 114, 1 (1974).
[13]C. Bernard, M. Ducarrior, and F. Teyssandier, *J. Less-Common Metals*, 78, 269 (1981).
[14]C. Bernard, M. Ducarrior, and F. Teyssandier, *J. Electrochem. Soc.*, 135, 225 (1988).

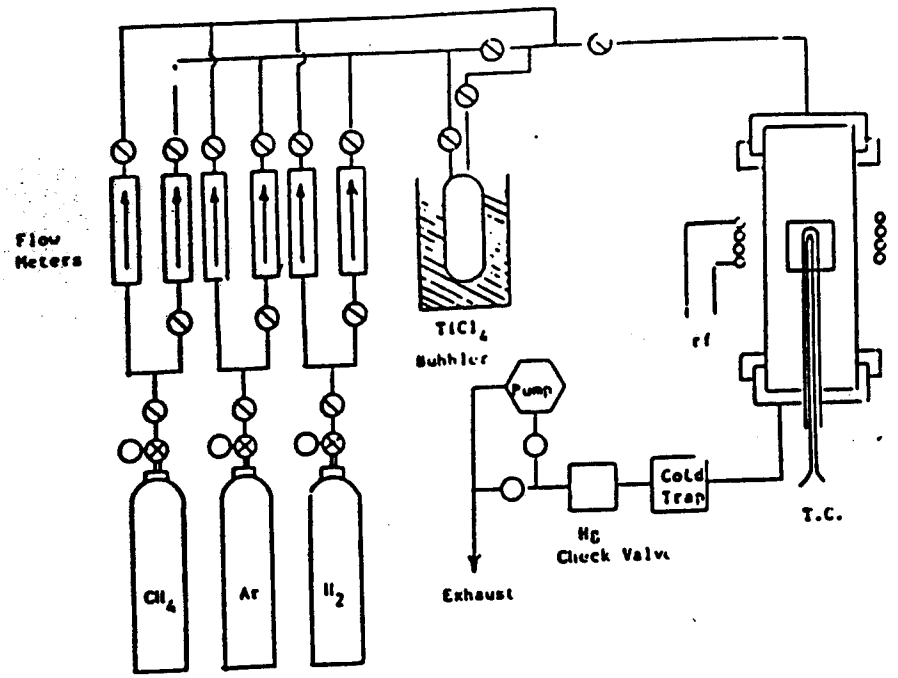

Fig. 1. Schematic of CVD system.

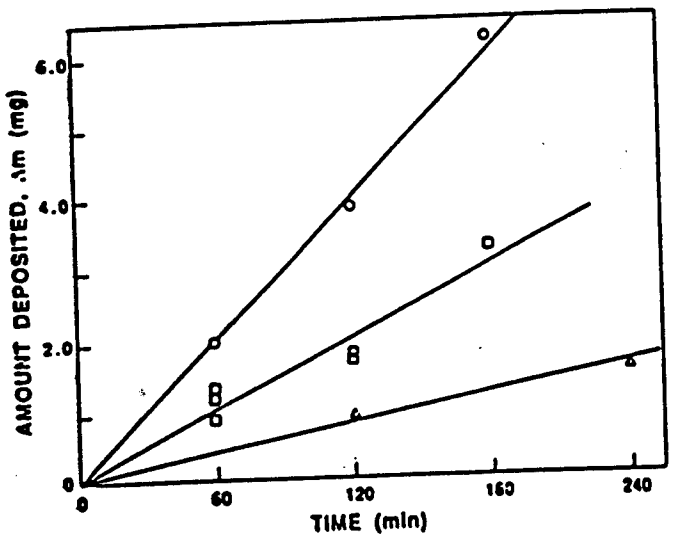

Fig. 2. Amount of TiC_x deposited on Al_2O_3 substrates as a function of deposition time for three deposition temperatures: O, 1500 K; ⊡, 1400 K; Δ, 1300 K. The deposition pressure was 1 atm and inlet flow rates were: $TiCl_4$, 5 sccm; CH_4, 5 sccm; and H_2, 490 sccm.

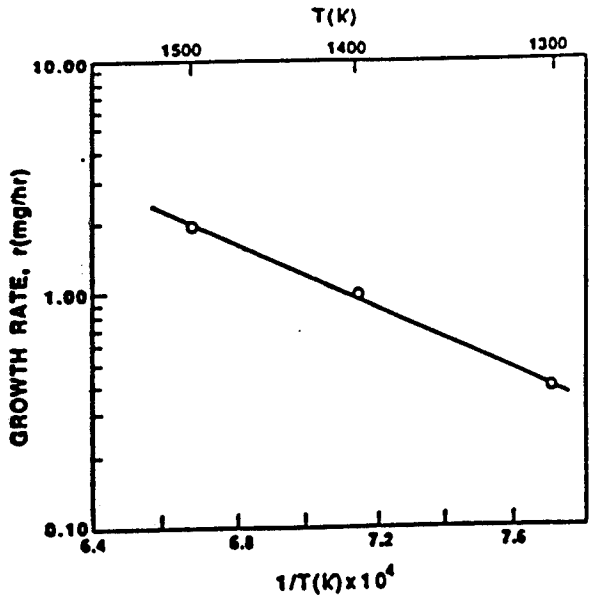

Fig. 3. Growth rate, mg/h, of TiC_x as a function of reciprocal deposition temperature.

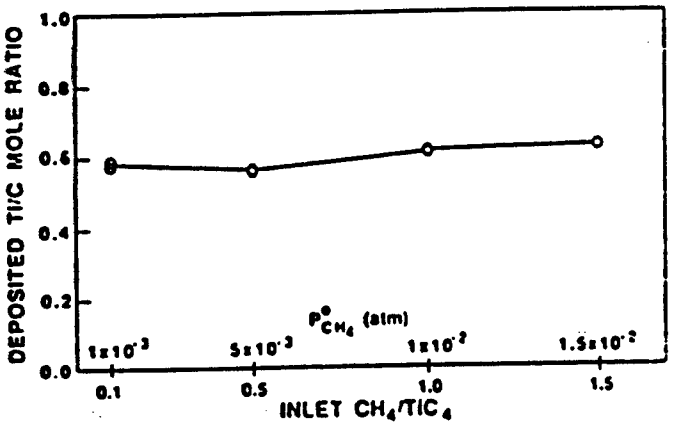

Fig. 4. Effect of inlet $CH_4/TiCl_4$ molar ratio on the stoichiometry of deposited TiC_x at 1500 K. The total flow rate was 1000 sccm and the $TiCl_4$ flow rate was constant at 10 sccm.

Fig. 5. Scanning electron micrographs of TiC_x deposited on Al_2O_3 substrates by CVD at 1 atm pressure and total flow rate of 500 sccm: (*a*) clean Al_2O_3 substrate; (*b*) deposition temperature, 1500 K, $CH_4/TiCl_4$ inlet molar ratio, 1.0; (*c*) deposition temperature, 1600 K, $CH_4/TiCl_4$ inlet molar ratio, 0.5; (*d*) deposition temperature, 1600 K, $CH_4/TiCl_4$ inlet molar ratio, 1.0; (*e*) deposition temperature, 1600 K, $CH_4/TiCl_4$ inlet molar ratio, 3.0; (*f*) deposition temperature, 1600 K, $CH_4/TiCl_4$ inlet molar ratio, 4.0.

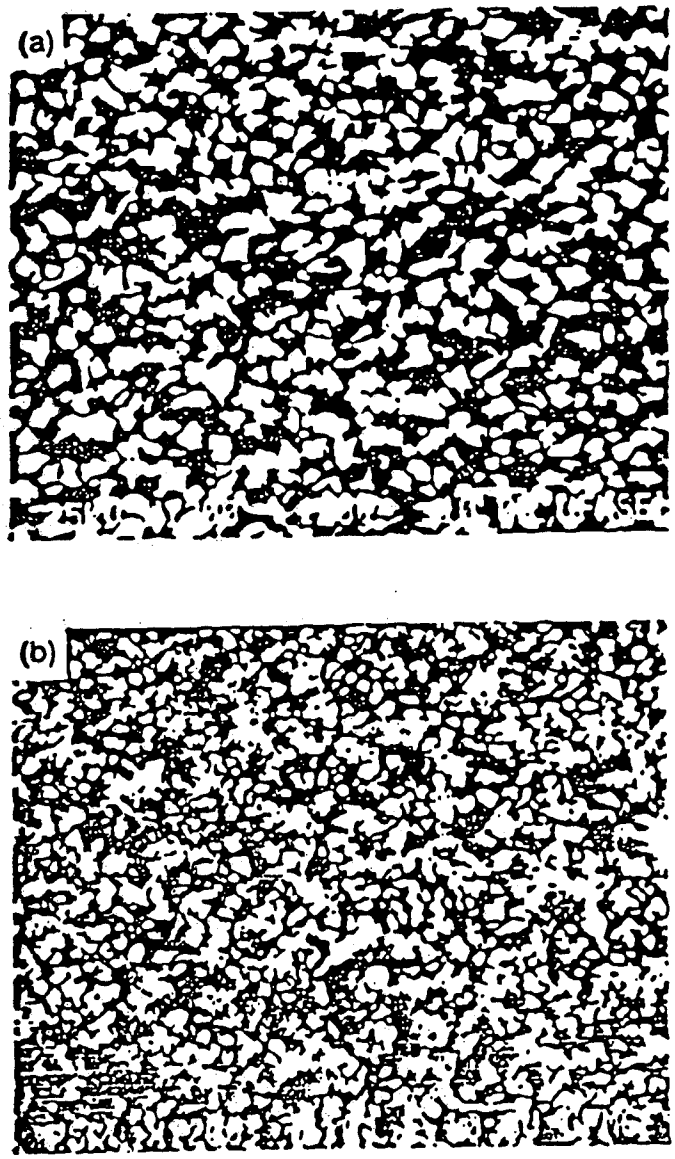

(c)

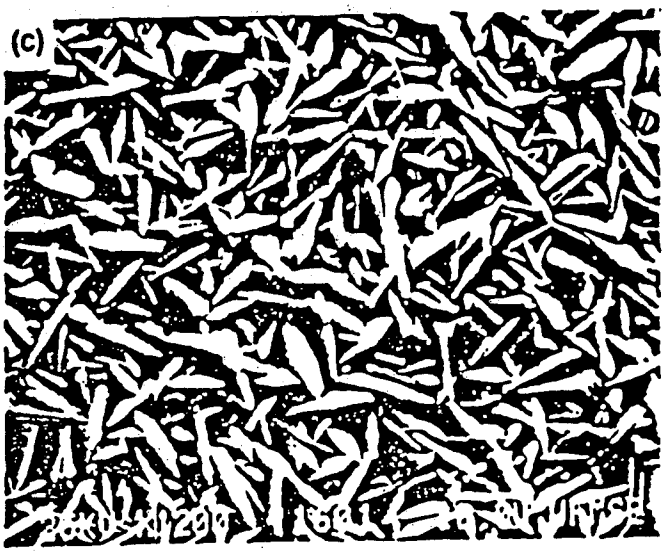

(d)

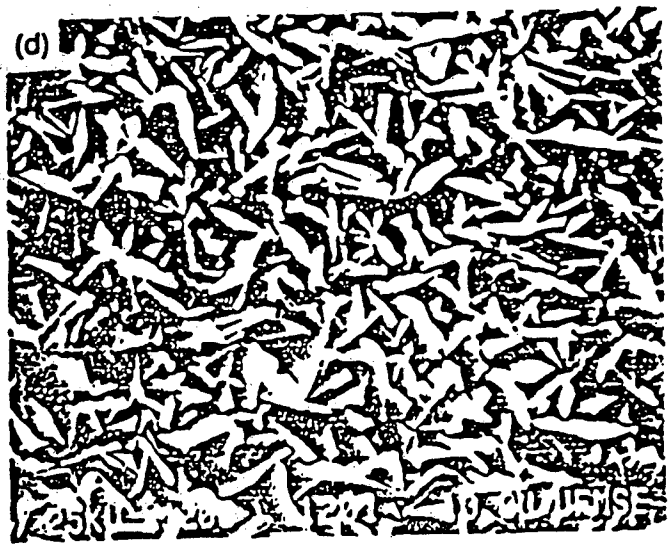

(e)

(f)

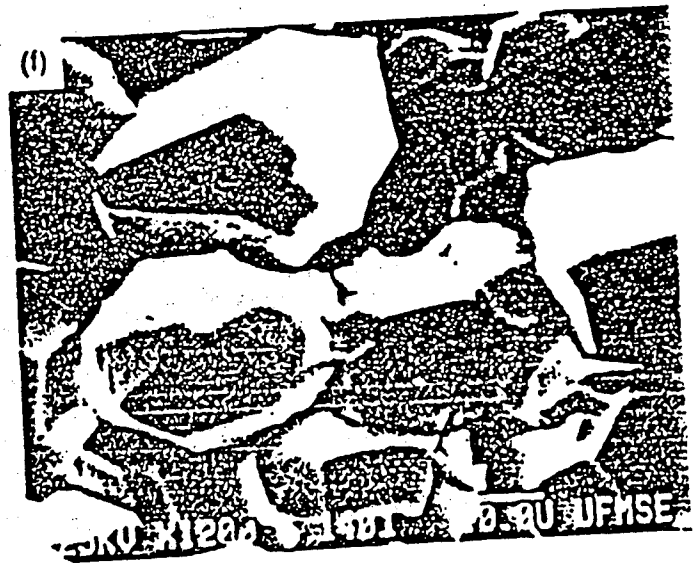

CVD OF TiC_x ON REFRACTORY MATERIALS

M.S. Dariel[1], R. Aparicio[2], T.J. Anderson[2] and M.D. Sacks[1]

[1] Materials Science and Engineering Department
[2] Chemical Engineering Department
University of Florida
Gainesville, FL 32611

Chemical vapor deposition of TiC_x from $TiCl_4$ and CH_4 sources in a H_2 carrier gas was studied on a variety of substrates. Values of apparent activation energies were determined to be 81 kJ/mol for a Ta substrate, 110 kJ/mol for graphite, 121 kJ/mol for Al_2O_3 and 210 kJ/mol for Nicalon. Deposition was reaction limited in the temperature range 1300 to 1500 K. Different preferred grain orientations and surface morphologies were observed on each substrate. The properties of the deposited films were characterized by SEM, XRD and EMPA.

A. INTRODUCTION

TiC_x has been proposed as a matrix phase in hybrid carbon/carbon composites because of its hardness, high melting temperature and resistance to wear (1). These same properties have made TiC_x attractive for applications such as bulk ceramic tools used in industrial cutting technology and, in combination with oxidation resistant Al_2O_3 films, first coatings of fusion reactors (2,3).

Deposition of TiC_x films on refractory materials is of particular interest as a potential reinforcing phase for high temperature ceramic matrix composites. In the present study, the growth rate of TiC_x is reported as a function deposition temperature on a variety of substrates including Si-C-O (Nicalon) fibers, polycrystalline graphite, SiO_2, Al_2O_3, Mo and Ta. The influence of the inlet gas composition on the elemental composition of the films deposited on Nicalon, graphite and Al_2O_3 was measured by EMPA. The surface morphology and grain orientations were characterized as a function of deposition temperature and substrate type.

B. EXPERIMENTAL

TiC_x was deposited on planar substrates in a vertical pedestal type reactor using $TiCl_4$ and CH_4 in H_2 as reactant sources. The pedestal susceptor was made of graphite, and was

heated by a 7.5 kW rf generator. The substrate temperature was measured by both a sheathed type S thermocouple placed in the center of the susceptor and a two-color optical pyrometer focused on the top surface of the substrate through a gas-swept quartz viewport. The reactor was enclosed by a 76 mm diameter quartz tube which was sealed at both ends by water-cooled flanges. The reaction chamber was purged before each deposition by sequential pumping and back-filling with Ar.

Deposition of TiC_x on stacked Nicalon fiber weaves was accomplished by the temperature gradient, forced flow CVI method. The stacks, consisting of 3 weave discs were packed together with a graphite holder and separated from the top of the pedestal susceptor with a graphite ring. Radiation absorption by the stack from the susceptor provided a temperature gradient of approximately 200°C across the stack. As a result, the top layers of the stack (gas inlet) were at a lower average temperature than the bottom layers, thus allowing a reaction front to move in a direction opposite to that of the gas flow. Passage of the gases through weaves was ensured by plugging the reactor wall-susceptor annulus with graphite felt and providing an exit through an axisymetric hole in the susceptor.

All depositions were performed at atmospheric pressure and reactant partial pressures were in the range $7x10^{-3}$ to $2x10^{-2}$ atm for $TiCl_4$ and $1x10^{-2}$ to $2.8x10^{-2}$ atm for CH_4. The H_2 carrier gas flow rate range was 570 to 970 sccm. The deposition temperature was varied in the range 950 to 1270°C and the deposition time varied from 1 to 12 hrs. Substrates consisted of Nicalon 12-harness satin weave cloth preforms, polished graphite, alumina or silica, and high purity Mo or Ta foils.

SEM observations were made on as-deposited coatings, on fracture planes, and on polished cross sections of infiltrated weaves or coated plates, cast in acrylic or epoxide resins. In addition, the coatings were analyzed by XRD and EPMA to obtain information on crystallinity, preferred orientation and elemental composition. For EPMA measurements special care was taken to avoid surface contamination from carbon containing materials used in polishing or other preparation steps.

C. RESULTS AND DISCUSSION

Deposition Rates

The growth rate of TiC_x on various substrates was determined as a function of growth temperature at constant reactant inlet compositions (10 sccm $TiCl_4$, 20 sccm CH_4 and

970 sccm H_2). Since the surface was nonplanar, growth rates were determined by measuring the weight change of the substrate and normalizing by the exposed surface area. The measured weight gain expressed in mg/hr is shown as a function of reciprocal temperature in Figure 1. For all substrates examined, the growth rate was a linear function of inverse temperature. Values of the apparent activation energies were calculated from the results of a linear regression analysis and found to be 81 kJ/mol for Ta, 110 kJ/mol for graphite, 121 kJ/mol for Al_2O_3 and 210 kJ/mol for Nicalon. An apparent activation energy for deposition on Mo was not determined since only 2 growths were performed. No rate data were obtained for SiO_2. Of the substrates used in this study, only graphite has a previously reported atmospheric pressure activation energy (159 kJ/mol) (1,4).

Previous studies on a variety of other substrates as well as the results of this study suggest that deposition of TiC_x is limited by heterogeneous reaction (5). An increase in the CH_4 partial pressure was found to increase the TiC_x deposition rate, consistent with previous studies(6). Stjernberg et al. have suggested that deposition occurs by the Langmuir-Hinshelwod adsorption mechanism[6]. In their model $TiCl_4$ undergoes rapid homogeneous thermal decomposition to yield subchlorides which adsorp on one type of site. The decomposition product HCl and CH_4 compete for the available adsorption sites of the second type. Differences in the observed activation energies are attributed to differences in the surface chemistry of different grain orientations (as discussed below) which affect the nucleation mechanism and are determined by substrate type.

Composition of TiC_x Films

The elemental composition of TiC_x films on Al_2O_3, Nicalon and graphite was determined by EMPA. No data was obtained for the films on SiO_2, Ta and Mo.

For both Nicalon and graphite substrates, the C/Ti elemental ratio in the films was in the range 0.91-0.93 at a $CH_4/TiCl_4$ input gas ratio of 2, (partial pressure of $TiCl_4$ = 1 x 10^{-2}) and temperature of 1200°C. Increasing the $CH_4/TiCl_4$ ratio to 3.5 at 1200°C resulted in an C/Ti elemental ratio of 1.07, indicating the formation of free carbon. At 1050°C, the films become richer in Ti, with an elemental ratio of 0.82 at an input gas ratio of 2. As for the TiC_x films on Al_2O_3, the C/Ti ratio remained constant at 0.6 as the input gas ratio and the temperature varied from 0.1 to 1.5 and 1000°C to 1200°C, respectively. Comparison of the experimentally measured compositions with theoretical equilibrium values show

excellent agreement for deposition of TiC_x films on Nicalon and graphite at 1200°C(7). However, neither of the compositions on Nicalon and graphite at 1050°C nor those on Al_2O_3 agree with the equilibrium diagrams.

Surface Morphology and Grain Orientation

The substrates examined in this work have a wide range of chemical compatibility with TiC_x. Graphite is a semimetal and C is a component of the TiC_x solid solution, thus providing a carbon source in addition to the gas phase. Mo and Ta are metals which can form stable compounds with C during the initial stages of growth. Al_2O_3 and SiO_2 are insulators which should be relatively inert in the presence of TiC_x. The properties of Nicalon (Si-C-O) are close to those of SiC and thus similar to TiC_x. As expected, quite dissimilar grain orientations and surface morphologies were observed for different substrates.

The reactor geometry for growth of TiC_x on Nicalon was different than that for other substrates. In this system a temperature gradient was imposed across the stack and significant mass transfer limitations were present in the inner portions of the stack. As the deposition temperature increased from 1000°C to 1200°C, the structure of TiC_x grown on Nicalon fibers changed (Figure 2 a-d) from pyramidal needles 0.2 - 1 μm in size to more rounded, equiaxed grains smaller than 0.2 μm. Fracture sections of coatings showed the grains grown at the lower temperature were columnar and aligned perpendicularly away from the fiber surface (Figure 3). X-ray patterns of all TiC_x films on Nicalon show a random orientation of the crystals despite the variety of microstructures.

Nodular growths were observed on fibers directly facing the gas inlet orifice. In these growths, locally accelerated deposition occurs in spite of the overall lower growth temperature of the fibers on which the gas stream is impinging. Features of these growths are markedly different from the regular type of growth observed on most of the fiber surface, and they consist of blocky crystals with step-ledge like features as shown in Figure 4 a-b. Since no mass transfer limitation was believed to exist on this exposed plane, these growth features are not attributed to local gas phase disturbances but rather to a nucleation phenomenon(8). A possible explanation is related to deposition of powdery, purplish colored titanium subchloride particles on the cold reactor walls in depositions with a $CH_4/TiCl_4$ ratio of 2. Particles above the sample apparently became dislodged and settled onto the upper layer of the stack, thus providing

different nucleation sites that develop into the nodular growths. This explains why no such growths were found when very little subchloride deposition was observed on the reactor walls ($CH_4/TiCl_4$ inlet molar ratio was increased to 7/2).

At deposition temperatures above 1200°C, a third type of growth feature was observed on the fibers located in between the graphite holders. In this region the gas flow was greatly restricted. While the fine grained TiC_x structure on the Nicalon surface was retained (Figure 5), whiskers, 10-15 microns long with an aspect ratios of about 10, were also grown. In their study of Ni-catalyzed TiC_x deposition, Wukulski et al. have reported whisker growth to occur at low reactant concentrations and system pressures (9). Apparently TiC_x whisker growth on Nicalon is promoted by reactant depletion effects within the restricted regions inside the graphite holder. Despite these marked dissimilarities in surface morphology, the X-ray diffraction spectra of both the low and the high temperature forms of TiC_x grown on Nicalon are identical and correspond to that of randomly oriented TiC_x, (Figure 6a).

For CVD of TiC_x on graphite more conventional dome-shaped structures were obtained. Magnification of films grown below 1000°C showed small needle-like aggregates 0.1 by 1 μm in size (Figure 7a). X-ray diffraction results indicated these needles were of random orientation (Figure 6b). TEM analysis of the needle showed them to be composed of grains with very diffuse, weakly defined boundaries, less than 30 nm in size. As the temperature of deposition was increased, their shape became more rounded and equiaxed grains appear (Figure 7b). As the growth temperature was further increased to 1200°C, the crystal edges grew sharper, forming blocky, faceted stacks 5-15 μm in size (Figure 7c,d). Simultaneously, the (220) diffraction line became much stronger (Figure 6c). Lee and Chun studied the deposition of TiC_x on WC-12Co substrates using the same deposition chemistry as this study. They reported the preferred orientation of the films to be independent of deposition time and gas phase composition (10). In addition, they observed a very similar trend in orientation; a random orientation at 1050°C changing to (220) between 1100°C and 1150°C.

TiC_x films deposited on fused silica at 1000°C were weakly adhered to the substrate. SEM analysis of the films revealed heaps of knobby, small (< 0.1 μm) amorphous-like particles covering larger, faceted crystallites (Figure 8). The X-ray diffraction peaks were broader, indicating amorphous areas (Figure 6d). Preliminary TEM measurements showed randomly oriented grains, up to several microns in size, with well developed boundaries. The randomness of grain orientation is

also confirmed by the XRD pattern.

The effect of growth temperature on the morphology of the TiC_x grown on alumina tended to be the reverse as that observed on other substrates. As the temperature increased from 1200°C (Figure 9a) to 1300°C (Figure 9c) the TiC_x grains change from a round, faceted shape to a more elongated form. The reactant composition, however, had the opposite effect. Figure 9b-d shows the microstructure of TiC_x grown at different values of $CH_4/TiCl_4$ gas inlet ratios. The grains changed in the previously observed pattern from a needle-shaped to round, equiaxed crystals. X-ray analysis showed (111) preferred orientation.

CVD of TiC_x on the metals Mo and Ta produced wedge shaped, sharply defined crystallinities at a lower growth rate than on the other substrates (Figure 10a,b). X-ray diffraction results for TiC_x grown on Mo at 1150°C (Figure 6e) show that the (220) line is enhanced; the ratio of peak intensities (220)/(220) has the value of 7 compared to the value 0.6 for the random powder (Figure 6h). At 1200°C growth temperature, the ratio of peak intensities decreased to a value of 0.2 (Figure 6f). This behavior is opposite to that observed for deposition on graphite. The x-ray diffraction spectrum at 1200°C also shows weak Mo_2C lines which is formed during the initial stages of deposition by reaction between the substrate and CH_4. Similar behavior was observed for deposition on Ta substrates with the reaction product TaC forming adjacent to the substrate. The X-ray diffraction analysis shows the (220) lines as dominant, suggesting random orientation, though the (311) line was also strongly enhanced (Figure 6g).

D. SUMMARY

The deposition of TiC_x on a variety of refractory substrates using a chloride chemistry was limited by heterogeneous reaction at a temperature near 1200°C. Values of the apparent activation energies ranged from 81 kJ/mol for Ta to 210 kJ/mol for Nicalon. Under identical growth conditions the morphology and grain orientations were strongly influenced by substrate type and growth temperature. Random grain orientations were deposited on Nicalon, SiO_2 and at low temperature, on graphite. A preferred orientation was observed on Al_2O_3 (111), Ta (311), Mo (220) at low temperature, and graphite (220) at high temperature.

ACKNOWLEDGEMENTS

This work was supported by the Defense Advanced Research Project Agency under Navy grant No. MDA972-88-J-1006.

REFERENCES

1. J.Y. Rossignol, F. Langlais and R. Naslain, Proc. 9th Int. Conf. on CVD, 596 (1985)

2. D.G. Kim, J.S. Yoo and J.S. Chun, Thin Solid Films, 165, 149(1988).

3. M. Okada, Thin Solid Films, 108, 373(1983).

4. L. Agour, E. Fitzer and J. Schlichting, Proc. 5th Int. Conf. on CVD, 600(1975).

5. J.N. Lindstrom and S. Aubrey, Proc. 4th Int. Conf. on CVD, 115(1973).

6. K.G. Stjernberg, Thin Solid Films, 40, 81(1977).

7. C. Bernard, M. Ducarrior and F. Teyssandier, J. Less-Common Metals, 78, 269-274(1981).

8. W.R. Holman and F.J. Huegel, J. Vac. Sci. Technol., 11, 701(1974).

9. L. Wokulski and, K. Wokulska, J. Crystal Growth, 62, 439 (1983).

10. C.W. Lee and J.S. Chun, Proc. 8th Int. Conf. on CVD, 563(1981).

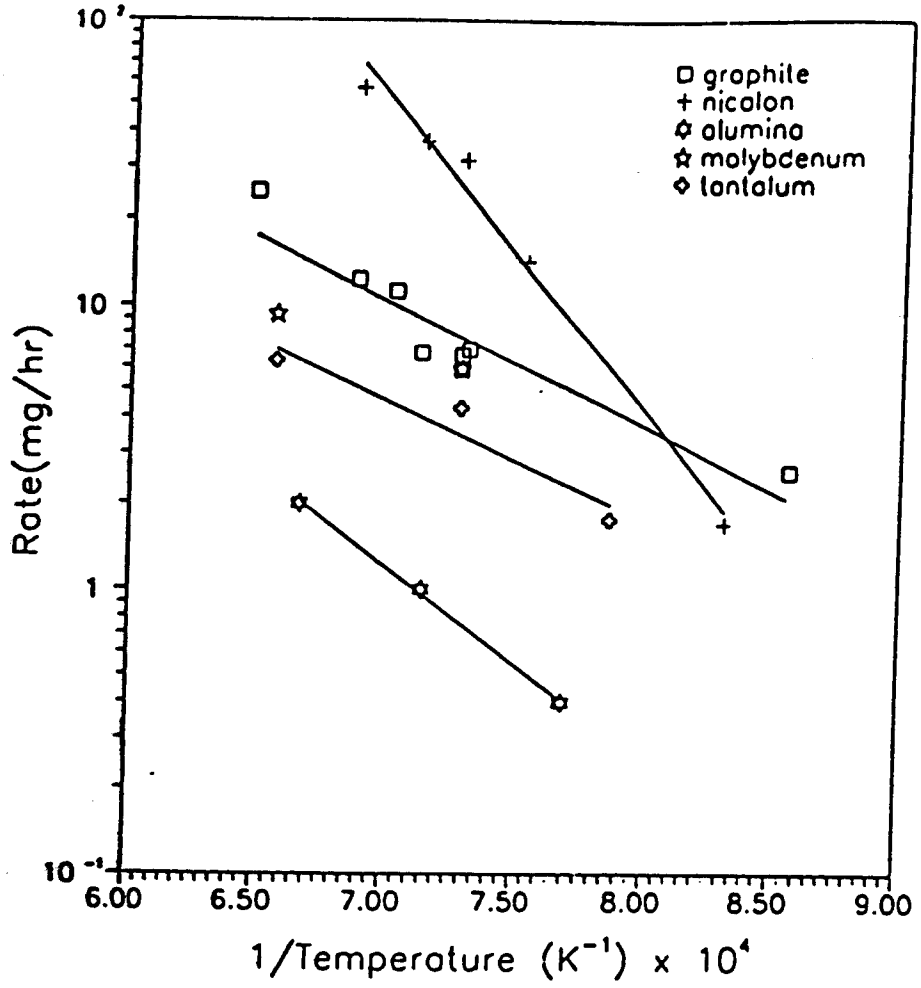

Fig. 1. Growth rate of TiC_x on various substrates as a function of reciprocal temperature.

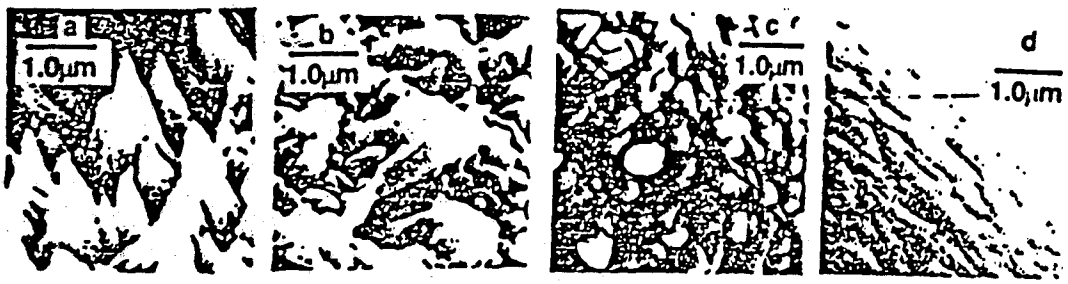

Fig. 2. Effect of temperature on the microstructure of TiC_x on Nicalon (Si-C-O) fibers. Temperature varied from 1000°C to 1200°C.

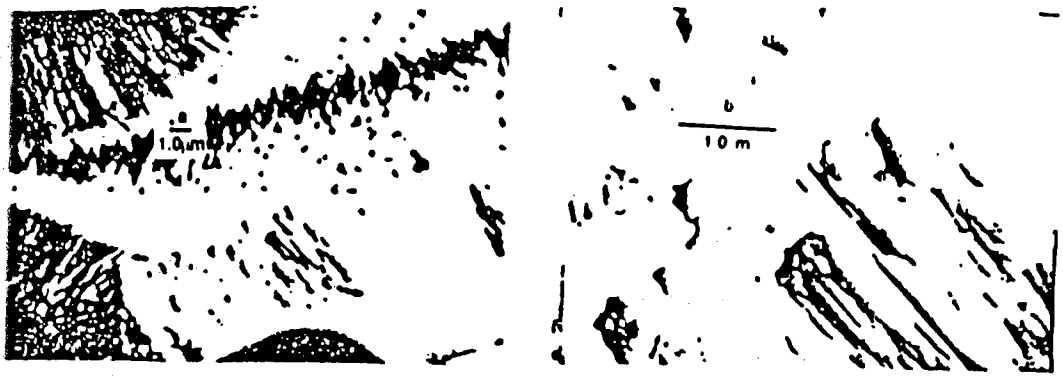

Fig. 3. Microstructure of TiC_x on Nicalon at 1000°C.

Fig. 4. Nucleation nodes of TiC_x on Nicalon.

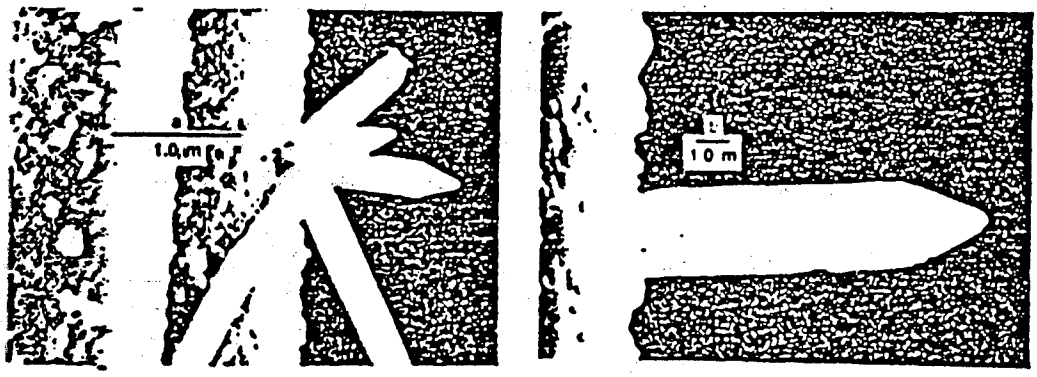

Fig. 5. TiC_x whiskers resulting from reactant depletion.

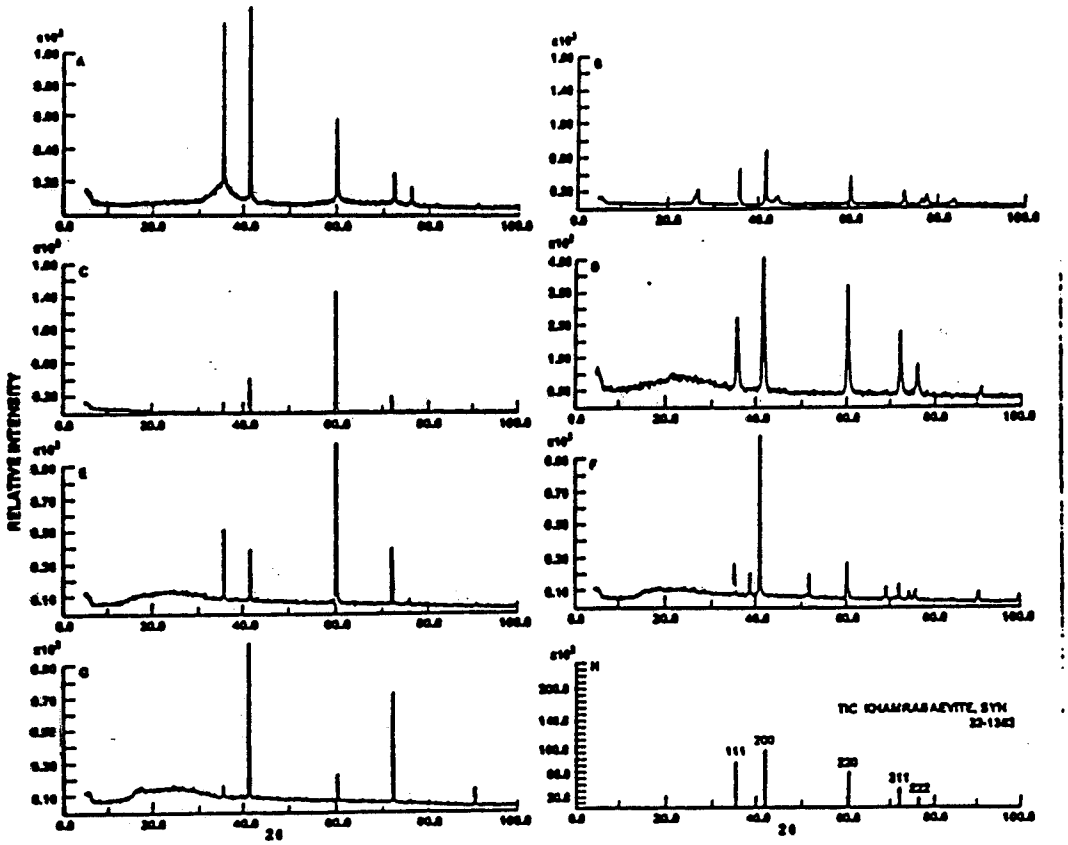

Fig. 6. X-ray diffraction patterns of TiC_x on: a) Nicalon (1000-1200°C), b) Graphite (1000°C), c) Graphite (1200°C), d) Silica (1000°C), e) Molybdenum (1150°C), f) Molybdenum (1200°C), g) Tantalum (1150°C), h) Standard powder pattern.

Fig. 7. Microstructure of TiC_x on Graphite at: a) 1000°C, b)1100°C and c) and d) 1200°C.

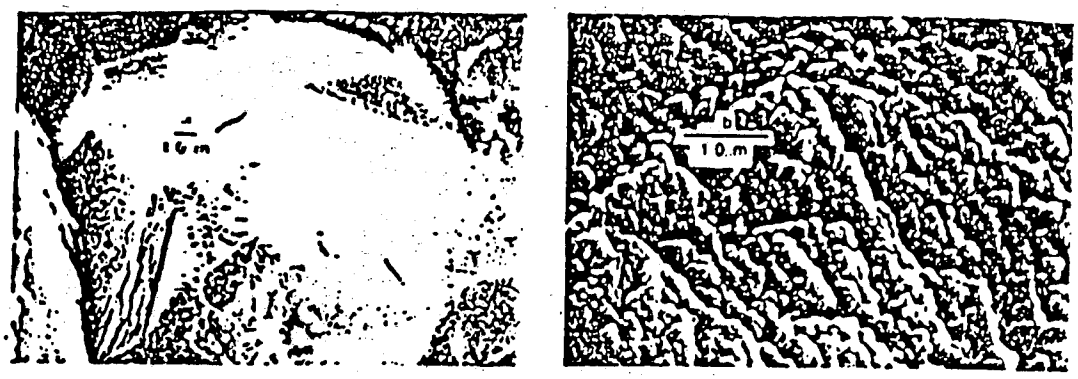

Fig. 8. Microstructure of TiC_x on Silica.

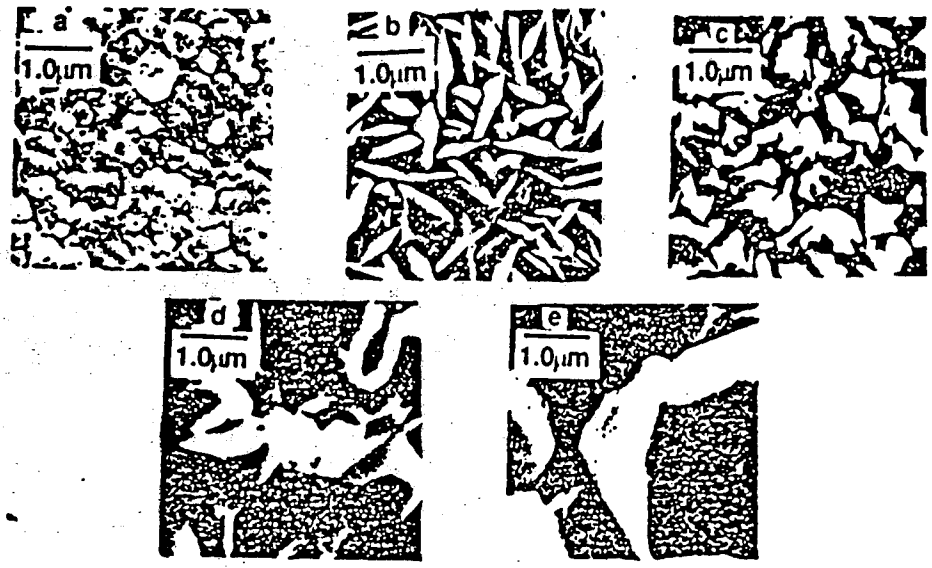

Fig. 9. Microstructure of TiC_x on Alumina at: a) 1200°C and $CH_4/TiCl_4$= 1.0, b) 1300°C and $CH_4/TiCl_4$= 0.5, c) 1300°C and $CH_4/TiCl_4$=1.0, d) 1300°C and $CH_4/TiCl_4$=3, e) 1300°C and $CH_4/TiCl_4$=4.0.

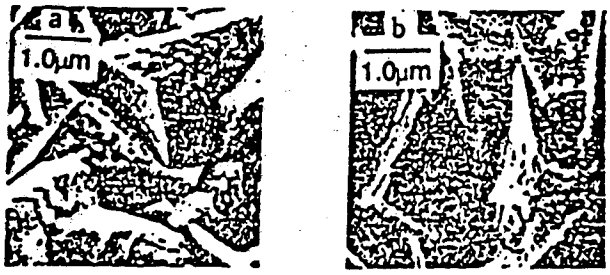

Fig. 10. Microstructure of TiC_x on a) Molybdenum, b) Tantalum.

CVD OF TiC_x ON SINGLE CRYSTAL Al_2O_3

R.A. Aparicio[1], E.F. Allen[1], T.J. Anderson[1], and M.D. Sacks[2], [1]Department of Chemical Engineering and [2]Department of Materials Science and Engineering, University of Florida, Gainesville, FL 32611

ABSTRACT

The kinetics of chemical vapor deposition of TiC_x from CH_4 and $TiCl_4$ sources on single crystal Al_2O_3 were investigated. Experimental growth rates show an Arrhenius dependence on deposition temperature, with apparent activation energies of 296 KJ/mol on (0001) Al_2O_3 and 328 KJ/mol on (1$\bar{1}$02) Al_2O_3. The growth rate was also found to have a linear dependence on the CH_4 partial pressure. Various grain orientations were observed in the films depending on the deposition temperature, deposition thickness, and substrate orientation. The measured grain orientations, however, were independent of the CH_4 partial pressure.

INTRODUCTION

TiC_x is a material with high strength and hardness, high melting temperature, and good resistance to wear and oxidation. These properties make TiC_x an attractive candidate as a matrix phase in ceramic-ceramic composites. The use of TiC_x in such applications has, however, received only recent attention.[1] Chemical vapor infiltration (CVI) is a useful technique to densify ceramic composites, particularly for systems such as fiber reinforced composites. CVI of TiC_x into ceramic preforms should also be feasible given the similarity of deposition chemistry and recent successes demonstrated for SiC.[2,3,4]

Successful CVI requires that reaction-limited deposition conditions be approached. Thus, an understanding of the kinetics regulating the deposition process, particularly in isolation from mass transfer effects, would be useful in designing suitable CVI reactors and in specifying appropriate operating conditions. In this study, the kinetics of TiC_x deposition on flat Al_2O_3 substrates were investigated in the reaction-limited regime. The influence of the temperature, substrate orientation, and CH_4 partial pressure on the deposition rate is reported. In addition, the coatings were characterized by X-ray diffraction (XRD), electron microprobe analysis (EMPA), and scanning electron microscopy (SEM) to determine the effect of the above parameters on the grain orientation, composition, and surface morphology.

EXPERIMENTAL

The experimental system used to deposit the TiC_x films has been previously described.[6] The films were deposited simultaneously on flat single crystal (0001) and (1$\bar{1}$02) Al_2O_3 substrates.* All depositions were carried out at atmospheric pressure. The methane (CH_4) partial pressure varied from 250 to 4050 Pa, while the titanium tetrachloride ($TiCl_4$)** partial pressure was held constant at 1010 Pa. Hydrogen was used as the carrier and diluent gas in the atmospheric pressure reactor. The total gas flow rate ranged from 4 to 250 std. cm^3/s, and deposition time varied from 1 to 4 hours. Experiments were performed in the temperature range of 1278-1383 K. The deposition temperature was measured with a dual-wavelength (ratio) optical pyrometer focused on the surface of the substrate.

RESULTS AND DISCUSSION

Effect of Deposition Parameters on the Deposition Rate

The influence of the total flow rate on the growth rate was investigated at 1383 K. The rate was observed to increase with flow rate to approximately the one-half power, up to 17 std. cm^3/s. For higher flows, the rate remained constant at values determined by the temperature and reactant gas partial pressures. This result indicates that the boundary between the mass-transfer and reaction-controlled regimes is somewhat less than 17 std. cm^3/s total flow rate. The growth of TiC_x should therefore be reaction-limited for temperatures less than 1383 K and total flow rates greater than or equal to the above value.

The temperature dependence of the deposition rate was determined at constant reactant partial pressures of 2030 Pa for CH_4 and 1010 Pa for $TiCl_4$ and a total flow rate of 17 std. cm^3/s. In order to quantify the apparent rate of deposition, the weight increase of the substrates was measured as a function of time for various temperatures (Fig. 1) and the growth rate was obtained from the slope of the weight change curve. For both substrate orientations, the growth rate followed an Arrhenius dependence on temperature (Fig. 2). The calculated apparent activation energies were 296 KJ/mol (±142 KJ/mol) for (0001) Al_2O_3 and 328 KJ/mol (±128 KJ/mol) for (1$\bar{1}$02) Al_2O_3. These activation energies are nearly 2.5 times higher than those reported for hot pressed polycrystalline Al_2O_3.[5]

The effect of CH_4 partial pressure is shown in Fig. 3. The deposition temperature and the $TiCl_4$ partial pressure were held constant at 1383 K and 1010 Pa, respectively. The slope of the curve is 1.06, indicating first-order

---

* Commercial Crystal Laboratories, Inc., Naples, Florida.

** Fisher Scientific, Fair Lawn, NJ. 98.0% purity reported by the manufacturer.

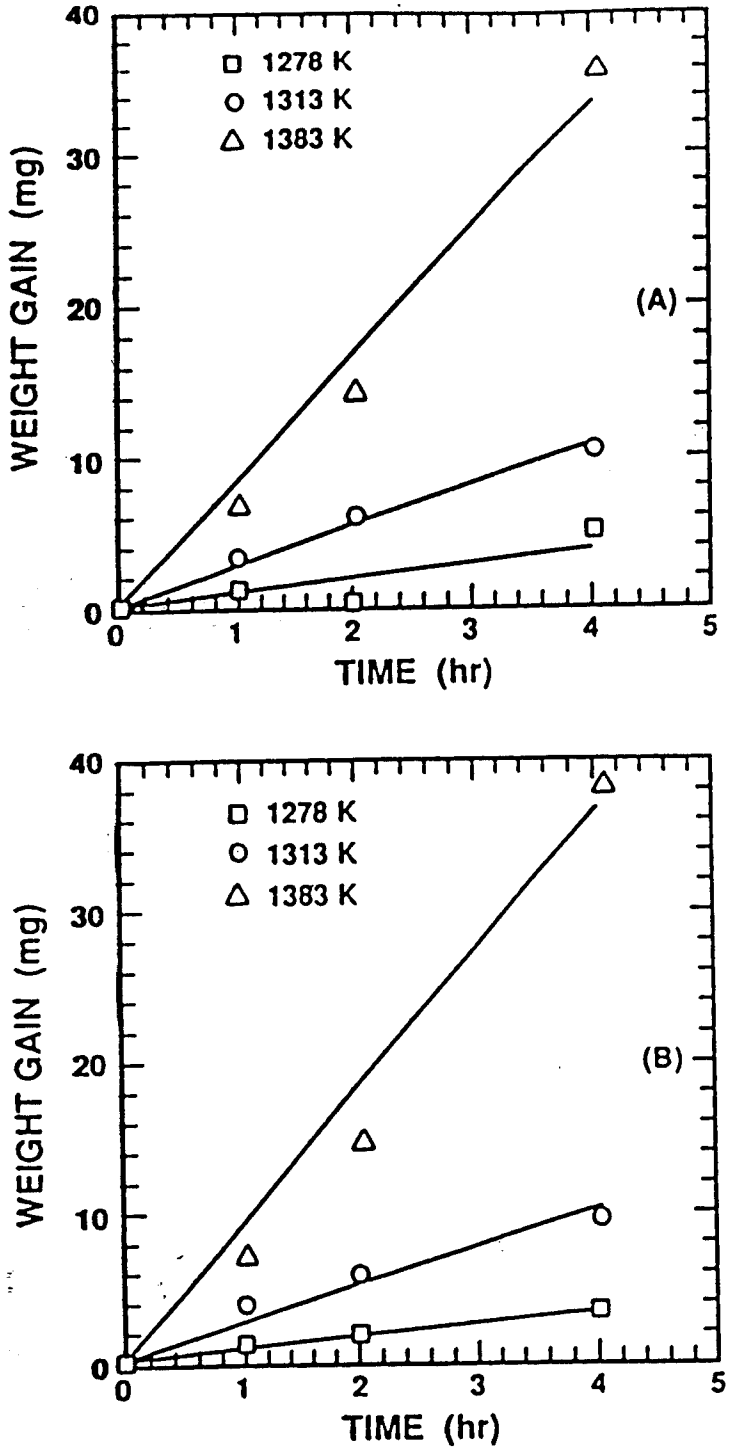

FIG. 1. Weight of TiC_x deposited on (A) (0001) and (B) $(1\bar{1}02)$ Al_2O_3 as a function of deposition time.

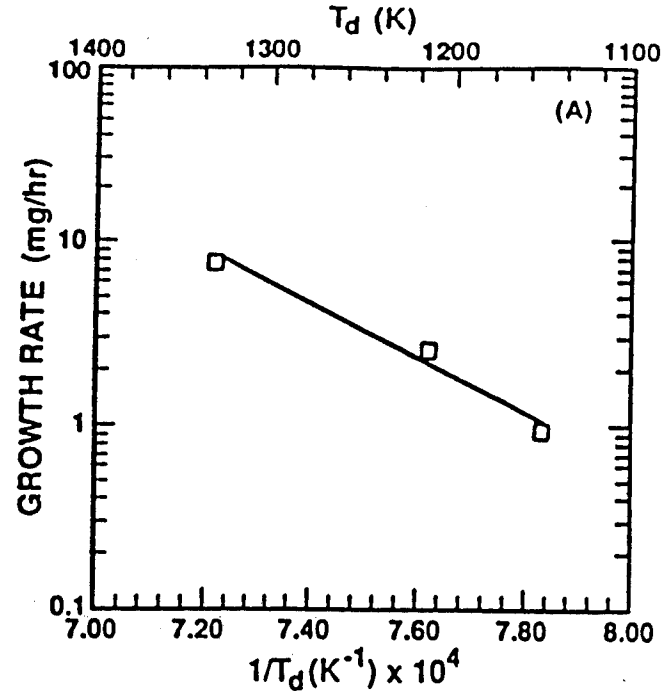

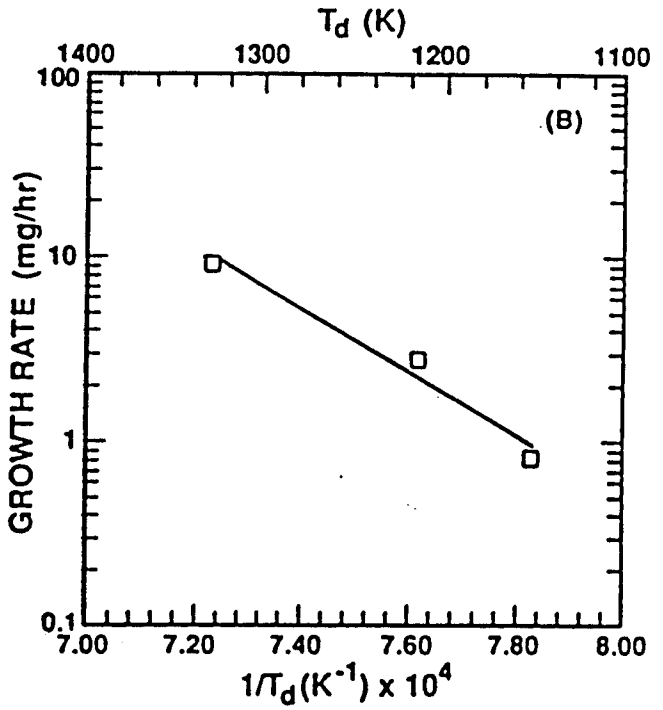

FIG. 2. Arrhenius plots of the TiC_x growth rate on (A) (0001) and (B) $(1\bar{1}02)$ Al_2O_3 as a function of temperature.

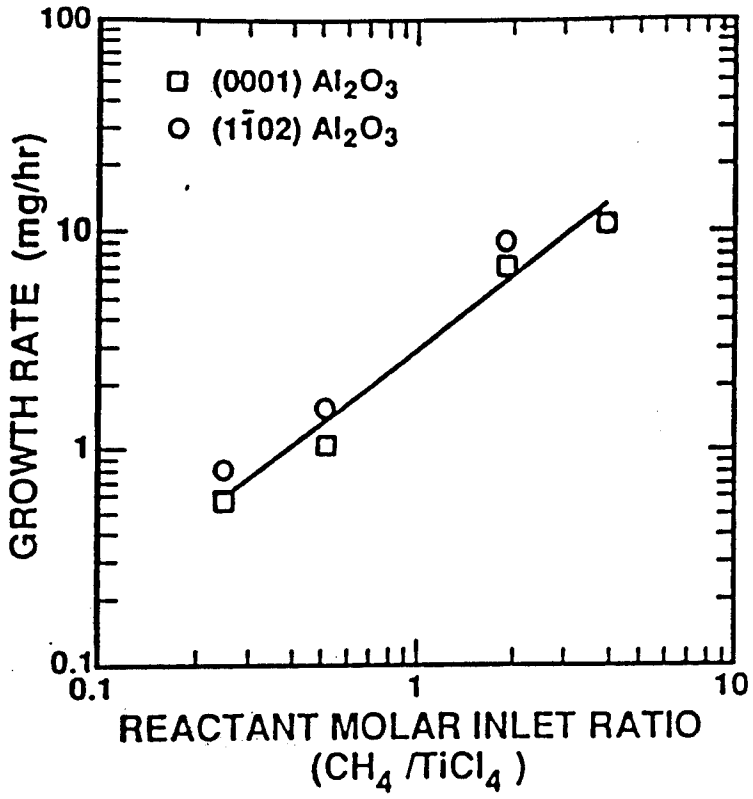

FIG. 3. TiC_x growth rate as a function of the ratio of CH_4 to $TiCl_4$ in the inlet gas. The $TiCl_4$ partial pressure was held constant at 1010 Pa.

dependence of the deposition rate on the CH_4 partial pressure. This result is consistent with work by Stjernberg et al.,[6] who proposed a Langmuir-Hinshelwood mechanism in which the growth rate also follows a first order dependence on the CH_4 partial pressure. Because of this trend, CH_4 decomposition has been postulated as the rate-limiting step in the deposition of TiC_x. For comparison, the above activation energies are in agreement with the activation energy of homogeneous CH_4 pyrolysis at 2273 K (312 KJ/mol).[7]

Surface Morphology, Grain Orientation, and Film Composition

Figure 4 shows the morphological evolution of the coatings on (0001) Al_2O_3 as the temperature was varied from 1278 to 1383 K. The grain size increased with temperature and the grain shape changed from a globular to a faceted structure, presumably caused by an increase in growth rate. A similar trend was observed for the coatings on (1$\bar{1}$02) Al_2O_3.

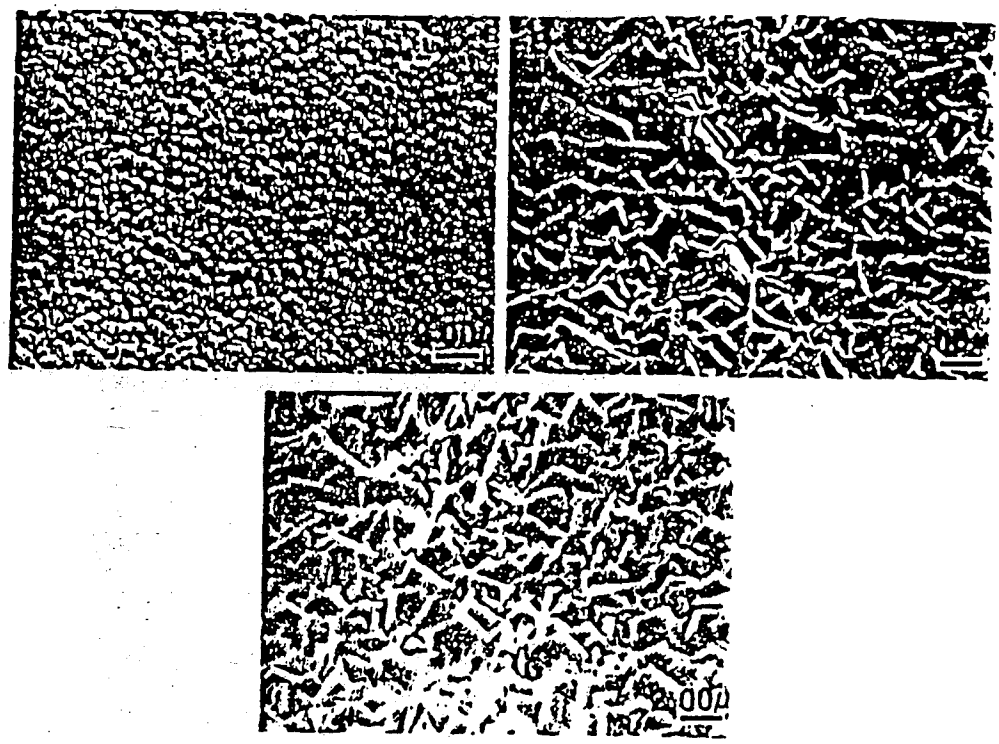

FIG. 4. Microstructure of TiC_x on (0001) Al_2O_3 at: (A) 1273 K, (B) 1323 K, and (C) 1373 K.

The effect of the CH_4 partial pressure on the surface morphology of the films (Fig. 5) is similar to the temperature effect (Fig. 4). There is an increase in grain size; however, the grain shape remains unchanged. Once again, this trend is the same for both Al_2O_3 substrate orientations.

Each film displayed a strong preferred orientation which varied with substrate orientation, deposition time, and deposition temperature (Table 1). For long deposition times and higher growth temperatures, the coatings appeared to be oriented in directions of highest atomic packing. Grain orientations did not, however, vary with CH_4 partial pressure.

The measured film composition remained constant (C/Ti = 0.52 ±0.05) as the ratio of CH_4 to $TiCl_4$ partial pressures in the inlet gas was varied from 0.25 to 4.0. The apparent independence of the film composition on the inlet gas concentration ratio is attributed to the errors in the EMPA measurement, caused by the film surface roughness. Improvement in the measurement could not be achieved by polishing due to poor adhesion of the film to the substrate.

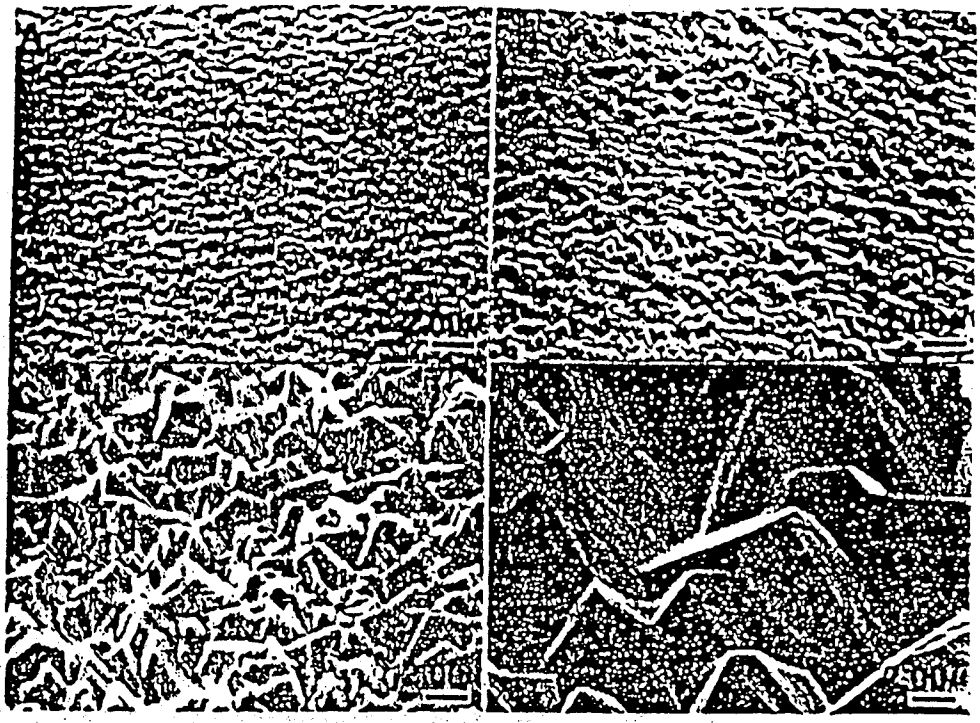

FIG. 5. TiC_x microstructures on $(1\bar{1}02)$ Al_2O_3 for various $CH_4/TiCl_4$ ratios: (A) 0.25, (B) 0.50, (C) 2.00, (D) 4.00. $TiCl_4$ partial pressure was constant (1010 Pa).

TABLE 1. Preferred Orientation of TiC_x Films as a Function of Substrate Orientation, Deposition Time and Temperature.

Substrate Orientation: (0001)

Deposition Temperature (K)	Deposition Time (hr)		
	1	2	4
1278	(200)	(200)	(111)
1313	(111)	(111)	(220)
1383	(111)	(111)	(111), (220)

Substrate Orientation: $(1\bar{1}02)$

Deposition Temperature (K)	Deposition Time (hr)		
	1	2	4
1278	(200), (111)	(200), (111)	(111)
1313	(200), (311)	(200), (311)	(200)
1383	(200)	(220)	(220)

SUMMARY

The deposition rate of TiC_x on single crystal Al_2O_3 from CH_4 and $TiCl_4$ sources followed an Arrhenius dependence on growth temperature, with activation energies of 296 KJ/mol to 328 KJ/mol for (0001) and (1$\bar{1}$02) substrate orientations, respectively. The deposition rate was also a linear function of the CH_4 partial pressure. Reaction-limited growth could be achieved at flow rates greater than or equal to 17 std. cm^3/s, below which the rate depended on the total gas velocity. Grain orientations were affected strongly by the substrate orientation, deposition time, and deposition temperature. As the thickness of the film increased, orientations along planes of highest atomic packing, i.e., (111) and (220), became dominant.

ACKNOWLEDGEMENTS

This work was supported by the Defense Advanced Research Projects Agency under Navy grant No. MDA972-88-J-1006. The authors would also like to thank Pete Axson, Juan Casero, and Amy Hoelzer for their assistance.

REFERENCES

1. J.Y. Rossingnol, F. Langlais, and R. Naslain, "A Tentative Modelization of Titanium Carbide C.V.I. Within the Pore Network of Two-Dimensional Carbon-Carbon Composite Preforms," Electrochem. Soc. Proc. 9th Int. Conf. on Chemical Vapor Deposition, 596-614 (1984).

2. D.P. Stinton, A.J. Caputo, R.A. Lowden, and T.M. Besmann, "Improved Fiber-Reinforced SiC Composites Fabricated by Chemical-Vapor Infiltration," Ceram. Eng. Sci. Proc., 7 (7-8) 983-989 (1986).

3. D.P. Stinton, A.J. Caputo, and R.A. Lowden, "Synthesis of Fiber-Reinforced Silicon Carbide Composites by Chemical Vapor Infiltration," Am. Ceram. Soc. Bull., 65 (2) 347-350 (1986).

4. W.J. Lackey, "Review, Status, and Future of the Chemical Vapor Infiltration Process for Fabrication of Fiber-Reinforced Ceramic Composites," Ceram. Eng. Sci. Proc., 10 (7-8) 577-584 (1989).

5. R. Aparicio, J.L. Ponthenier, F. Hong, T.J. Anderson, M.D. Sacks and G. Johnson, "Chemical Vapor Deposition of TiC_x on Al_2O_3 Substrates," Ceram. Eng. Sci. Proc., 10 (9-10) 1462-1471 (1989).

6. K.G. Stjernberg, "The Rate of Chemical Vapor Deposition of TiC," Thin Solid Films, 40 81-88 (1977).

7. W.C. Gardiner, Jr., J.H. Owen, T.C. Clark, J.E. Dove, S.H. Bauer, J.A. Miller, and W.J. McLean, "Rate and Mechanism of CH_4 Pyrolysis from 2000°C to 2700°C," Symp. Int. Combust. Proc., 15 857-868 (1975).